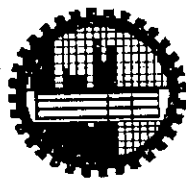# *Investigation Of The Dose Distribution By Irregular Field-Shaping Device For Photon Beam Radiation*

By

LAILA ZAMAN

#100847#

A Thesis Submitted TO The Department Of Physics, Bangladesh University Of Engineering And Technology In Partial Fulfilment Of The Requirement For The Degree Of Master Of Philosophy

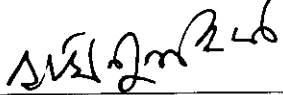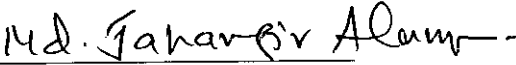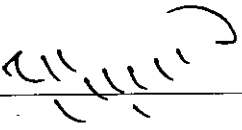Bangladesh University Of Engineering And Technology
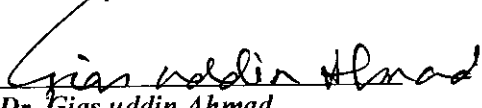Dhaka, Bangladesh

December 2004

BANGLADESH UNIVERSITY OF ENGINEERING AND TECHNOLOGY
DEPARTMENT OF PHYSICS

Certification of Thesis work

*The thesis titled "**Investigation of the Dose Distribution by Irregular Field-Shaping Device for Photon Beam Radiation**", submitted by Laila Zaman, Roll No. 9614007F, Session 1995-96-97 has been accepted as satisfactory in partial fulfillment of the requirement for the degree of Master of Philosophy on 28th December 2004.*

BOARD OF EXAMINERS

1.
   Prof. Mominul Huq (Supervisor)
   Professor
   Department of Physics, BUET, Dhaka   Chairman

2.
   Mr. M. Jahangir Alam (Co-Supervisor)
   Senior Medical Physicist   Member
   Delta Medical Centre Ltd., Dhaka

3.
   Head   Member
   Department of Physics, BUET, Dhaka

4.
   Dr. Gias uddin Ahmad
   Professor of Physics, (Retired) BUET   Member
   Resortessa Apartment # S-2
   Dhanmondi R/A, Dhaka

5.
   Dr. Nazma Zaman   Member
   Professor
   Department of Physics, BUET, Dhaka

6.
   Dr. Mir. Md. Akramuzzaman
   Professor   Member
   Department of Physics
   Jahangirnagar University, Savar, Dhaka

CANDIDATES DECLARATION

It is hereby declared that this thesis or any part of it has not been submitted elsewhere for the award of any degree or diploma.

Signature of the Candidate

Laila Zaman

(Laila Zaman)
Session 1995-96-97
Roll No. 9614007F

Acknowledgements

This work which I carried out at the Department of Physics, Bangladesh University of Engineering & Technology (BUET), Dhaka, Bangladesh, is the result of a few years of my life's academic involvement. Many people have supported me during this research work, I would like to thank all of them.

Firstly, I must thank my supervisor Professor Md. Mominul Huq, Department of Physics for giving me the opportunity to carry out this research. Thanks to Prof. Huq for his continuous interest in my work, for constant and unflinching support, for being so optimistic as well as helping with fruitful discussions and ideas.

I would like to express my sincere gratitude to Professor Dr. Gias uddin Ahmad, Prime Asia University, Dhaka for his continuous advise. He has given me a great chance for advancing my career to pursue higher study. I want to thank him not only for giving me support but also for reviewing my thesis paper and making valuable suggestions.

I am very much grateful to Dr. Mir. Md. Akramuzzaman, Professor, Department of Physics, Jahangirnagar University, Savar, Dhaka for his important suggestion during writing up my thesis.

I am grateful to my Co-Supervisor, Md. Jahangir Alam, Senior Physicist, Delta Medical Centre, for permitting me to carry out part of my research work in his Institute and for his continuous help and cooperation in my work.

I am also grateful to Prof. Md. Abu Hashan Bhuiyan, Prof. Nazma Zaman, Dr. Md. Nazrul Islam, Ms. Afia Begum and Mr. Rafi Uddin who encouraged me throughout the research work.

I want to express special gratitude to Mr. Md. Liaquat Ali, Mr. Swpan Kumar Das and other staffs of the Department of Physics, BUET and all technicians of the Onchology Department of Delta Medical Centre Ltd. for their valuable help.

ABSTRACT

This research work reports the investigation of dose distribution by the irregular field shaping device for photon beam radiation. In this work phantom of size 50 cm × 45 cm, thickness 1.5 cm and the irradiation facilities Co-60 teletherapy unit were used.

During dose measurement 0.6 cc ionization chamber and PTW-UNIDOS electrometer were used. At first open field doses for various field sizes such as 5×5cm; 10×10cm, 15×15cm, 20×20 cm, 25×25 cm for lateral, vertical and diagonal distances were investigated.

The "Half-beam device" which is used for the breast cancer treatment was used as one of the irregular field shaping devices. Three other irregular field shaping devices were made with several rectangular blocks (made of shielding material) inserting into the shielding tray. The doses on points of both side of the central axis were measured by using the irregular field shaping devices.

The data were analyzed by making graphs using the points of dose measurement vs. the dose rate of these points and thus showing the effect of the irregular field-shaping device, which are used for the treatment of cancer.

Another special block (made of lead alloy) which is routinely used for the pelvis cancer treatment was used with tissue-compensator for the dose measurement of various points, thus to find the effect of the tissue-compensator. For finding the percentage of deviation for doses, the open field data was compared with the blocked field data for the same field size 15×15cm. The estimated deviations were satisfactory.

To my Husband
and
Daughter

CONTENTS

i

Tissue and Bone

CHAPTER 4: Radiotherapy Technique for Cancer Treatment

CHAPTER 5: Equipment and Experimental Methods

CHAPTER 6: Results and Discussion

CHAPTER-7: Summary, Recommendation and Conclusion

CHAPTER 1 Introduction

1.1. General

Radiotherapy also called radiation therapy, is used for the treatment of cancer and other diseases with ionizing radiation. Ionizing radiation deposits energy that injures or destroys cells in the area being treated (the "target volume") by damaging their genetic material, making it impossible for these cells to continue their growth. Although radiation damages both cancer cells and normal cells, the latter are able to repair them and function properly. Radiotherapy may be used to treat localized solid tumors, such as cancers of the skin, tongue, larynx, brain, breast, or uterine cervix. It can also be used to treat leukemia and lymphoma (cancers of the blood-forming cells and lymphatic system, respectively).

One type of radiation therapy commonly used involves photons, "packets" of energy. X-rays were the first form of photon radiation to be used to treat cancer. Depending on the amount of energy they possess, the rays can be used to destroy cancer cells on the surface of or deeper in the body. The higher the energy of the x-ray beam, the deeper the x-rays can go into the target tissue. Linear accelerators and betatrons are machines that produce x-rays of different energy. The use of machines to focus radiation (such as x-rays) on a cancer site is called external beam radiotherapy.

Gamma rays are another form of photons used in radiotherapy. Gamma rays are produced during spontaneous decay of certain elements (such as radium, uranium, and cobalt 60). Each element decays at a specific rate and gives off energy in the form of gamma rays and other particles. X-rays and gamma rays have the same effect on cancer cells.

Another technique for delivering radiation to cancer cells is to place radioactive implants directly in a tumor or body cavity. This is called internal

radiotherapy. Brachytherapy, interstitial irradiation, and intracavitary irradiation are types of internal radiotherapy. In this treatment, the radiation dose is concentrated in a small area, and the patient stays in the hospital for a few days. Internal radiotherapy is frequently used for cancers of the tongue, uterus, and cervix.

Several new approaches to radiation therapy are being evaluated to determine their effectiveness in treating cancer. One such technique is intraoperative irradiation, in which a large dose of external radiation is directed at the tumor and surrounding tissue during surgery.

Another investigational approach is particle beam radiation therapy. This type of therapy differs from photon radiotherapy in that it involves the use of fast-moving subatomic particles to treat localized cancers. A very sophisticated machine is needed to produce and accelerate the particles required for this procedure. Some particles (neutrons, pions, and heavy ions) deposit more energy along the path they take through tissue than do x-rays or gamma rays, thus causing more damage to the cells they hit. This type of radiation is often referred to as high linear energy transfer (high LET) radiation.

Scientists also are looking for ways to increase the effectiveness of radiation therapy. Two types of investigational drugs are being studied for their effect on cells undergoing radiation. Radiosensitizers make the tumor cells more likely to be damaged, and radioprotectors protect normal tissues from the effects of radiation. Hyperthermia, the use of heat, is also being studied for its effectiveness in sensitizing tissue to radiation.

Other recent radiotherapy research has focused on the use of radiolabeled antibodies to deliver doses of radiation directly to the cancer site (radioimmunotherapy). Antibodies are highly specific proteins that are made by the body in response to the presence of antigens (substances recognized

as foreign by the immune system). Some tumor cells contain specific antigens that trigger the production of tumor-specific antibodies. Large quantities of these antibodies can be made in the laboratory and attached to radioactive substances (a process known as radiolabeling). Once injected into the body, the antibodies actively seek out the cancer cells, which are destroyed by the cell-killing (cytotoxic) action of the radiation. This approach can minimize the risk of radiation damage to healthy cells. The success of this technique will depend upon both the identification of appropriate radioactive substances and determination of the safe and effective dose of radiation that can be delivered in this way. [1]

Radiation therapy may be used alone or in combination with chemotherapy or surgery. Like all forms of cancer treatment, radiation therapy can have side effects. Possible side effects of treatment with radiation include temporary or permanent loss of hair in the area being treated, skin irritation, temporary change in skin color in the treated area, and fatigue. Other side effects are largely dependent on the area of the body that is being treated.

In the past 100 years, diagnostic radiology, nuclear medicine and radiation therapy have evolved from the original crude practices to advanced techniques that form an essential tool for all branches and specialties of medicine. The inherent properties of ionizing radiation provide many benefits but also possess certain element of risk.

In the practice of medicine, there must be a judgement made concerning the benefit /risk ratio. This requires not only knowledge of medicine but also of the radiation risks. Interventional cardiologists, radiologists, orthopedic and vascular surgeons and others, who actually operate medical x-ray equipment or use radiation sources, should possess more information on proper technique and dose management. [2]

However, it should be remembered that radiotherapy is often accompanied by adverse side effects. Some adverse effects are unavoidable and often resolve spontaneously or with treatment. Serious adverse effects may occur and result from the proximity of sensitive normal tissues to the treatment field or rarely as a result of individual radiation sensitivity. They do not undermine the purpose of radiotherapy. Appropriate use of radiotherapy saves millions of lives every year. Even if only palliative treatment is possible, the therapy substantially reduces suffering.

The magnitude of risk from radiation is dose-related with higher amounts of radiation being associated with higher risks. Since large amounts of radiation are required in radiation therapy, the risk of radiation related adverse effect is measurably higher.

The aim of managing radiation exposure is to minimize the putative risk without sacrificing, or unduly limiting, the obvious benefits in the prevention, diagnosis and also in effective cure of diseases (optimization). It should be pointed out that when too little radiation is used for diagnosis or therapy there is an increase in risk although these risks are not due to adverse radiation effects per sec. Too low an amount of radiation in diagnosis will result in either as image that does not have enough information to make a diagnosis and in radiation therapy, not delivering enough radiation will result in increased mortality because the cancer being treated will not be cured. [2]

1.2. Prevalence of Cancer

Incidence of cancer has been increasing in almost non-linear fashions in recent years, which is alarming in the context of socioeconomic condition of our country. According to estimates made by International Agency for Research on Cancer (IARC) there are more than 9 million new cancer cases

worldwide with slightly more than half of the new cases in developing countries. By the year 2015, this figure is expected to increase to about 15 million cases, of which two thirds will occur in developing countries [3]. The distribution of cancer cases between the sexes worldwide is fairly even having 4.77 millions in males and 4.55 million cases in females. Since the incidence of cancer increases with age, the majority of new cases occur in the age group 65+ years. The age distribution of cancer cases is, however quite different in developed and developing countries; there are significantly more cancer cases in childhood, adolescence and young ages in developing countries, while in developed countries this feature is quite reverse where cancer in the elderly still dominates (Fig. – 1.1).
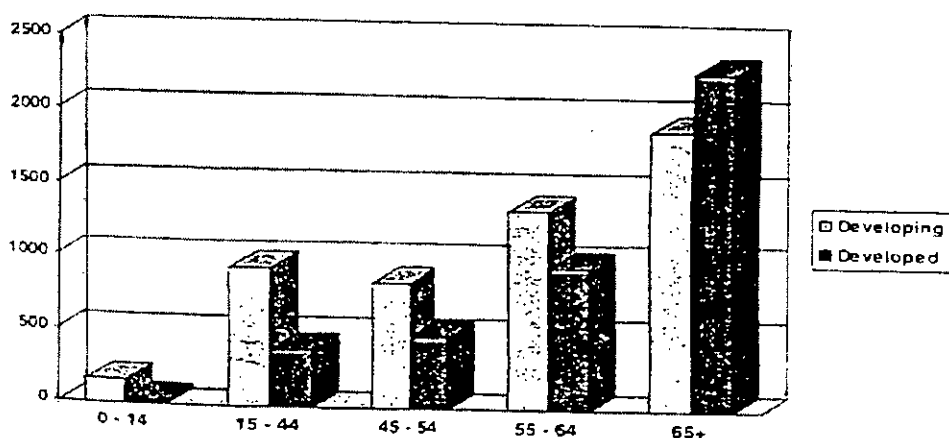
Fig. 1.1 Age distribution of cancer cases in developed and developing countries in 1990. In the age group 0 – 14 years there are 5 times more cases in developing countries and in the age group 15 – 45 years almost three times more (IARC 1990 estimate).

Overall, the most common tumor worldwide is cancer of the lung with an annual incidence of almost 1.2 million cases, followed by the stomach cancer (0.90 million), breast cancer (0.84 million), colorectal cancer (0.80 million) and cancer of the mouth and pharynx (0.51 million) (Fig. – 1.2).
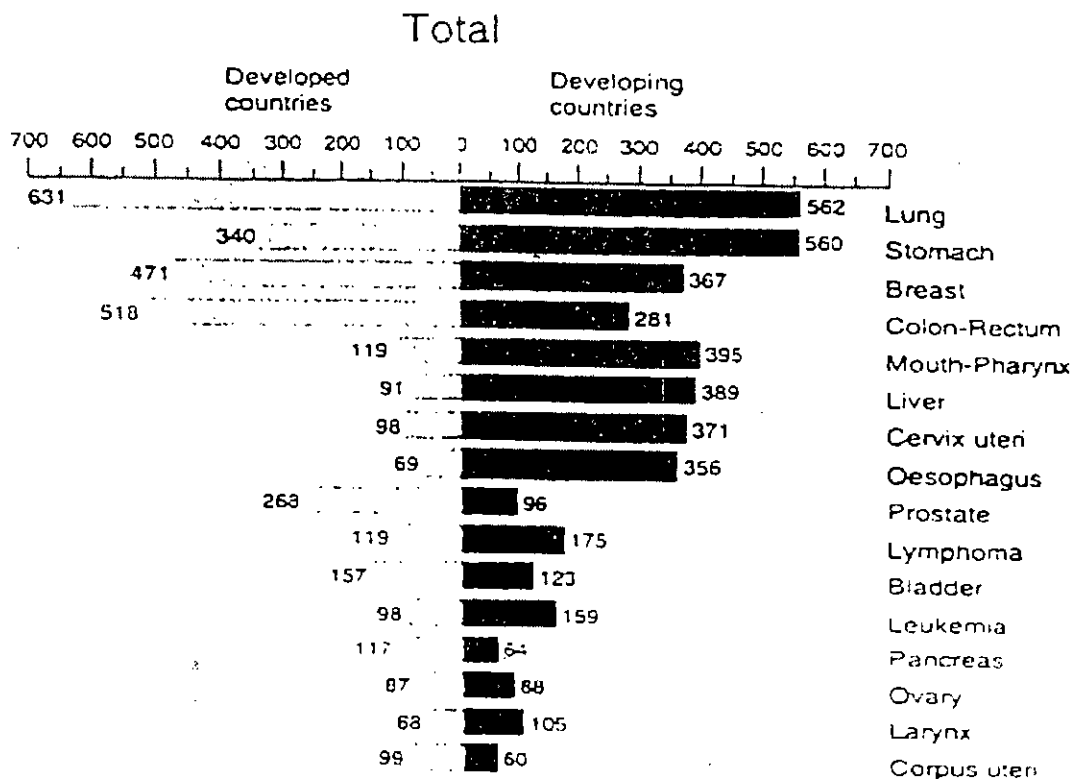
Total

Fig.1.2 Worldwide distribution of cancer types in 1990, ranked by total number of cases for various diagnoses (IARC 1990 estimate).

In males the common tumor is cancer of the lung, followed by stomach (Fig. – 1.3). In females, breast cancer is the most common type followed by cancer of the cervix (Fig. – 1.4). However, in Bangladesh, prostrate cancer is the most common in male followed by lung cancer while in female, cervix is the most common cancer type followed by breast cancer.

Male

Developed countries — Developing countries

500 400 300 200 100 0 100 200 300 400 500

Developed	Developing	Cancer type
472	417	Lung
203	355	Stomach
252	150	Colon-Rectum
258	96	Prostate
89	254	Mouth-Pharynx
59	273	Liver
50	232	Oesophagus
118	94	Bladder
66	108	Lymphoma
61	86	Larynx
53	87	Leukemia
60	36	Pancreas
57	32	Kidney
35	14	Mal. Melanoma
18	15	Myeloma
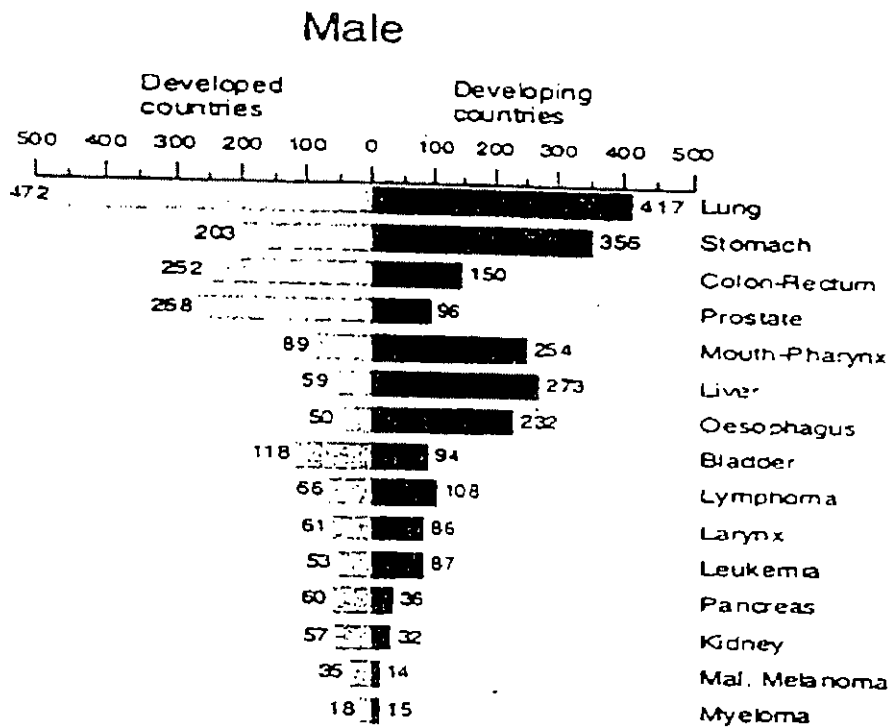
Fig. 1.3 Worldwide distribution of cancer types in 1990, ranked by total number of cases for various diagnoses for males (IARC 1990 estimate)

Female

Developed Countries — Developing Countries

500 400 300 200 100 0 100 200 300 400 500

Developed	Developing	Cancer type
471	367	Breast
98	371	Cervix uteri
266	131	Colon-Rectum
137	204	Stomach
159	145	Lung
87	88	Ovary
30	141	Mouth-Pharynx
99	60	Corpus uteri
32	116	Liver
19	124	Oesophagus
53	67	Lymphoma
45	72	Leukemia
57	28	Pancreas
39	29	Bladder
38	23	Kidney
40	17	Mal. Melanoma
18	11	Myeloma
7	19	Larynx

Fig. 1.4 Worldwide distribution of cancer types in 1990, ranked by total number of cases for various diagnoses for females (IARC 1990 estimate)

According to WHO statistics, there were about 0.8 million cancer patients in Bangladesh in 1993 among a total population of 110 million (0.73%) at least half of them needing radiotherapy treatment at various stages of the disease. Each year additional 0.3 million new cancer patients are diagnosed, representing 0.25% of the current population of 120 million. Among the female cancer patients, constituting about 50% of the total, some 30% have been suffering from cancer of the cervix, meaning about 45,000 new cervical cancer cases each year [4,3].

Almost 50% of these require management comprising surgery, radiotherapy and chemotherapy, which are being considered as the basis of the management of patients with cancer. A radiotherapy department shall be integrated in a comprehensive cancer treatment programme. The radiation oncologists will determine the overall treatment techniques and specific treatment procedures keeping in mind that those procedures evolve in time. The physicist will need to prepare the technical work and instruments associated with each type of treatment, such as procedures for calculation of doses and treatment times, source handling and associated quality control (QC) steps etc. The importance of careful planning for each type of radiotherapy treatment should be appreciated by all, since the correct execution of the treatment is the purpose of the entire program [5]. Unfortunately, aforesaid requirements are very often ignored in the most of our radiotherapy establishments. Except a few, therapy establishments in our country do not have any physicist to take care of the aforesaid physical aspects of radiotherapy treatment planning system which actually causes serious problem in the proper management of physics part of the therapy procedure.

1.3. Field Irregularity and Dose Distribution

Any field other than square, rectangular or circular fields may be termed irregular fields. These irregularly shaped fields are frequently encountered in radiotherapy practices. Irregular shaped fields, in fact, appear when radiation sensitive structures are shielded from the primary beam or when the field extends beyond the irregularly shaped patient's body contour. Since basic standard dosimetric data are available for rectangular or square fields only, special methods including several correction factors are necessary to use these basic data for calculation of doses in irregularly shaped fields. For certain specific irregular fields, some special methods are in general use. However, irregular fields are not universal rather, it can be different for different clinical situations. Therefore, several approaches are in progress for making generally applicable methods for calculation of doses in individual irregular field.

1.4. Organs at Risk

It is well understood that exposure to ionizing radiation causes biological effects in living tissue resulting in cells death and other complicated consequences. Fatal diseases like leukemia and several forms of cancers can occur from excessive exposure to ionizing radiation [6]. Increased likelihood of cancers is the delayed effects of exposure to radiation. This delayed effect of radiation, however, can be considered as stochastic effect and is of somewhat less important but survivability of the patient usually gets preference in radiotherapy treatment planning. On the other hand, short term (acute) or non-stochastic effects of ionizing radiation are considerable and are very carefully accounted for during application of therapy doses. These acute effects of radiation are associated with levels of radiation dose applied to the patients and generally known as acute radiation syndromes. These are categorized as:

a) haematopoietic syndrome

b) gastrointestinal syndrome and

c) cerebrovascular syndrome etc.

The occurrences of these effects differ according to the relative radiosensitivity of the involved organ and doses to it. It has been observed that a dose level of a few grays can inactivate a significant number of the stem cells of the haematopoietic system, which may lead to bone marrow depression. Epithelial cells that line the intestinal surface are highly vulnerable to radiation injury resulting in diarrhoea, haemorrhage, electrolyte imbalance, dehydration and other gastrointestinal effects within a few days as a consequence of cell damage by radiation dose. At dose above about 50 Gy, cellular injury may be severe in the relatively radiation insensitive neurologic and cardiovascular compartments of the body. This effect may produce life-threatening damages almost immediately after exposure. Deaths in a few hours or days usually caused by destruction of the blood vessels in the brain, fluid accumulation and neuronal damage result [7,8]. A single dose of about 0.15 Gy to male testis causes temporary sterility while permanent sterility may occur at dose above 3.5 Gy. Single ovarian doses of above 0.65 Gy may cause temporary sterility in female while permanent sterility has been observed at doses above 2.5 Gy. Doses required to produce temporary or permanent sterility are increased by orders of magnitude if delivered in fractions or simultaneously at low dose rate [9,10].

Under the above circumstances, it is very important for physicist, oncologists and dosimetrists that during treatment planning, extra attention must be paid so that no undesired dose burden can take place in any organs, particularly low tolerant organs, outside the treatment volume. Dose rate per fraction and number of fractions in therapy completion must also be taken into account so that possible acute radiation syndrome can be controlled. In order to fulfill the aforesaid criteria, beam modification for

achieving required irregular photon fields is very often and important as well in routine radiotherapy practices.

1.5. Tissue Type and Response to Radiation

The biological targets of radiation are the cells, which make up the body's various tissues. Radiation is particularly lethal to cells during cell division (mitosis). The end result is cell death or the loss of reproductive capacity. The exact mechanism by which the cell loses their reproductive capability is yet unknown [9]. The specific target of radiation is the DNA molecule, which lies within the chromosomes of the cell's nucleus and constitutes the genetic blueprint for future reproduction. The growth of both normal and malignant tumor cells is influenced by different proportion of cells in their cycles of completion. In the malignant tumor, the normal control of cell division has been lost, resulting in inappropriate cellular proliferation and thus become more sensitive to radiation than normal tissue cells. In conventional radical radiotherapy, daily doses of the order of 2 Gy are usually delivered. Each dose of 2 Gy roughly reduces the surviving tumor population by 50% [4,7,11].

The purpose of radiotherapy treatment planning is to confine the applied radiation dose to the treatment or tumor volume and minimize the dose to normal tissues. This is easier for superficial than deep-seated tumors. In radiotherapy treatment procedure, development of a system for providing zero doses to the normal tissue and 100% dose to the target volume is not practically possible. Quite necessarily some normal tissue is included in the treatment volume with a view to cover the microscopic spread of malignant tissues beyond the visible limits of the tumor margin. There are certain definite limits to the amounts of radiation that normal tissues will tolerate. This maximum radiation dose that tissue of a particular organ can receive without showing any significant biological effects is referred to as the tolerance dose of that organ. Exceeding this dose may result in major and

sometimes fatal complications. The tolerance dose will vary with the type, amount of tissue irradiated, the quality of radiation and its application strategy. However, beam modification by using shielding blocks as per target outline can save some normal tissue volume from necessary or unnecessary radiation exposure to certain extent which helps providing required and adequate radiation dose to the target volume without crossing the normal tissue tolerance thereby resulting no known biological effects to the normal tissue [12,13].

1.6. Radio-Sensitivity and Dose Fractionation

Radio-sensitivity of cells is a very common word in radiotherapy practices normally contemplated by the treatment planning team usually comprised of radiation oncologists, medical physicists, dosimetrists during making a blueprint for therapy applications. The term "Radio-sensitivity" means the relative vulnerability of cells to be damaged by ionizing radiation. Radio-sensitivity is measurable in cell survival curves using the capacity of cells to reproduce following irradiation as the end point. Both normal and malignant tissues have different sensitivities, mainly determined by their different growth rates. This is the basis of the law of Bergonie and Tribondeau (1904). The biological action of ionizing radiation is greater where the reproductive activity of the cell is higher, the longer the period of its mitosis and the less the degree of differentiation. It has been observed that the radio-sensitivity of the rapidly dividing germ cells of the reproductive organs such as "testes or ovary" is high, fortunately the cells of a malignant tumor of the testis or ovary have even higher radio-sensitivity, paving the way for application of radiotherapy to these highly radiosensitive organs. In contrast, a slow growing soft tissue sarcoma shares the low sensitivity of its parent tissue. However, adequate dose can be applied to the soft tissue sarcoma without causing extra dose burden to the critical organs by shaping the irradiation beam as per tumor outline so that irradiation beam zone

excludes the vulnerable critical organs. The various tissues and organs have a wide spectrum of radio-sensitivity. The highly sensitive tissues are rapidly damaged by fairly low doses while the most radio-resistant organs can withstand much higher dose without any obvious radiation induced effects. Radio-sensitivity of different living tissues can be categorized as follows:

a. High-sensitivity:
1) The epithelium of the skin (epidermis)
2) The epithelial lining (inner surface) of the alimentary tract.
3) The cells in the bone marrow which produces the blood cells i.e. the haematopoietic tissue.
4) The reproductive cells of the testes and ovary.

b. Intermediate sensitivity:
Liver, kidney, lung and many glands.

c. Less sensitive:
Muscle, bone, connective and nervous tissues etc. [14, 15]

These radiosensitive organs lying close to the malignant tumors can be saved from unwanted radiation exposure beyond their tolerance level by shaping the radiation fields using beam blocks so that it excludes these critical organs and exploiting the dose fractionation facility as well. It is well understood that different types of tissues respond differently to the same amount of radiation exposure. Dose fractionation exploits this benefit of variable responses of rapidly responding tumors and late responding normal tissues to ionizing radiation. Damage to DNA following irradiation is generally repaired over a period of hours. However, the degree of repair will vary from tissue to tissue. Slowly responding tissues (connective tissue and spinal cord) have a greater capacity for repair than tumor tissues as long as the gap between treatment fractions is at least 6 hours which is the conventional daily fraction. Since cell killing is logarithmic rather than linear, the difference in survival between normal and tumor cells is increased

exponentially. Ideally it is preferable to deliver a radiation dose over as short a time as possible within the limits of acute radiation tolerance. Giving radiotherapy in several small doses at regular intervals during the day (multiple daily fractions) may help overcome tumor repopulation. Conversely excessive prolongation of radical external beam irradiation over 7 – 8 weeks may allow significant tumor reproduction [16,17,18].

1.7. Dose Risk and Rationality

It would not be overwhelming to mention here that in routine clinical radiotherapy practices, radiation doses can not be lowered to that level so that there would certainly be no acute radiation syndrome. However, adapting necessary arrangements during treatment plan, the radiation doses to the organs outside the treatment volume are ascertained at least theoretically to a minimum and justifiable level so that no unwanted radiation effect could happen. The special arrangements to do so, involves modification of the therapy beam according to the target volume in such a manner that organs at risk like: bone marrow, gonads, bladder, rectum, spine and GI tract etc. would be well spared from the radiation exposure while adequate and requisite dose with optimum uniformity could be delivered to the malignant tumor volume. For radiation protection, an upper limit must be established for permissible radiation exposures. This limit should be reflected as a risk that is acceptable to the exposed individuals and to the society in general, without depriving society of the benefits derived from judicious use of ionizing radiation. In addition, it should be recognized that dose should always be kept as low as reasonably achievable (ALARA) consistent with reasonable costs and convenience and without compromising the benefits of radiation to the society [4,19,20].

1.8. Rationality

Application of radiotherapy for management of malignant diseases is primarily aimed to provide curative radiation dose to the treatment volume. Adequate as well as homogeneous dose to the target volume is a pre requisite for curative treatment of malignant diseases. Patient's clinical dosimetry is done on the basis of standard isodose distribution data which are collected under ideal conditions of the radiation beam striking perpendicularly a flat surface of a homogeneous water phantom [4]. The standard isodose curves are drawn for equal increments of percentage depth dose (% DD of PDD). The curves represent the lines of equal depth dose (DD) for a particular field size and source to surface distance (SSD) at a specific plane in water. They are different for different beams, showing the effects of dose distribution due to energy, source size, SSD and beam attenuation etc. However, patients have surfaces, which are curved rather than flat and tissue inhomogenieties like bone and lung rather than homogeneous water phantom. In addition, the target or treatment volume is often irregular in shapes in contrary to the square or rectangular fields employed in standard dose distribution data collection [4]. Organs at risk also limits adequate dose application to the treatment volume. Individual planning is needed to optimize each treatment by selecting an irradiation technique, beam incidence, radiation quality, dose weight, field size and shape to guarantee a certain dose and dose homogeniety to each target volume under optimal sparing of organs at risk [21]. The aforesaid curvature type patient's surface, tissue inhomogeniety and irregular shaped treatment volumes etc are apparently the prevailing constraints in application of standard isodose data for calculation of patient's radiation dose in clinical situations. Radiotherapy without necessary corrections for those incompatibilities can not provide desired results. Dose required as well as dose tolerated is different for different target volumes depending primarily on the number of tissue cells, beam quality, dose distribution and dose application strategy (treatment planning) etc. Beam modifications according

to the target shape, tissue compensator for curvature type surface and target tissue density values are essentially desired to meet clinical dosimetry requirements for adequate and homogeneous dose applications to the treatment volume. Investigations of dose distribution pattern in irregular photon fields are assumed to be an important parameter, which could play a vital role in radiotherapy practices in individual therapy unit. This type of study has not yet been done in Bangladesh and perhaps not accounted with sufficient attention in routine radiotherapy practices in most of the radiotherapy establishments of Bangladesh. It is also true that, in clinical institutions and hospitals where accuracy and precision are not maintained within a narrow range, there can be a tendency to avoid normal tissue complications by lowering the prescribed dose. The consequence is a drastic decrease in the probability of tumour control [5]. The only acceptable solution is improvement of accuracy and precision so that the right doses can be prescribed and applied. This practice of prescribing lower doses than desirable can not be considered negligible for potential exposure or accident since the problem is associated with the prescription itself. Successful accomplishment of the present study is greatly expected to help the radiotherapy establishments of the country for delivering the required doses to the target volume with simultaneous sparing of healthy normal tissues and organs at risk at an optimum level.

1.9. Objective with Specific Aims of the Study

Dose measurements are usually carried out on phantoms having flat and regular surfaces. However, the human body curvature is not regular and also varies from person to person. Individual planning is, therefore, needed for each patient depending on the modality of treatment, selection of appropriate radiation exposure technique, beam quality, dose-weighting factor, field size and shape to guarantee a certain specified dose and dose homogeneity in the target volume. Dose distribution in the irregularly

shaped field will be studied in the present work [22]. This will help in proper delivery of dose to target volume at the same time sparing the surrounding normal tissues and organs at risk[23, 24] .The findings are expected to play a significant role in the treatment of cancer.

The main objective of the study are given below,

1. To investigate the open field dose rate of various points of solid phantom for some specific field sizes.
2. To use the "half-beam device" as one of the irregular field shaping device for the measurement of dose rates in various interested points for field size 16x17 cm^2 and 9x17 cm^2 and thus finding the effect of the device for cancer treatment.
3. To use various shaped blocks to make other irregular field-shaping device termed as two-cornered block, four-cornered block, three-cornered block etc. for investigating dose rates at various interested points.
4. To find out the percentage of deviation of doses between calculated value and measured value as well as to investigate the reasons of deviation.
5. To investigate the dose rates using tissue compensator for different field size (blocked) and thus finding the effect of tissue conpensator.

CHAPTER-2   Review

2.1. Introduction

As discussed before, the numbers of cancer patients all over the world and also in our country is not negligible. Radiotherapy is one of the treatment fields for cancer. Gamma rays from ^{60}Co-teletherapy unit are used in radiotherapy. We know phantoms are used for experimental works and to get minimum doses to normal tissues various blocks or irregular-field shaping devices are used. Some of the previous works that are relevant to the present study are being reviewed in the subsequent pages.

2.2. Review of the Previous Works

Radhe Mohan et al.[48] worked on "Use of fast Fourier transformations in calculating dose distributions for irregularly shaped field for three-dimensional treatment planning". In the method presented in this paper, dose distribution for arbitrarily shaped beams are calculated by two-dimensional convolution of the relative primary photon fluence distributions and kernels representing the cross-sectional profiles of a pencil beam at a series of depths. The pencil beam dose distributions are computed, once and for all, with the Monte Carlo method for photon energy spectrum for each treatment machine. The finite size of the source, which is important for cobalt machines, is also taken into account using convolution of the source with the relative primary fluence distribution. Convolutions are performed using fast Fourier transforms on array processor. Results of calculations are in excellent agreement with measured data.

Jun Lian et al.[49] worked on "Therapeutic treatment plan optimization with probability density-based dose prescription". The purpose of their work was

to develop a statistical analysis-based inverse planning formalism to more effectively utilize the prior knowledge. They presented the details of the new dose optimization algorithm after a brief introduction of the concept of preference function. The formalism was then applied to a synthetic phantom case with C-shaped tumour target and a prostate case. Their results indicated that the statistical analysis-based formalism provides a general framework for inverse planning and is capable of producing conformal IMRT (Intensity Modulated Radiation Therapy) dose distribution.

Dietmar Georg et al [50] worked on "Empirical methods to determine scatter factors for irregular MLC shaped beams". The purpose of this article was to compare different empirical methods, which had been proposed for independent MU verification, to determine (1) output ratios in air (S_c) and (2) phantom scatter factors (S_p) for irregular MLC (Multileaf collimators) shaped fields. Ten dedicated field shapes were applied to five different types of MLCs. All calculations based on empirical relations were compared with measurements and with calculations performed by a treatment planning system with a fluence based algorithm. For most irregular MLC shaped beams output ratios in air could be adequately modeled with an accuracy of about 1%-1.5% applying a method based on the open field aperture defined by the leaf and jaw setting combined with the equivalent square formula suggested by Vadash and Bjarngard [51]. The accuracy of this approach was strongly dependent on the inherent head scatter characteristics of the accelerator in use and on the irregular field under consideration.

M. G. Davis et. al [52] worked on "Use of simple quality assurance procedures in the analysis of beam asymmetries on Cobalt-60 treatment units". One critical part of that program was the weekly analysis of symmetry and flatness characteristics on all modalities of all linear accelerators. Measurements were made at depth (10 cm water equivalent) three times per month and at d_{max} once a month. These measurements were typically made using Kodak XV electron field. Flatness and symmetry were specified

along the major axes within the region contained by 80% of the full with at half –maximum of the central axis value. The quality assurance program for Cobalt-60 units includes output spot checks and light field vs. radiation field congruence checks, each of which were carried out on a weekly basis. Measurements of symmetry and flatness were also required for all Cobalt-60 units at the time the asymmetry was detected, but only on an annual basis. These checks were not done more often because it was assumed that beam symmetry and flatness characteristics for Cobalt-60 units were predictably uniform.

Michael K. Fix et. al [53] worked on "Simple beam models for Monte Carlo photon beam dose calculation in radiotherapy". In this work, photons and electrons were assumed to be radiated from point sources. Four different models were investigated which involved different ways to determine the energies and locations of beam particles in the output plane. Depth dose curves, profiles and relative output factor were calculated with these models for six field sizes from 5x5 to 40x40 cm^2 and compared to measurements. Model 1 uses a photon energy spectrum independent of location in the PS (phase space) plane and a constant photon fluence in this plane. Model 2 takes into account the spatial particle fluence distribution in the PS plane. A constant fluence is used again in model 3, but the photon energy spectrum depends upon the off axis position. Model 4, finally uses the spatial particle fluence distribution and off axis dependent photon energy spectra in the PS plane. Depth dose curves and profiles for field sizes up to 10x10 cm^2 were not model sensitive. Good agreement between measured and calculated depth dose curves and profiles for all field sizes was reached for model 4. However, increasing deviation were found for increasing field sizes for model 1 – 3. Large deviations resulted for the profiles of models 2 & 3. This was due to the fact that these models over estimate and under estimate the energy fluence at large off axis distances. Relative out put factors consistent with measurement resulted only for model 4.

T.B. Tiourina et al [54] worked on "Measurements and calculations of the absorbed dose distribution around a ^{60}Co source". In this work dose measurements had been performed in air and in water around a activity ^{60}Co source used in high dose rate brachitherapy. Measurements were carried out to distances of 20 cm, using ionization chambers. These data show that at a distance of about 15 cm the amount of scattered radiation virtually equals the amount of primary radiation. This emphasizes the contribution of scattered radiation to the dose in healthy tissue far from the target volume, even with relatively high energy photon radiation of ^{60}Co. In addition to these measurements, the Monte Carlo code had been used to calculate separately primary dose and scattered dose from a cobalt point source.

Chen-Show Chuy et. al [55] worked on "A simplified intensity modulated radiation therapy technique for the breast". In this paper, the above mentioned technique for the breast was presented. The technique aimed to produce a uniform dose distribution in the entire breast volume. Using the standard tangential beam arrangement, the authors first determined for each pencil beam the mid point of the segment that intersected the treatment volume. The dose to the mid point from the open field was then calculated. The intensity of the pencil beam was determined as proportional to the inverse of the open field dose with that intensity modulated beam, the dose delivered to the mid point of each pencil beam segment that intersected the treatment volume was now equalized. The dose distribution in the entire treatment volume was nearly as uniform as could be achieved under the given beam arrangement. Fifteen left breast patients were planed with the sIMRT technique. For comparison, the same group of patients was also planned with the standard wedged pair technique and the full-fledged volume based IMRT (vIMRT) technique. Both the sIMRT and vIMRT techniques achieved more homogeneous dose in the treatment volume then the standard plan. Doses to the heart, the ipsilateral lung, and the contralateral breast were also reduced. The planning time and the treatment

time for the sIMRT technique were comparable to that of the standard technique, and significantly less than that required by the vIMRT technique. The sIMRT technique is practical for large-scale implementation in a busy clinic with out requiring significant increase of resources.

2.3. Comment on the Present Study

An important work related to the present study was carried out by H. Rashid [54]. He, in his Ph.D. thesis reported results on investigation of doses in irregular photon fields. In this work the author investigated the doses for photon beam from ^{60}CO teletherapy unit and 6 MV photon beam from Linac-mevatron 7445, side by side using several irregular photon fields for the treatment.

The present work is really an extension of this work. The main difference between the two is that in the past one various irregular fields were used for the investigation of doses. But in the present work various irregular-devices were used for the investigation of dose distribution. In this case, some of the irregular field-shaping devices were made by placing some small blocks (which are routinely used in the work station for cancer treatment) in the shielding tray. Previously the irregular fields were made by fabrication of blocks. Another important point is noticeable such as in the dose calculation, Day's method was used in the former work, but in the present work, dose value was calculated using Clarkson's method.

CHAPTER-3   Interaction of Radiation with Matter

3.1 Cell Biology

All living creatures and organisms consist of tiny structures known as cells. The basic components of the cell are the nucleus, a surrounding liquid known as the cytoplasm and a membrane, which forms the cell wall. Fig 3.1 shows the structures of typical human cell.
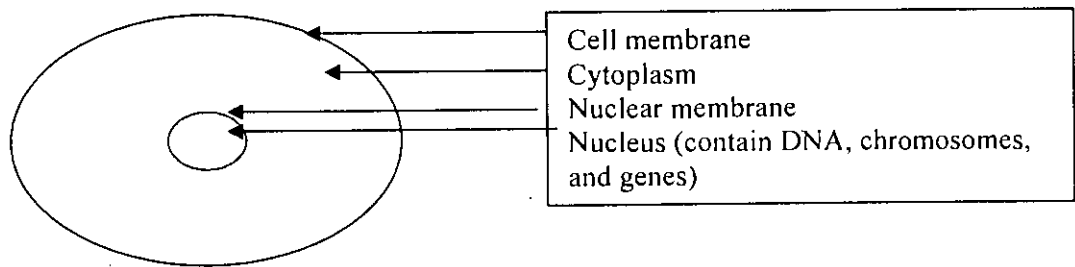
Fig. 3.1 The simplest picture of the cell

The simplest picture of the cell is that the cytoplasm is the factory of the cell while the nucleus contains all the information, which the cell needs to carry out its function and reproduce itself. The cytoplasm breaks down food and converts it into energy and small molecules. These small molecules are later converted into complex molecules needed by the cell either for maintenance or duplication.

The nucleus contains the chromosomes which are tiny threadlike structures made up of genes. A human cells normally contains 46 chromosomes. The genes consist of de-oxyribonucleic acid (DNA) and protein molecules and carry the information, which determines the characteristics of the daughter cell [25].

Cells are able to reproduce to compensate for cells, which die. The life of different types of human cell, and hence the rate of reproduction, varies from a few hours to many years. Reproduction of cells occurs in two ways, known as mitosis and meiosis.

3.2. The Interaction of Radiation with Cell

The basic difference between nuclear radiation and the more commonly encountered radiation such as heat and light is that the former has sufficient energy to cause ionization. In water, of which cells are largely composed, ionization can lead to molecular changes and to the formation of chemical species of a type which are damaging to the chromosome material [26,27]. The damage takes the form of changes in the construction and the function of the cell. In the human body, these changes may manifest themselves as clinical symptoms such as radiation sickness, cataracts, or in the longer term, cancer.

Most of the body is water, and most of the direct action of radiation therefore is on water. The result of this energy absorption by water is the production, in the water, of highly reactive free radicals that are chemically toxic and which may exert their toxicity on other molecules.

The processes leading to radiation damage are complex and are often considered in four stages:

(i) The initial physical stage, lasting only a minute fraction ($\sim 10^{-16}$) of a second in which energy is deposited in the cell and causes ionization. In water the process may be written as:

$$H_2O \xrightarrow{\text{radiation}} H_2O^+ + e^-$$

24
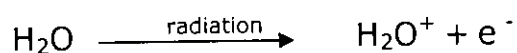
Where H_2O^+ is the positive ion and e^- is the negative ion.

(ii) The physico-chemical stage, lasting about 10^{-6} seconds in which the ions interact with other water molecules resulting in a number of new products. For example, the positive ion dissociates:

$$H_2O^+ \longrightarrow H^+ + OH$$

The negative ion, that is the electron, attaches to a neutral water molecule, which then dissociates:

$$H_2O + e^- \longrightarrow H_2O^-$$

$$H_2O^- \longrightarrow H + OH^-$$
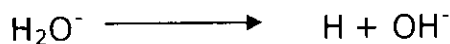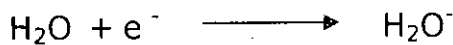
Thus the products of the reactions are H^+, OH^-, H and OH. The two former ions, which are present to quite a large extent in ordinary water, take no part in subsequent reactions. The other two products, H and OH, are called free radicals meaning that they have an unpaired electron and are chemically highly reactive. Another reaction product is hydrogen peroxide H_2O_2 which is a strong oxidizing agent:

$$HO + HO \longrightarrow H_2O_2$$

(iii) The chemical stage, lasting a few seconds in which the reaction products interact with the important organic molecules of the cell. The free radicals and oxidizing agents may attack the complex molecules, which form the chromosomes. They may, for example, attach themselves to molecules or cause links in long chain molecules to be broken.

(iv) The biological stage, in which the time scale varies from tens of minuets to tens of years depending on the particular symptoms. The chemical

changes can affect an individual cell in a number of ways. For example they may result in:

a) The early death of the cell,

b) The prevention or delay of cell division, or

c) A permanent modification, which is passed on to daughter cells.

3.3. Effects of Radiation on Human Body

The effects of radiation on the human body are the result of damage to the individual cells. These effects may be conveniently divided into two classes, namely somatic and hereditary. The somatic effects arise from damage to the ordinary cells of the body and affect only the irradiated person. The hereditary effects, on the other hand, are due to damage to the cells in the reproductive organs, the gonads. The important difference is that, in this case, the damage may be passed on to person's children and subsequently to later generations.

There are two basic categories of the biological effects that may be observed in irradiated person [2]. These are;
1) due largely to cell killing (deterministic)
2) mutations, which may result in cancer and hereditary effects (stochastic or probabilistic).

Effects due to cell killing (such as skin necrosis) have a practical threshold dose below which the effect is not evident but in general when the effect is present its severity increases with the radiation dose. The threshold doses are not an absolute number and vary from individual to individual. Effects due to mutations (such as cancer) have a probability of occurrence that increases with dose, it is currently judged that there is not a threshold below which the effect will not occur and finally the severity of the effects is

independent of the dose. Thus a cancer caused by a small amount of radiation can be just as malignant as one caused by a high dose.

3.4. Deterministic Effect

These effects are observed after large absorbed doses of radiation and are mainly a consequence of radiation induced cellular death. They occur only if a large proportion of cells in an irradiated tissue have been killed by radiation, and the loss can not be compensated by increased cellular proliferation. The ensuring tissue loss is further complicated by inflammatory processes and if the damage is sufficiently extensive, also by secondary phenomena at the systemic level (e.g. fever, dehydration, bacteraemia etc.). In addition, eventual effects of healing processes, e.g. fibrosis, may contribute to additional damage and loss of function of a tissue or an organ. Clinical examples of such effects are necrotic changes in skin, necrosis and fibrotic changes in internal organs, acute radiation sickness after whole body irradiation, cataract, and sterility (Table 3.1).

Table 3.1 Deterministic effects after whole-body and localized irradiation by X and gamma rays; approximate absorbed threshold doses for single (short-term) and fractionated or low dose-rate (long- term) exposures [2].

Organs/tissue	Effect	Threshold absorbed dose in Gy	
		Short-term exposure (single doses)	Long-term exposure (Yearly-repeated for many years)
Testicles	Temporal sterility Permanent sterility	0.15 3.5-6.0	0.4 2.0
Ovaries	Sterility	2.5-6.0	>0.2
	Detectable opacities Visual impairment (cataract)	0.5-2.0 5.0	>0.1 >0.15
Bone marrow	Haemopoiesis impairment	0.5	>0.4
Skin	Erythema (dry desquamation) Moist desquamation Epidermal and deep skin necrosis Skin atrophy with complications and telangiectasia	2 18 25 10-12	- - - 1.0
Whole body	Acute radiation Sickness(mild)	1.0	-

Doses required to produce deterministic changes are in most cases large (usually in excess of 1–2 Gy). Some of those occur in a small proportion of patients as side effects of radiotherapy. They can also be found after complex interventional investigations (such as vascular stenting) when long fluoroscopy times have been used.

The relationship between the frequency of a given deterministic effect and the absorbed dose has a general form presented in Fig.3.2. It can be seen that the essential feature of this dose-response relationship is the presence of a threshold dose. Below this dose no effect may be diagnosed but with increasing dose the intensity of the induced damage increases markedly, in

some situations, dramatically. An example of the deterministic damage to the skin is presented in Fig 3.3.
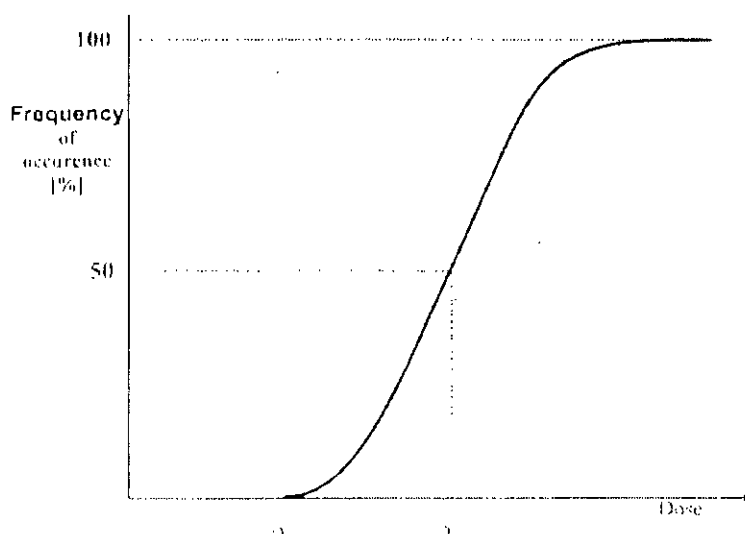
Fig. 3.2 A general dose response relationship for radiation induced deterministic (cell killing) effects. D_{Th} – Threshold dose
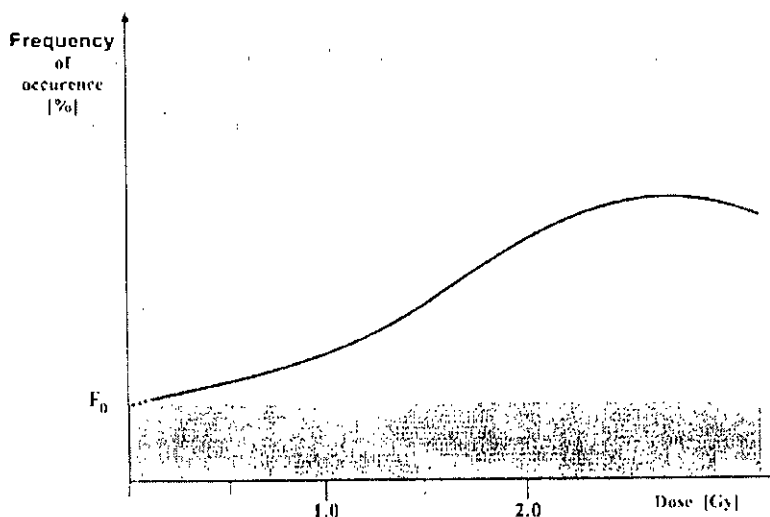

Fig. 3.3 A general dose response relationship for radiation induced stochastic effects (here cancer incidence may occur after gamma ray radiation)

Shaded area – controlled incidence (F_0) in a non-irradiated population
Broken line – extrapolation to the lowest doses for which there is no direct evidence.

Malformations induced by radiation in the conceptus in the period of organogenesis (3-8 week of pregnancy), are also due to cell killing and are classified as deterministic effects. The same applies to malformations of the forebrain - leading to mental retardation - induced by the exposure between 8 and 15 weeks (and to some extent up to 25 week) after conception. The threshold doses are however, substantially lower than those found for deterministic effects after irradiation in extrauterine life: thus, 100 – 200 mGy form a threshold-range for malformations induced between the 3rd and 8th week[2], and ~200 mGy for the aforementioned brain damage (8 – 25 week).

Stochastic Effects

As mentioned above, irradiated and surviving cells may become modified by induced mutations (somatic, hereditary). These modifications may lead to two clinically significant effects: malignant neoplasm's (cancer) and hereditary mutations.

Cancer

Ionizing radiation is a carcinogen although a relatively weak one. Careful follow-up of over 80,000 atom bomb survivors in Hiroshima and Nagasaki over the 50 years indicates that there have been 12,000 cancer cases of which less than 700 excess deaths were due to radiation. Expressed another way, only about 6% of the cancer occurring in these survivors is radiation-related.

These observations allow estimation of the probability with which a given dose may lead to diagnosis (incidence) and death (mortality) from various cancers. Among the latter there are several forms of leukemia and solid tumors of different organs, mostly carcinomas of the lung, thyroid, breast, skin and gastrointestinal tract. Radiation –induced cancers do not appear immediately after radiation exposure but require time to become clinically apparent (latent period). Examples of minimum latent periods are non-CLL

leukemia 2 years, about 5 years for thyroid and bone cancer and 10 years for most other cancers. Mean latent periods are 7 years for non-CCL leukemia and more than 20 years for most other cancers. It is important to note that some tumors do not appear to be radiation-induced or only weakly so. These include carcinomas of the prostate, cervices, uterus, lymphomas and chronic lymphatic leukemia.

Hereditary Effects

The risk of hereditary effects of ionizing radiation has been estimated on the basis of experiments on various animal species, because there are no demonstrated effects in humans.

From careful analysis of the experimental studies and epidemiological surveys it may be concluded that dose-response relationships for these two categories of stochastic effects have a distinctly different form from those characterizing deterministic sequelae. The principal features of dose-response relationship for cancer may be summarized as follows:

a. The induction of cancer by X or gamma rays yields increasing frequency of the effect with increasing dose up to a maximum.

b. Below ~ 100-200 mGy, any potential effect cannot be measured easily because statistical errors of the observations due to the large amount of spontaneous cancer and the impact of confounding factors. This should not be interpreted as the presence of a dose threshold. It is assumed that at the low doses (< 0.2 Gy), probability of the effect (frequency) increases most likely proportionally with the dose.

c. There is always a spontaneous frequency of the effect (mutations, cancer) in non-irradiated populations (F_0 in Fig. 2.3), which cannot be differentiated qualitatively from that induced by radiation. In fact, mutations or cancers induced by irradiation have the same morphological, biochemical and clinical etc. characteristics as the cases occurring in non-irradiated individuals.

31

In Table-3.2 the international commission of Radiological Protection (ICRP) [28] summarizes the probability of developing a fatal cancer as a result of irradiation. These data are representative for a population of equal numbers of men and women. The differences in gender are small except for the breast: the probability for women should be taken as 0.40% Sv^{-1} and for men as 0%Sv^{-1}.

Table 3.2 Nominal probability coefficients for individual tissues and organs [28]

Tissue or organ	Probability of induction of fatal cancer for the whole population (%Sv^{-1})
Bladder	0.30
Bone Marrow	0.50
Bone Surface	0.05
Breast	0.20
Colon	0.85
Liver	0.15
Lung	0.85
Esophagus	0.30
Ovary	0.10
Skin	0.02
Stomach	1.10
Thyroid	0.08
Remainder	0.50
Total	5.00

3.5. Dosimetric Aspect of Ionizing Radiation within Body

3.5.1. Introduction

The dominant mode of interaction of x-and gamma ray photons in a particular region of the body varies with the energy of the photons and with effective atomic number and electron density (electrons per kilogram) of the region. For purposes of dosimetry, the body may be divided into the following regions:

(1) Fat

(2) Muscles (or soft tissue excluding fat)

(3) Bone and

(4) Air-filled cavities.

The effective atomic number, average density and electron density are listed in Table-2.3 for these constituents of the body.

Table 3.3 Effective atomic number, physical density and electron density for air water and body constituents.

Material	Effective atomic no	Density (kg/cu m)	Electron density (electrons/kg)
Air	7.6	1.29	3.01×10^{26}
Water	7.4	1.00	3.34×10^{26}
Soft tissue	7.4	1.00	3.36×10^{26}
Fat	5.9-6.3	0.91	$(3.34-3.48) \times 10^{26}$
Bone	11.6-13.8	1.65-1.85	$(3.00-3.19) \times 10^{26}$

3.5.2. F-Factor

An exposure of 1R provides an absorbed dose of 0.876 rad in air:

$$D_{air} (rad) = 0.876(rad/R) \cdot X (R) \qquad \dots\dots (3.1)$$

The dose to a medium such as soft tissue is related to the dose in air at the same location by the ratio of energy absorption in the medium to energy absorption in air:

$$D_{med} = D_{air} \frac{[(\mu_{en})_m]_{med}}{[(\mu_{en})_m]_{air}} \qquad \dots\dots (3.2)$$

$$D_{med} = 0.876 \frac{[(\mu_{en})_m]_{med}}{[(\mu_{en})_m]_{air}} \qquad \dots\dots (3.3)$$

In equation (3.3), $[(\mu_{en})_m]_{med.}$ is the mass energy absorption coefficient in the medium for photons of the energy of interest. This coefficient describes the rate of energy absorption in the medium and $[(\mu_{en})_m]_{air}$ describes the rate of energy absorption in air. In equation (3.3), the expression may be simplified to

$$D_{med} = (f)(X) \qquad \dots\dots (3.4)$$

where
$$f = 0.869 \frac{[(\mu_{en})_m]_{med}}{[(\mu_{en})_m]_{air}} \qquad \dots\dots (3.5)$$

The expression denoted as f is known as the f-factor and varies with the nature of the absorbing medium and the energy of the radiation.
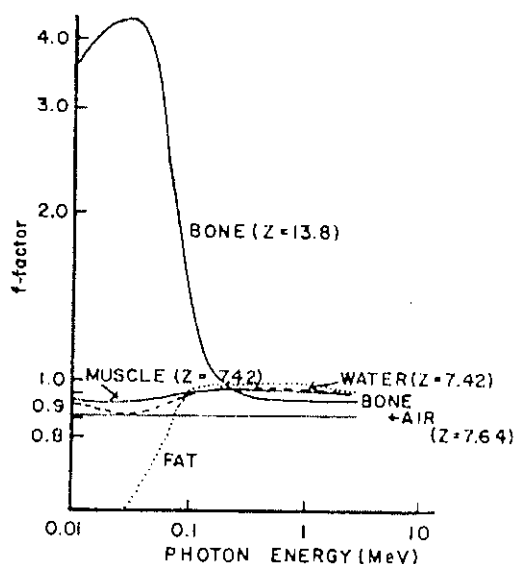
Fig. 3.4 The f-factor for conversion between roentgens and rads for air, water and different constituents of the body, plotted as a function of photon energy.

The f-factor is used to compute the absorbed dose D in rad in a medium receiving an exposure X in roentgens. The f-factor is plotted in Fig. 3.4 for air, water, fat, muscle and compact bone as a function of photon energy.

3.5.3. Attenuation of X and Gamma Rays in Fat

X- and gamma-ray photons with energy less than about 35 keV interact in soft tissue primarily by the photoelectric effect[29], with a probability for interaction that varies roughly as Z^3. Compared to muscle and bone, fat has a higher concentration by weight of hydrogen($\sim$11%) and carbon ($\sim$57%) and a lower concentration of nitrogen($\sim$1%), oxygen (30%) and high $-Z$ trace elements ($<$1%)[30]. Hence, the effective atomic number of fat (Z_{eff} = 5.9-6.3) is less than that for soft tissue (Z_{eff}=7.4) or bone (Z_{eff}=11.6-13.8), and low $-$energy photons are attenuated less rapidly in fat than in an equal mass of soft tissue or bone[30, 31] .The reduced attenuation in fat is reflected in a lower f-factor for photons of low energy in this body constituent (Fig.3.4).

35

X- or gamma-ray photons of higher energy interact primarily by Compton scattering, with a probability that varies with the electron density of the attenuating medium but not with the atomic number. The electron density of hydrogen is about twice that of other elements[29], because the nucleus of hydrogen contains no neutrons. Since more hydrogen is present in fat than in other body constituents, more Compton interaction occurs in fat than in mass of muscle or bone. For photons of intermediate energy, therefore, the f- factor for fat exceeds that for other body constituents.

The f factor cannot be defined rigorously for X- and gamma ray photons with energy greater than about 3 MeV, because the roentgen is not applicable to photons of higher energy. Consequently, f factors in Fig .3.3 are plotted to only 3 MeV. The attenuation of X- and gamma ray photons in fat may be estimated from attenuation measurements in mineral oil or polyethylene, because the effective atomic numbers, densities and electron densities of these materials are close to those for fat[29] .

3.5.4. Attenuation of X and Gamma Rays in soft Tissue

The effective atomic number and density of body fluids and soft tissues, excluding fat, are almost identical to those for water, because soft tissue is roughly 75% water and body fluids are 85 – 100% water. Soft tissue often is simulated by a water filled phantom or by Plexiglas, Mix-D or pressed wood (e.g., Masonite).

Hydrogen is absent from air, but contributes about 10% of the weight of muscle. Consequently, the electron density is greater for muscle than for air, and the f-factor for muscle exceeds that for air (Fig.3.4).

3.5.5. Attenuation of X and Gamma Rays in Bone

The effective atomic number and physical density (kg/cu m) are greater for bone than for soft tissue, hence, X-and gamma ray photons attenuated more rapidly in bone than in an equal volume (not necessarily mass) of soft tissue, and the absorbed dose is reduced to structures beyond bone. On the other hand, the absorbed dose to soft tissue adjacent to or enclosed within bone may be increased by photoelectrons liberated as photons interact with high-Z atoms (e.g., atoms of phosphorus and calcium) in bone.

3.5.6. Dose to Soft Tissue Near an Interface between Soft Tissue and Bone

Under conditions of electron equilibrium, the absorbed dose D in rad to compact bone is

$$D=(f)(X) \qquad \text{...... (3.6)}$$

Here X is the exposure in roentgens and f is the f-factor for the bone exposed to photons of a particular energy (Fig. 3.4). To compute the absorbed dose to soft tissue beyond the range of electrons escaping from bone, the f-factor for soft tissue is used in equation (3.8). The absorbed dose to soft tissue near bone is less than the absorbed dose in bone but greater than the absorbed dose in soft tissue beyond the range of electrons from bone. In tissue irradiated by diagnostic or orthovoltage X rays, the region of increased dose to soft tissue extends over a distance of 100μ or less from an interface between soft tissue and bone. These transition zones of increased doses are illustrated in Figs. 3.5 to 3.7 for X-ray beams of different qualities.
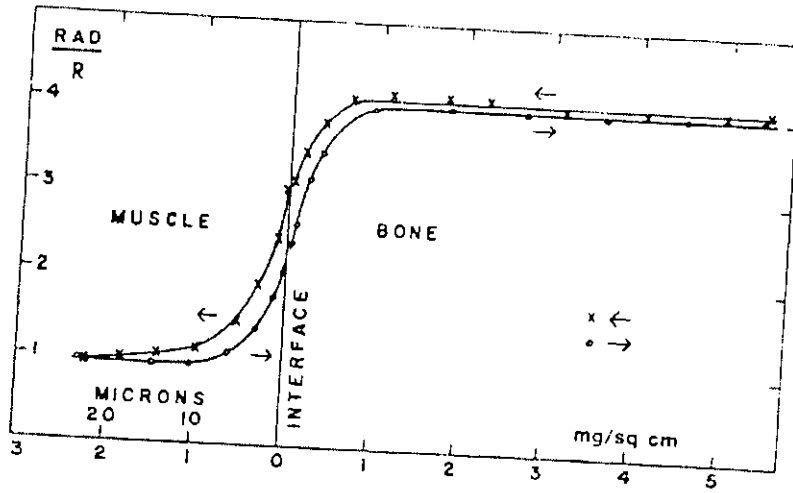
Fig. 3.5 The f-factor (rad/R) for 50 -kV$_p$, 0. 08 mm Cu HVL X-rays near an interface between soft tissue and bone. Arrows indicate the direction of the X-ray beam.
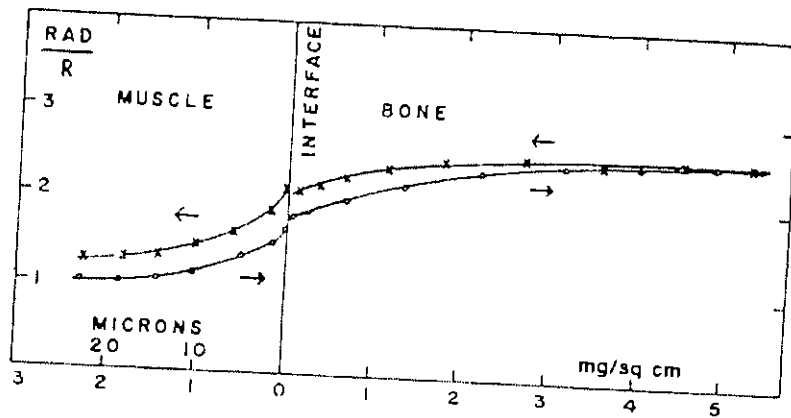
Fig.3.6 The f-factor (rad/R) for 140 -kV$_p$, 0.7 mm Cu HVL X-rays near an interface between soft tissue and bone. Arrows indicate the direction of the X- ray beam.
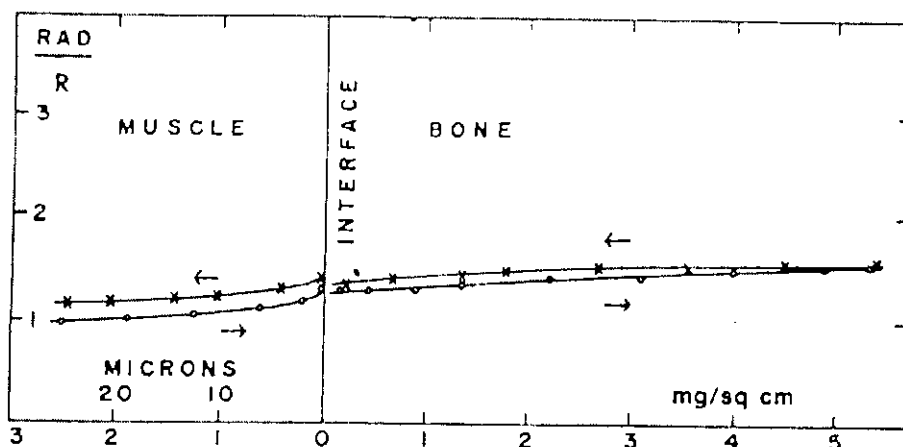
Fig.3.7 The f-factor (rad/R) for 210 –kVp, 2.1 mm Cu HVL X-rays near an interface between soft tissue and bone. Arrows indicate the direction of the X ray beam.

The radiation dose delivered to soft tissue near an interface between soft tissue and bone may be computed with an f-factor intermediate between those for soft tissue and bone. The f-factor for photons of different energies are plotted in Fig. 3.8 as a function of the distance from the interface.
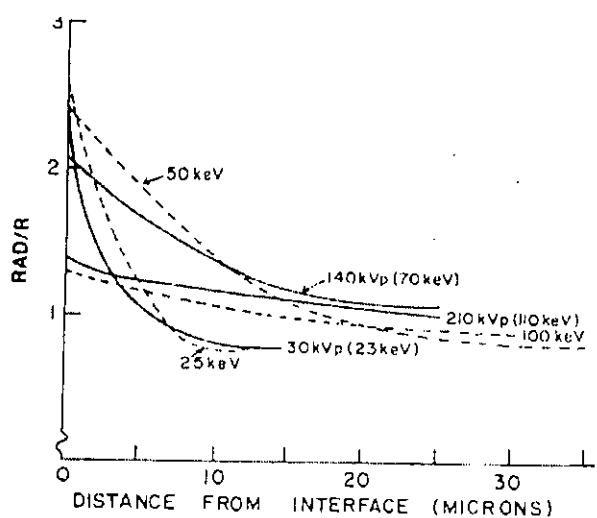
Fig.3.8 Calculated and measured f-factors as a function of the distance in soft tissue from an interface between soft tissue and bone.

3.5.7. Dose to Soft Tissue within Bone

Soft tissue that occupies cavities within bone includes the soft tissue components of Haversian system. These components include osteocytes about 5μ in diameter, connective tissue along the walls of Haversian canals, and blood vessels in the walls of the canals. Haversian canals vary from 50 to 100μ in diameter. In trabecular bone, spaces occupied by bone marrow are relatively large, averaging about 400μ across.

The absorbed dose in small (diameter< 1μ) inclusions of soft tissue within compact bone is close to that computed with equation (3.8) and an f-factor for bone. The dose to larger (diameter> 1μ) soft tissue inclusions is less than that estimated with equation (3.8) and an f-factor for bone. In larger inclusion, the absorbed dose varies from a maximum at the bone tissue interface to a minimum at the center of the inclusion (Fig. 3.9).
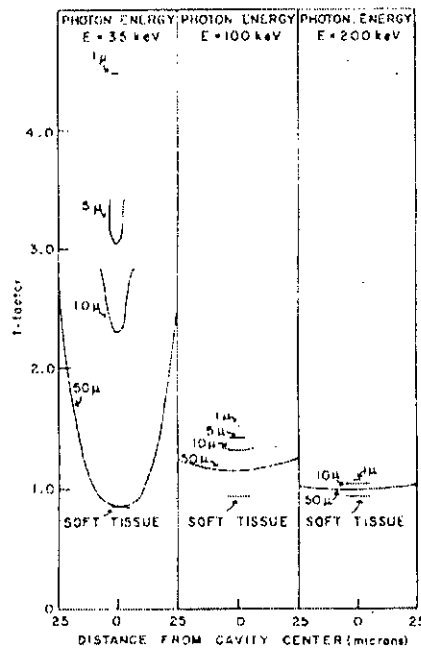
Fig. 3.9 The f-factor for photons of various energies, as a function of the distance from the center of cavities of different sizes. A layer of bone around cavity provides electron equilibrium.

The absorbed dose across these larger inclusions is difficult to determine. Average f-factors in Table-3.4 were computed by Spiers [33] for osteocytes, for typical soft tissue inclusion excluding bone marrow and for the soft tissue lining of a typical Haversian canal. The average f-factors are highest for osteocytes because these components occupy very small cavities. Haversian canal, on the average are much smaller than spaces in trabecular bone that contain bone marrow, and the average dose to bone marrow usually is not much greater than that delivered to soft tissue in the absence of bone. The increase in average absorbed dose in bone marrow spaces of different sizes is plotted in Fig.3.10 as a function of the energy of incident photons. For marrow cavities of all sizes, the increase in dose is less than 50% of the dose to soft tissue without bone.
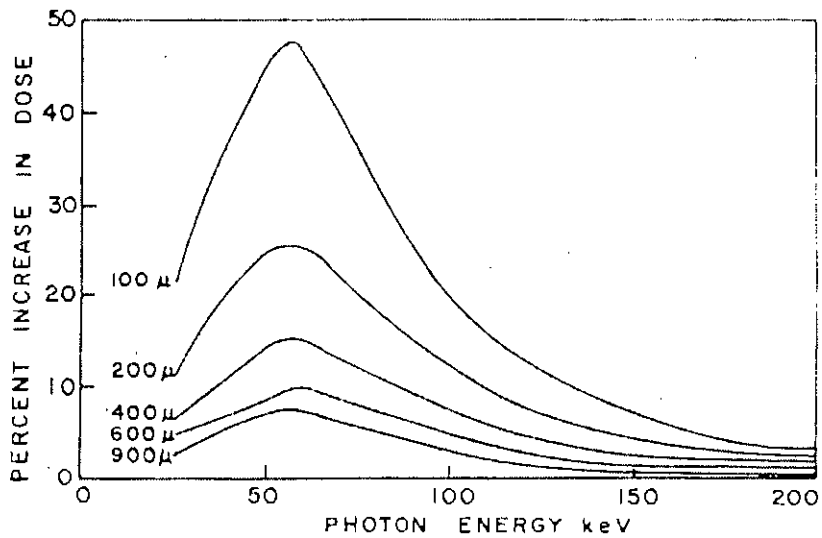
Fig. 3.10 Percent increase in average absorbed dose to bone marrow cavities, averaged over cavities of various sizes.

Table 3.4 Average f-factors for inclusions of soft tissue in bone[32]

Photons Energy (keV)	Osteocyte 5 μ diameter	Typical soft tissue in bone	10 μ lining of 50 μ Haversian canal
25	2.80	1.73	1.50
35	3.12	2.05	1.76
50	3.25	2.27	1.89
75	2.40	1.85	1.60
100	1.52	1.36	1.26
200	1.05	1.03	1.02

The probability of pair production increases, with the atomic number of the attenuating medium. Consequently, the dose delivered by high-energy photons is greater in bone than in soft tissue. For example, the dose delivered by 10-MeV photons is about 15% greater in bone than in soft tissue receiving an identical exposure. Electrons released during pair production interactions have an average range of about 2-3 cm in soft tissue and more than 1 cm in bone. For a thickness of bone less than that required for electron equilibrium, it is difficult to estimate the dose to bone and to soft tissue inclusions within bone.

3.5.8. Dose to Soft Tissue beyond Bone

The dose delivered to soft tissue by X- or gamma-ray is reduced by bone interposed between the soft tissue and the surface. The reduction in absorbed dose to soft tissue in influenced by:

a) The increased attenuation of primary photons in bone caused by the higher atomic number and density of this constituent of tissue.

b) Changes in the amount of radiation scattered to soft tissue beyond the location of bone. The changes depend upon many factors, including field size, quality of radiation and the distance between the bone and the soft tissue of interest.

Low energy X- or γ-ray photons are attenuated primarily by photoelectric interactions, and the attenuation of these photons is much greater in bone than in an equal mass of soft tissue or fat. For photons of higher energy, Compton scattering replaces photoelectric absorption as the dominant interaction. The probability for Compton interaction depends on the electron density of the attenuating medium, but not on its atomic number. The electron density is slightly less for bone than for soft tissue or fat, and the energy absorbed per gram of bone is slightly less than the energy absorbed per gram of muscle or fat exposed to photons of intermediate energy. However, the physical density (kg/cum) of compact bone is almost twice the density of fat or muscle. Therefore, the energy absorbed per unit volume of compact bone is almost twice that absorbed in an equal volume of fat or muscle exposed to an identical number of X- or γ-ray photons of intermediate energy.

The effect of bones to the radiation exposure and absorbed dose at various depths within a patient exposed to diagnostic or orthovoltage X-rays is illustrated in Fig.3.11. The radiation exposure, which always is measured in a small volume of air, is reduced at locations B, C and D by bone interposed between the locations and the surface. The reduction in exposure at these locations reflects primarily the increased attenuation of photons in overlying bone, the dose absorbed in bone is increased at A, B, and C, because the attenuation of diagnostic or orthovoltage X rays increases with the atomic number of the attenuating medium. The absorbed dose is reducing to soft tissue beyond bone because greater number photons are removed from the beam, by the overlying bone.
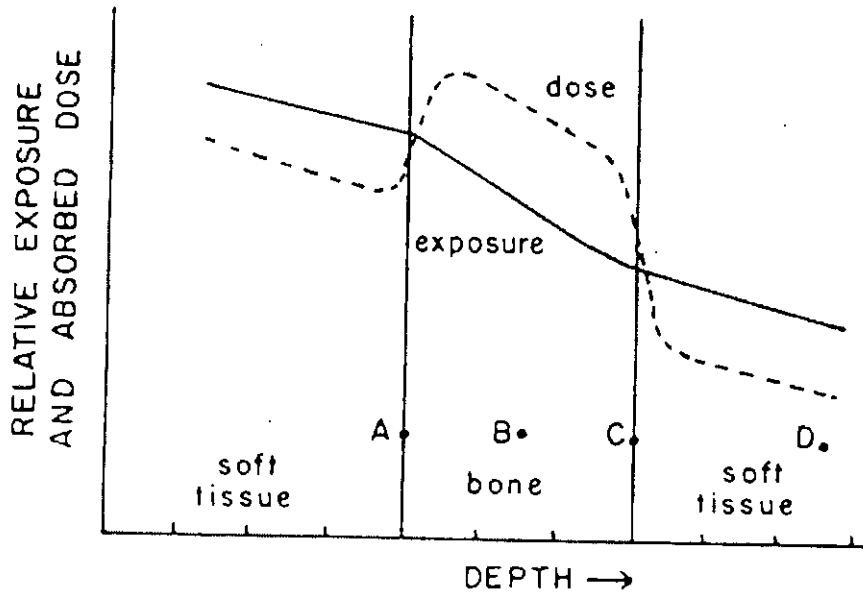
Fig. 3.11 Radiation exposure and absorbed dose plotted as a function of depth in soft tissue containing bone.

3.6. Measurement of Absorbed Dose

3.6.1. Radiation Absorbed Dose:

The current definition of absorbed dose or simply dose, is the quotient $d\dot{\varepsilon}/dm$, where $d\dot{\varepsilon}$ is the mean energy imparted by ionizing radiation to material of mass dm. The old unit of dose is rad (radiation absorbed dose) and represents the absorption of 100 ergs of energy per gm of absorbing material.

$$1 \text{ rad} = 100 \text{ ergs/g} = 10^{-2} \text{ J/kg}$$

The SI unit for absorbed dose is the gray; and rad is

$$1 \text{ Gy} = 100 \text{ rad}$$

or $\quad 1 \text{ rad} = 10^{-2} \text{ Gy}$

Since gray is a larger unit than rad, there is a practical problem in switching from rad to grays. For instance, if a patient receives treatments of 175 rad/day, the dose will have to be racorded as 1.75 grays. A subunit, centri gray (cGy), has often been used as being equivalent to rad.

3.6.2. Relationship between Kerma, Exposure and Absorbed Dose

a) **Kerma :** The quantity Kerma (K)(kinetic energy released in the medium) is defined as " the quotient of dE_{tr} by dm, where dE_{tr} is the sum of the initial kinetic energies of all the charged ionizing particles(electrons and positrons) liberated by uncharged particles(photons) in a material of mass dm"

$$K = dE_{tr} / dm \qquad \text{.................. (3.7)}$$

The unit for kerma is the same as for dose, i.e., J/kg. The name of its SI unit is gray (Gy) and its special unit is rad.

For a photon beam traversing a medium, kerma at a point directly proportional to the photon energy fluence Ψ and is given by

$$K = \Psi(\overline{\mu_{tr}}/\rho)$$

where $\overline{\mu_{tr}}/\rho$ is the mass energy transfer coefficient for the medium averaged over the energy fluence spectrum of photons.

Kerma can be divided into two parts:

$$K = K^{col} + K^{rad}$$

where K^{col} and K^{rad} are the collision and the radiation parts of Kerma, respectively.

b) Exposure and Kerma

The quantity exposure is defined as dQ/dm where dQ is the total charge of the ions of one sign produced in air when all the electrons (negatrons and positrons) liberated by photons in (dry) air of mass dm are completely stopped in air. Exposure is the ionization equivalent of the collision kerma in air. It can be calculated from K^{col} by knowing the ionization charge produced per unit energy deposited by photons. The mean energy required to produce an ion pair in dry air is almost constant for all electron energies and has a value of $\overline{W}$ = 33.97 eV/ ion pair. If e is the electronic charge (=1.602 x 10^{-19} C), then $\overline{W}$/e is the average energy required per unit charge of ionization produced. Since 1eV=1.602 x 10^{-19} J, $\overline{W}$/e=33.97 J/C. Exposure (X) is given by

$$X = (K^{col})_{air.}(e/\overline{W})$$

The SI unit for exposure is C/kg and the special unit is roentgen (1R= 2.58x10^{-4}C/kg).

Determination of absorbed dose from exposure is readily accomplished under conditions of electron equilibrium. However, for energies in the megavoltage range, the electron fluence producing absorbed dose at a point is characteristics of photon energy fluence some distance upstream. Consequently, there may be appreciable photon attenuation in the distance. The calculation of absorbed dose from exposure when rigorous electronic equilibrium does not exist is much more difficult, requiring energy-dependent corrections. Therefore, the determination of exposure and its conversion to absorbed dose is practically limited to photon energies up to ^{60}Co.

In the presence of charged particle equilibrium (CPE), dose at a point in any medium is equal to the collision part of kerma. Dose to air (D_{air}) under these conditions is given by

$$D_{air} = (K^{col})_{\overline{air}} = X.W/e \qquad \text{.............. (3.8)}$$

Inserting units
$$D_{air}(J/kg) = X(R).2.58 \times 10^{-4}(C/kg).33.97(J/C) = 0.876 \times 10^{-2} J/kg/R).X \ (R)$$

Since
1 rad = 10^{-2} J/kg,

$$D_{air}(rad) = 0.876(rad/R).X(R) \qquad \text{.................. (3.9)}$$

From the above equation it is seen that the roentgen-to-rad conversion factor for air, under the conditions of electronic equilibrium, is 0.876.

3.6.3. Environmental Conditions

If the ion chamber is not sealed, its response is affected by air temperature and pressure. In fact, most chambers are unsealed and communicate to the outside atmosphere. Since the density of air depends on the temperature and pressure, in accordance with the gas laws, the density of air in the chamber volume will likewise depend on these atmospheric conditions. The density or the mass of air in the chamber volume will increase as the temperature decreases or pressure increases. Since exposure is given by the ionization charge collected per unit mass of air, the chamber reading for a given exposure will increase as the temperature decreases or as the pressure increases.

Standard laboratory calibrates chambers under the conditions present at the time of calibration. This factor is then converted to specific atmospheric conditions, namely, 760 mm Hg pressure and 22^0 temperature. The correction $C_{T.P}$ for conditions other than the above reference conditions can be calculated.

$$C_{T.P} = (760/P) \times \{(273+t)/295\} \quad\text{..............................(3.10)}$$

where P is the pressure in millimeters of mercury and t is temperature in degree Celsius. The second bracketed term gives the ratio of temperature t to the reference temperature (22^0), both converted to the absolute scale of temperature (in degree Kelvin) by adding 273 to the Celsius temperatures.

3.7. Exposure Measurement Technique

Exposure can be measured in roentgen with either a thimble or a Farmer type ionization chamber connected with appropriate electrometer. A Farmer type chamber is usually assumed to provide more stable and reliable dosimetric performances. However, each of them must have an exposure calibration factor N_c (say) that is traceable to primary standard dosimetry laboratory (PSDL) for a given quality of radiation. The chamber is to be placed at the desired point of measurement with its axis perpendicular to the radiation beam axis as well as the same geometry as used during chamber calibration configuration as shown in Fig. 3.12.
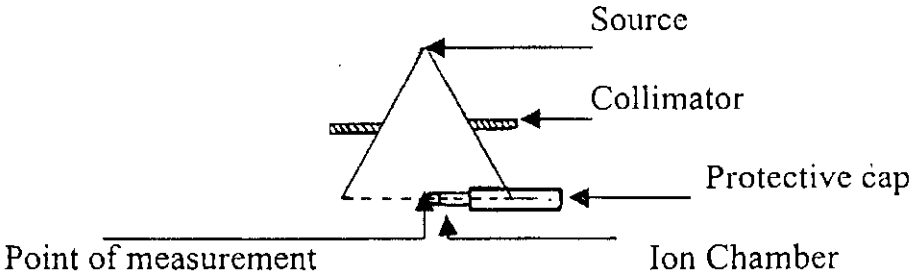
Fig.3.12 Geometry of exposure measurement with an ion chamber

48

For measurement in air, the effective point of measurement is usually specified to be the center of the chamber cavity for cylindrical or thimble shaped chambers. After the application of the calibration factor, the dosimeters reading will give the value of air kerma at a point in air corresponding to the center of the chamber, with the chamber replaced by air[39,40,41] .Necessary precautions are to be taken to avoid media, other than air, in the vicinity of the chamber, which might scatter radiation. Suppose for a given exposure, the electrometer reading is M. This exposure reading can be converted to roentgen as follows:

$$X = M.N_c.C_{T.P}.C_s.C_{st} \ldots\ldots\ldots\ldots\ldots\ldots 3.11$$

where $C_{T.P}$ is the correction for temperature and pressure, C_s is the correction for loss of ionization as a result of recombination, and C_{st} is the correction for stem leakage. The quantity obtained from the above expression is the exposure that would be expected in free air at the point of measurement in absentee of the chamber. In other words, the correction for any perturbation produced in the beam by the chamber is inherent in the chamber calibration factor N_c . For low-energy radiation such as applied in the superficial or orthovoltage range, no built up cap is required with the assumption that at this energy range, the chamber's wall thickness would be sufficient to provide necessary electronic equilibrium and also at this energy range, the chambers are usually calibrated without build up caps under the aforesaid assumption. However, for higher energies such as [60]Co(Cobalt-60), a build-up cap of lucite or other suitable material is to be used unless the chamber wall is already thick enough to provide electronic equilibrium. In either case, the correction to zero wall thickness is inherent in the chamber calibration factor N_c. It should be noted that no chamber should be used for measurement purpose unless its characteristics have not been clearly evaluated and found acceptable[42]. The transfer of energy from a photon beam to the medium takes place in two stages. The 1st stage involves the interaction of photon with an atom, causing an electron or

electrons to be set in motion. The 2nd stage involves the transfer of energy from the high-energy electron to the medium through excitation and ionization.

3.8. Scattering Effects in Radiotherapy Practices

The exposure at the surface of a phantom or any medium other than air is substantially greater than the exposure at the same point if no phantom or medium were present. Therefore, phantom or other media material is responsible for scattering of radiation back to the surface and this contribution is known as back scattering effect. The contribution due to back scatter at the point where the beam axis enters the phantom or other medium is expressed as percentage of the contribution due to primary radiation and is termed as percentage back scatter. This percentage backscatter increases with the area of the field irradiated and with the thickness of the underlying tissues . The amount of back scatter is larger for comparatively low energy photon beam and decreases with increasing beam energy [43].

3.9. Dose Build Up

At megavoltage energies, the scattered radiation is more in the forward direction and gives rise to less scattered radiation outside the edges of the beam. This effect is evidenced in the isodose charts of orthovoltage and megavoltage photon beams. Analysis of Compton scattering also shows that the recoil electron is ejected more and more in the forward direction with increasing kinetic energy. The range of recoil electron in orthovoltage is extremely small but in the case of megavoltage, the range of recoil electron is considerable and thus there is an initial build up of dose which becomes more and more pronounced as the energy is increased. In the case of

orthovoltage or low energy x-rays, the dose builds up to a maximum on or very close to the surface. But for higher-energy beams, the point of maximum dose lies deeper into the tissue or phantom. The region between the surface and the point of maximum dose is called the dose build up region. A simple explanation of this effect is that excessive thin layer of tissue produces fast electrons, which in turn deposits their energy in several layers of tissue beyond their point of origin. Although kerma in these layers is constant, the energy deposited in each layer (absorbed) depends on the number of electrons passing through the layer, and the number increases as each layer adds electrons to the electron flux from the preceeding layers. This increase continues until the electrons released only replaced those, which have come to the end of their range. The dose build up thus reaches a maximum at a depth determined by the range of the electrons and therefore by the energy of the photon beam. In practice, the kerma is not quite constant but falls as the primary radiation undergoes absorption and attenuation, with the result that the depth of the dose maximum is slightly less than the maximum range of the secondary electrons. The depth of the peak in centimeters is approximately a quarter of the x-ray energy in megavolts (2 cm at 8 MV etc.), ^{60}Co being approximately equivalent to 2 MV x-rays, has a peak approximately 0.5 cm [43,44,45]. Higher energy beams have greater penetrating power and thus deliver a higher percentage depth dose. If the effects of inverse square law and scattering are not considered, the percentage depth dose variation with depth is governed approximately by exponential attenuation. Thus the beam quality affects the percentage depth dose by virtue of the average attenuation coefficient, μ which when decreases, the more penetrating the beam becomes, resulting in a higher percentage depth dose at any given depth beyond the build up region.

3.10. Skin Sparing Advantages

For megavoltage beam such as ^{60}Co and higher energies the surface dose is much smaller than the dose at the depth of the d_{max}. The dose build up effect of the high energy beam is clinically known as the skin sparing effect and offers a distinctive advantage over the lower energy beams for which the d_{max} occurs at the skin surface. Thus, with high-energy (megavoltage) photon beams, higher doses can be delivered to deep-seated tumour without exceeding the tolerance of the skin. This, of course, is possible because of both the higher percent depth dose at the tumour and the lower surface dose at the skin[46]. A simple explanation of this is that as the high-energy photons enter a patient or phantom, they set electrons into motion, primarily through Compton interactions. In such interactions, the motion of the Compton electrons is predominantly in the forward direction so there is a net flow of electrons deeper into the patient. The concurrent slowing of these electrons deposits energy in the patient. Therefore, the dose begins to rise as the electrons slow down and deposit their energy. Thus, a depth related to the average distance that the Compton electrons travel is spared some of the dose of the incoming beam [47].

CHAPTER – 4   Radiotherapy Technique for Cancer Treatment

4.1. Treatment Volume Concept in Radiotherapy

Determination of treatment volume plays vital role in radiotherapy treatment in regards to complete irradiation of the malignant cells. A target volume consists of the demonstrable tumour(s), if present and any other tissue with presumed tumour is to be determined as 1st step for commencing radiotherapy treatment. This is the volume which needs to be irradiated to a specified or prescribed absorbed dose with optimum uniformity. In delineating the target volume, comprehensive attention must be paid to consider the local invasive capacity of the malignant tumour and its potential spread to the regional lymph nodes. Therefore, determination of target volume is a crucial one, which should include sufficient margins around the tumour to allow for the uncertainty in anatomic location of this volume. Further to this, additional margins must be provided around the above mentioned target volume to allow for limitations of the treatment technique (Fig.4.1). Thus, the minimum target dose should be represented by an isodose surface which adequately covers the target volume in order to provide that margin. The volume enclosed by this isodose surface is called the treatment volume. This treatment volume is, in general, larger than the target volume and depends on particular treatment technique and concerned target.
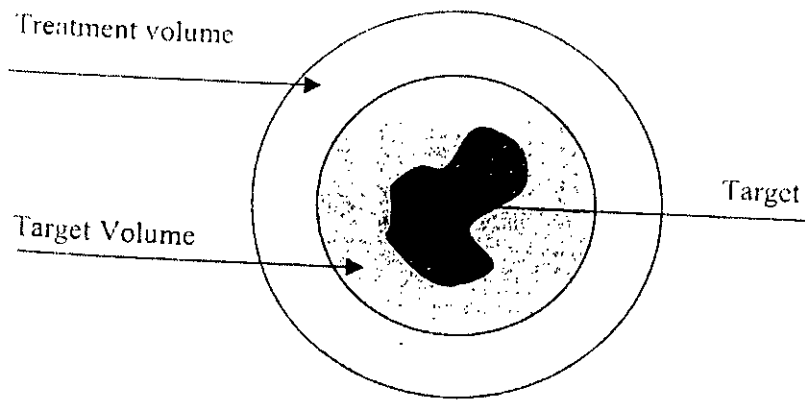
Fig. 4.1 Target, target volume and treatment volume

4.2. Tissue Missing

The standard dose distribution data are collected under an ideal condition using a homogeneous phantom with flat surface on which the beam is incident. However, in clinical practice, very often this is not the case. The patients body contour is not flat but rather have curvature which results in variation of SSD on the body contour. An increase or decrease of the SSD (source to surface distance) at the central axis results in changes in

a) Field size at the surface
b) % DD at depth below the skin and
c) Maximum dose rate at a certain depth dose below skin [11].

Under such conditions necessary corrections regarding SSD, %DD and given dose rate (maximum tissue dose rate) etc are needed for dose calculation. The off-axis %DD data are normally obtained from an isodose chart that assumes a flat incidence surface. If the surface is not a flat one (which is very often true in clinical conditions), rather an irregular one having air gaps with respect to the maximum tissue depth, then the %DD obtained from the isodose chart should be corrected for this air gap which is termed as

correction for tissue missing in radiotherapy practices. Therefore, the higher the tissue missing, the lower the photon beam attenuation or the increase in dose, resulting more variation of % of DD in areas other than maximum tissue depth. This decrease in attenuation or increase in dose, for various energies was evaluated and observed for ^{60}Co and 6 MV photon beams. The averaged values of these dose increments per cm of air gap or tissue missing for field sizes varying from 10x10 to 20x20 cm and depths approximately 10 cm are about 5% and 3.5% respectively.

4.2.1. Tissue Compensator

The missing tissue resulting from the beam incident on an irregular or sloping surface changes the desired uniform dose distribution pattern in the target volume. The degree of heterogeneity varies with the amount of missing tissue along incident beam. In certain clinical situations, surface irregularity gives rise to unacceptable dose heterogeneity in the target volume or causes excessive irradiation of sensitive structures such as spinal cord. Many techniques are in use to overcome this problem, including the use of wedged fields, multiple fields and the addition of bolus material or compensators. Bolus is a tissue equivalent material placed directly on the skin with a view to fill up the air gap (the region having missing tissue) and thus to even out the irregular contours of a patient to present a flat surface normal to the beam so that one is treating a surface as if there is no missing tissue present. Placing bolous directly on the skin surface is satisfactory for treatment with low energy orthovoltage radiation, but for high-energy megavoltage beams, this bolus technique results in the loss of its inherent skin sparing advantage. For such radiations, a compensating filter is used, which approximates the effect of the bolus as well as preserves the skin-sparing effect. Therefore, a compensator is simply an absorber inserted into the radiation beam. The thickness of the compensator at different points of the beam is such that it will attenuate the primary radiation just enough to

compensate the increase in dose due to the missing tissue at that point. To preserve the skin-sparing properties of the megavoltage beams, the position of the compensator should be such that electron contamination from it is minimal. For ^{60}Co and other megavoltage radiation beams, the compensator should be placed at a suitable distance usually 15-20 cm away from the patient's skin [42].

4.3. Dose Calculation Parameters

The dose to a point in a medium may be analyzed into primary and scattered components. The primary dose is contributed by the initial or original photons emitted from the source and the scattered dose is the result of the scattered photons. The scattered dose can be further analyzed into collimator and phantom components, since the two can be varied by blocking. For example, blocking a portion of the field does not significantly change the output or exposure in the open portion of the beam but may substantially reduce the phantom scatter. The above analysis presents one practical difficulty, namely, the determination of primary dose in a phantom, which excludes both the collimator and phantom scatter. However, for megavoltage photon beams, it is reasonably accurate to consider collimator scatter as part of the primary beam so that the phantom scatter could be calculated separately.

We therefore, define an effective primary dose as the dose due to the primary photons as well as those scattered from the collimating system. The effective primary dose in a phantom may be thought of as the dose at depth minus the phantom scatter. Alternatively, the effective primary dose may be defined as the depth dose expected in the field when scattering volume is reduced to zero while keeping the collimator opening constant.

4.3.1. Collimator Scatter Factor

The beam output measured in air depends on the field size. As the field size is increased, the output increases because of the increased collimator scatter, which is added to the primary beam. The collimator scatter factor (S_c) is commonly called the output factor and may be defined as the ratio of the output in air for a given field to that for a reference field (10x10 cm). S_c may be measured with an ion chamber with a build –up cap of a size large enough to provide maximum dose buildup for the given energy beam.

4.3.2. Phantom Scatter Factor

The phantom scatter factor (S_p) takes into account the change in scatter radiation originating in the phantom at a reference depth as the field size is changed. S_p may be defined as the ratio of the dose rate for a given field at a reference depth (e.g., depth of maximum dose) to the dose rate at the same depth for a reference field size (e.g., 10x10 cm), with the same collimator opening. For photon beam for which the backscatter factors can be accurately measured (e.g., ^{60}Co and 4 MV), S_p at the depth of maximum dose may be defined simply as the ratio of backscatter factor (BSF) for the given field to that for the reference field. Mathematically,

$$S_p (r) = BSF(r) / BSF(r_0) \qquad \text{..............(4.1)}$$

where r_0 is the side of the reference field size (10x10 cm).

4.3.3. Tissue-Phantom and Tissue-Maximum Ratio

Tissue-Phantom Ratio (TPR) is defined as the ratio of the dose at a given point in phantom to the dose at the same point at a fixed reference depth, usually 5 cm. This is illustrated in Fig 4.2. The corresponding quantity for the scattered dose calculation is called the scatter-phantom ratio (SPR).
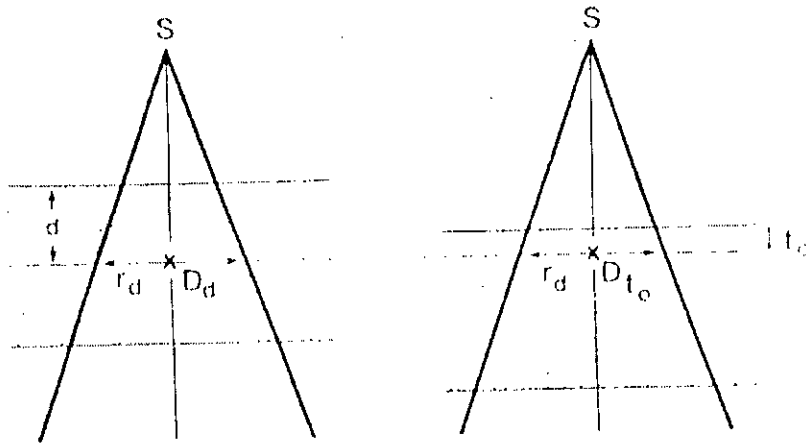
Fig.4.2 Diagram illustrating the definitions of tissue-phantom ratio (TPR) and tissue-maximum ratio (TMR). TPR(d,r_d)=D_d/D_{t0}, where t_0 is a reference depth. If t_0 is the reference depth of maximum dose, then TMR(d,r_d) = TPR(d,r_d).

The point of central axis D_{max} has a simplicity that is very desirable in dose computations. If adopted as a fixed reference depth, the quantity TPR gives rise to the TMR. Thus TMR is a special case of TPR and may be defined as the ratio of the dose at a given point in phantom to the dose at the same point at the reference depth of maximum dose (Fig.4.2).

4.3.4. Scatter-Maximum-Ratio (SMR)

The scatter-maximum ratio (SMR), is used for the calculation of scattered dose in a medium. It may be defined as the ratio of the scattered dose at a given point in phantom to the effective primary dose at the same point at the reference depth of maximum dose. Mathematically,

$$SMR(d, r_d) = TMR(d, r_d)\{S_p(r_d)/S_p(0)\} - TMR(d, 0) \quad \ldots\ldots\ldots 4.2$$

As at the reference depth of maximum dose (t_0), TMR is unity by definition, Eq.3.22 becomes

$$SMR(t_0, r_{t0}) = S_p(r_{t0})/S_p(0) - 1 \quad \ldots\ldots\ldots\ldots\ldots\ldots 4.3$$

4.3.5. Tissue-Air-Ratio (TAR)

Tissue-air-ratio (TAR) or "tumor-air-ratio" is defined as the ratio of the dose (D_d) at a given point in the phantom to the dose in free space (D_{fs}) at the same point. This is illustrated in Fig.4.3. For a given quality of beam, TAR depends on depth d and field size r_d at that depth:

$$TAR(d, r_d) = D_d/D_{fs} \quad \ldots\ldots\ldots\ldots\ldots 4.4$$

a) Effect of Distance on Variation of TAR

One of the most important properties attributed to TAR is that it is independent of the distance from the source. Since TAR is the ratio of the two doses (D_d and D_{fs}) at the same point, the distance dependence of the photon fluence is removed.

b) Variation with Energy, Depth and Field size

Tissue-air-ratio varies with energy, depth, and field size very much like the percentage depth dose. For the mega voltage beams, the tissue-air-ratio builds up to a maximum at the depth of maximum dose (d_m) and then decreases with depth more or less exponentially. For a narrow beam or a 0x0 field size in which scatter contribution to the dose is neglected, the TAR beyond d_m varies approximately exponentially with depth

$$TAR(d,0) = e^{-\overline{\mu}(d-d_m)} \qquad \dots\dots\dots\dots\dots 4.5$$

Where $\overline{\mu}$ is the average attenuation coefficient of the beam for the given phantom.
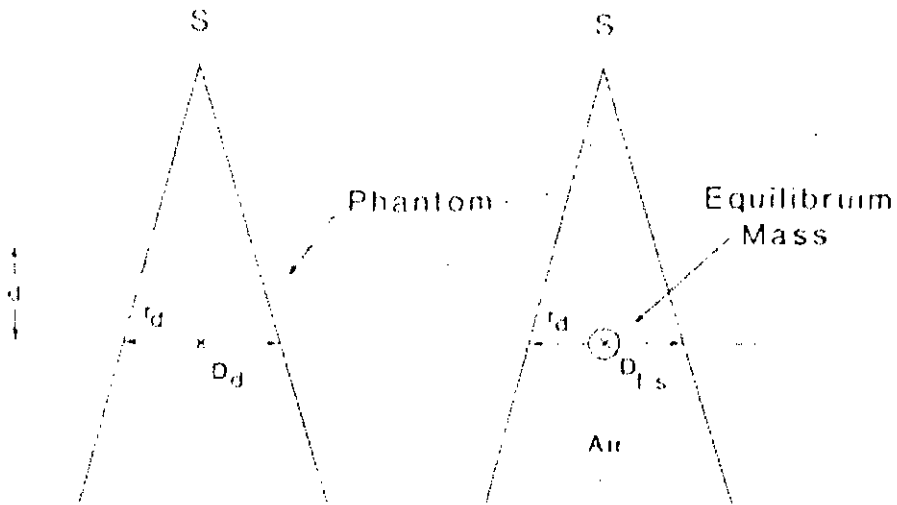
Fig.4.3 Illustration of the definition of tissue-air ratio, $TAR(d,r_d) = D_d/D_{fs}$.

4.3.6. Backscatter Factor

The term backscatter factor (BSF) is simply the tissue-air ratio at the depth of maximum dose on central axis of the beam. It may be defined as the ratio of the dose on central axis at the depth of maximum dose to the dose at the same point in free space. Mathematically,

$$BSF = D_{max}/D_{fs}$$

or

$$BSF = TAR(D_m, r_{dm})$$

where r_{dm} is the field size at the depth d_m of maximum dose.

The backscatter factor, like the tissue-air ratio, is independent of distance from the source and depends on the beam quality and field size.

4.3.7. Scatter-Air-Ratio (SAR)

Scatter-air-ratios are used for the purpose of calculating scattered dose in the medium. The computation of the primary and the scattered dose separately is useful in the dosimetry system of irregular fields.

Scatter-air ratio may be defined as the ratio of the scattered dose at a given point in the phantom to the dose in free space at the same point. The scatter–air-ratio like the tissue –air ratio is independent of the source-surface distance but depends on the beam energy, depth, and field size.

Since the scattered dose at a point in the phantom is equal to the total dose minus the primary dose at that point, scatter-air ratio is mathematically given by the difference between the TAR for the given field and the TAR for the 0x0 field.

$$SAR(d, r_d) = TAR(d, r_d) - TAR(d, 0) \dots\dots\dots\dots\dots\dots 4.6$$

Here TAR(d,0) represents the primary component of the beam.

4.3.8. Dose Calculation in Irregular Fields: Clarkson's Method

Any field other than the rectangular, square, or circular field may be termed as irregular. Irregularly shaped fields are encountered in radiotherapy when radiation sensitive structures are shielded from the primary beam or when the field extends beyond the irregularly shaped patient body contour. Examples of such fields are mantle and inverted Y fields employed for the

treatment of Hodgkin's decease. One method for dose calculation for irregular fields was proposed by Clarkson and later developed by Cunninghum. Clarkson method is based on the principle that the scattered component of the depth dose, which depends on the field size and shape, can be calculated separately from the primary component, which is independent of the field size and shape. A special quantity, SAR, is used to calculate the scattered dose.

Let us consider an irregularly shaped field shown in Fig.4.4. Assume this field cross-section to be at depth d and perpendicular to the beam axis. Let Q be the point of calculation in the plane of the field cross-section. Radii are drawn from Q to divide the field into elementary sectors. Each sector is characterized by its radius and can be considered as part of a circular field of that radius. If we suppose the sector angle is 10^0, then the scatter contribution from this sector will be $10^0/360^0 = 1/36$ of that contributed by a circular field of that radius and centered at Q. Thus the scatter contribution from all the sectors can be calculated and summed by considering each sector to be a part of its own circle the scatter-air ratio of which is already known and tabulated.

Using a SAR table for circular fields, the SAR values for the sectors are calculated and then summed to give the average scatter-air ratio ($\overline{SAR}$) for the irregular field at point Q. For sectors passing through a blocked area, the net SAR is determined by subtracting the scatter contribution by the blocked part of a sector. For example,

net$(SAR)_{QC} = (SAR)_{QC} - (SAR)_{QB} + (SAR)_{QA}.$
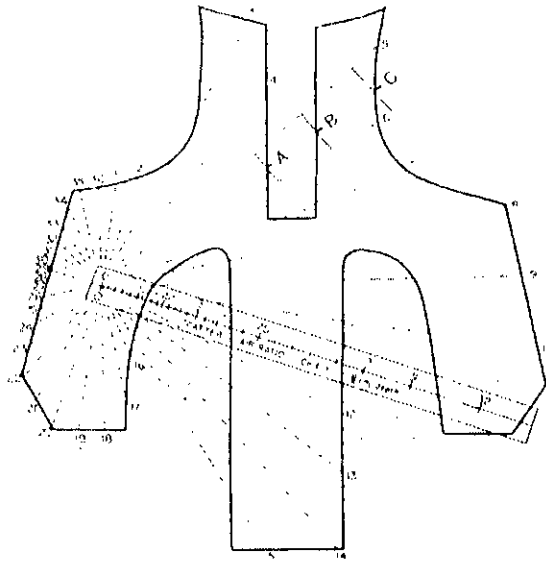
Fig.4.4 Outline of mantle field in a plane perpendicular to the beam axis and at a specified depth.

The computed $\overline{SAR}$ is converted to average tissue-air ratio $(\overline{TAR}$) by the equation

$$(\overline{TAR}) = TAR(\overline{0}) + \overline{SAR} \qquad \text{...................(4.7)}$$

where TAR(0) is the tissue-air ratio for 0x0 field, i.e., $TAR(0) = e^{-\overline{\mu}(d-d_m)}$, where $\overline{\mu}$ is the average linear attenuation coefficient for the beam and d is the depth of point Q.

CHAPTER-5   Equipment and Experimental Methods

5.1. Cobalt-60 Unit

5.1.1. Source

Irradiating ordinary stable ^{59}Co with neutrons in a reactor produces the ^{60}Co source. The nuclear reaction can be represented by ^{59}Co(n,γ)^{60}Co.

The ^{60}Co source, usually in the form of a solid cylinder, discs, or pallets, is contained inside a stainless-steel capsule and sealed by welding. This capsule is placed into another steel capsule, which is again sealed by welding. The double-welded seal is necessary to prevent any leakage of the radioactive material.
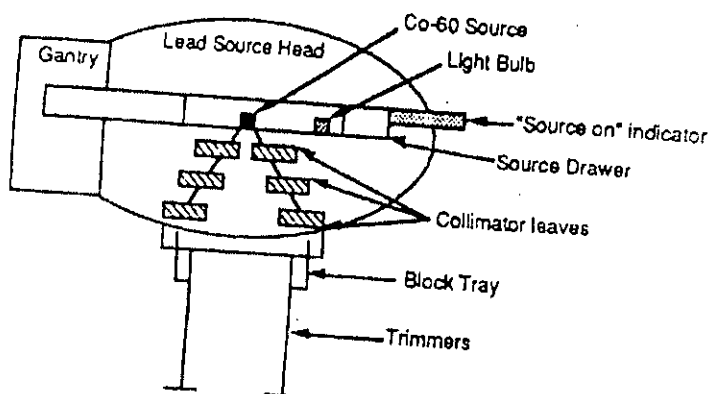
Fig.5.1 Cross sectional view of cobalt-60 teletherapy head

The ^{60}Co source decays to ^{60}Ni with the emission of β particles (E_{max} = 0.32 MeV) and two photons per disintegration of energies 1.17 and 1.33 MeV[33]. The decay scheme is shown in Fig.5.2. These γ rays constitute the usual treatment beam. The β particles are absorbed in the cobalt metal and the stainless-steel capsules resulting in the emission of bremsstrahlung x-rays and a small amount of characteristic x-rays. However, these x-rays of average energy around 0.1 MeV do not contribute appreciably to the dose in the patient because they are strongly attenuated in the material of the

source and the capsule. The other "contaminants" to the treatment beam are the lower-energy γ rays produced by the interaction of the primary γ radiation with the source itself, the surrounding capsule, the source housing, and the collimator system. The scattered components of the beam contribute significantly (~10%) to the total intensity of the beam [34]. All these secondary interactions, thus to some extent, result in heterogeneity of the beam. In addition, electrons are also produced by these interactions and constitute what is usually referred to as the electron contamination of the photon beam.
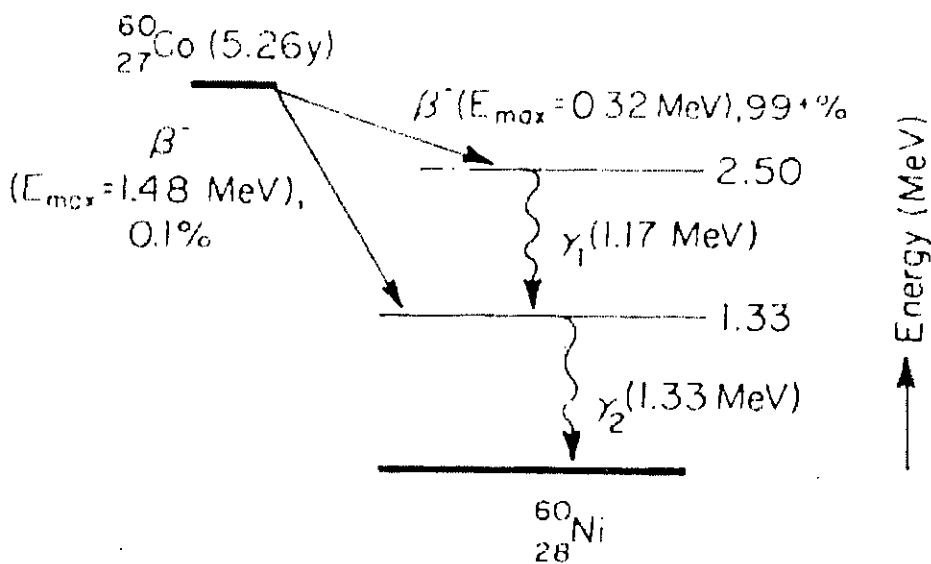
Fig.5.2 Decay scheme of [60]Co.

A typical teletherapy ^{60}Co source is a cylinder of diameter ranging from 1.0 to 2.0 cm and is positioned in the cobalt unit with its circular end facing the patient. The fact that the radiation source is not a point source complicates the beam geometry and gives rise to what is known as the geometric penumbra.
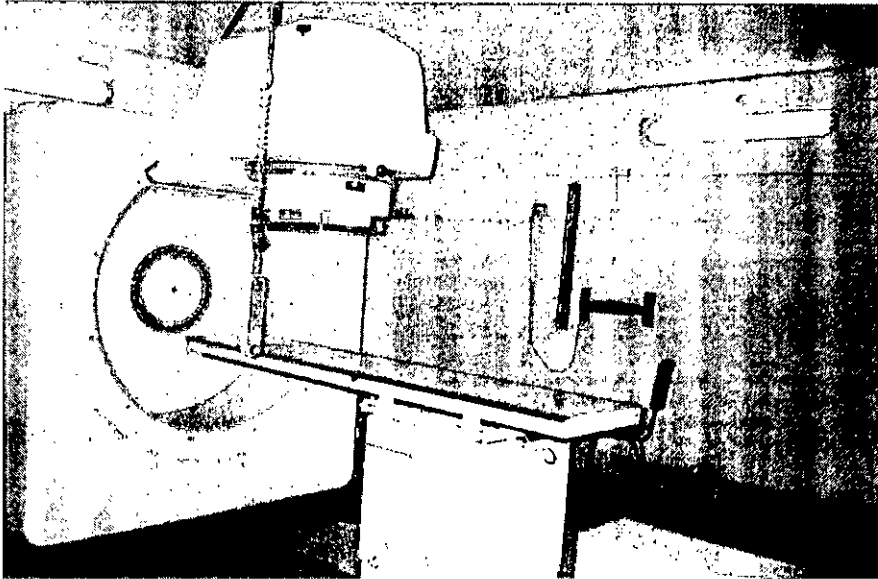
Fig. 5.3 A photograph of Co-60 teletherapy unit

5.1.2. Source Housing

The housing for the source is called the source head. It consists of a steel shell filled with lead for shielding purposes and a device for bringing the source in front of an opening in the head from which the useful beam emerges. Also, a heavy metal alloy sleeve is provided to form an additional primary shield when the source is in the "off" position.

A number of methods have been developed for moving the source from the "off" position to the "on" position. These are:

(a)   the source mounted on a rotating wheel inside the source head to carry the source from the "off" position to the "on" position;

(b)   the source mounted on a heavy metal drawer plus its ability to slide horizontally through a hole running through the source head-in the "on" position the source faces the aperture for the treatment beam

and in the "off" position the source moves to its shielded location and a light source mounted on the same drawer occupies the "on" position of the source;

(c)   mercury is allowed to flow into the space immediately below the source to shut off the beam; and

(d)   the source is fixed in front of the aperture and the beam can be turned on and off by a shutter consisting of heavy metal jaws. All of the above mechanisms incorporate a safety feature in which the source is returned automatically to the "off" position in case of a power failure.

5.1.3 Beam Collimation and Penumbra

A collimator system is designed to vary the size and shape of the beam to meet the individual requirements. The simplest form of a continuously adjustable diaphragm consists of two pairs of heavy metal blocks. Each pair can be moved independently to obtain a square or a rectangle-shaped field. Some collimators are multivane type, i.e., multiple blocks to control the size of the beam. In either case, if the inner surface of the blocks is made parallel to the central axis of the beam, the radiation will pass through the edges of collimating blocks resulting in what is known as the transmission penumbra. The extent of this penumbra will be more pronounced for larger collimator openings because of greater obliquity of the rays at the edges of the blocks. The effect has been minimized in some designs by shaping the collimator blocks so that the inner surface of the blocks remains always parallel to the edge of the beam. In these collimators, the blocks are hinged to the top of the collimator housing so that the slope of the blocks is coincident with the included angle of the beam. Although the transmission penumbra can be minimized with such an arrangement, it cannot be completely removed for all field sizes [33].

The term penumbra, in a general sense, means the region, at the edge of a radiation beam, over which the dose rate changes rapidly as a function of distance from the beam axis. The transmission penumbra, mentioned above, is the region irradiated by photons, which are transmitted through the edge of the collimator block.

Another type of penumbra, known as the geometric penumbra, is illustrated in Fig 5.4. The geometric width of the penumbra (P_d) at any depth (d) from the surface of a patient can be determined by considering similar triangles ABC and DEC. From geometry we have;

$$\frac{DE}{AB} = \frac{CE}{CA} = \frac{CD}{CB} = \frac{MN}{OM} = \frac{OF+FN-OM}{OM} \quad \text{.......} \quad (5.1)$$

If AB =s, the source diameter, OM =SDD, the source to diaphragm is distance, OF =SSD, the source to surface distance, then from the above equation, the penumbra (DE) at depth d is given by

$$P_d = \frac{s(SSD + d - SDD)}{SDD} \quad \text{.........} \quad (5.2)$$

The penumbra at the surface can be calculated by substituting d=0 in Eq.5.2.
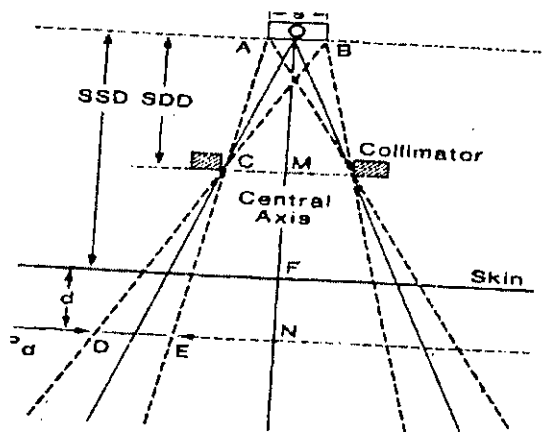
Fig.5.4 Diagram for calculating geometry penumbra

As Eq. 5.2 indicates, the penumbra width increases with increase in source diameter, SSD and depth but decreases with an increase in SDD. The geometric penumbra, however, is independent of field size as long as the movement of the diaphragm is in one plane, i.e. SDD stays constant with increase in field size.

Since SDD is an important parameter in determining the penumbra width, this distance can be increased by extendable penumbra trimmers. These trimmers consist of heavy metal bars to attenuate the beam in the penumbra region, thus "sharpening " the field edges. The penumbra, however, is not eliminated completely but reduced since SDD with the trimmers extended is increased. The new SDD is equal to the source to trimmer distance. An alternative way of reducing the penumbra is to use secondary blocks, placed close to the patient, for redefining or shaping the field. The blocks should not be placed closer than 15 to 20 cm from the patient because of excessive electron contaminants produced by the block-carrying tray.

The combined effect of the transmission and geometric penumbras is to create a region of dose variation at the field edges. A dose profile of the beam measured across the beam in air at a given distance from the source would show dosimetrically the extent of the penumbra. However, at a depth in the patient the dose variation at the field border is a function of not only geometric and transmission penumbras but also the scattered radiation produce in the patient. Thus, dosimetrically, the term physical penumbra width has been defined as the lateral distance between two specified isodose curves (the lines passing through points of equal dose) at a specified depth.

5.2. Measurement of Ionization Radiation

Introduction

Charged particles such as electrons, protons, and α particles are known as directly ionizing radiation provided they have sufficient kinetic energy to produce ionization by collision as they penetrate matter. The uncharged particles such as neutrons and photons are indirectly ionizing radiation since they liberate directly ionizing particles from matter when they interact with matter.

Ionizing photons interact with the atoms of a material or absorber to produce high-speed electrons by three major processes: photoelectric effect, Compton effect and pair production.

Radiation is invisible and thus its presence can not be detected directly. However, ionizing radiation produces observable effects in medium, through which it is passing, which in turn can be detected by several methods. In fact, measurement of these effects regarding their extent is an indirect and only strategic method of measuring ionizing radiation. In the early days of x-ray usage for diagnosis and therapy, attempts were made to measure ionizing radiation on the basis of their chemical and biological effectiveness. Radiation effects on photographic emulsions, changes in the color of some chemical compounds and reddening of human skin were related to the amount of radiation absorbed. For radiotherapy purposes, the reddening of the skin during therapy application was related to a radiation unit known as skin erythema dose (SED) which was defined as that amount of x or γ radiation that just produces reddening of the skin. However, this SED unit had many drawbacks and used as a crude estimation of radiation dose which depends on many factors such as type of skin, the quality of radiation, the extent of skin exposed to radiation, dose fractionation and skin reaction characteristics. With a view to avoid the aforesaid uncertainties

and to have more appropriate and precise unit for the measurement of ionizing radiation. In 1928 ICRU (International Commission on Radiological Unit and Measurement) recommended adoption of two physical quantities "Roentgen" as exposure unit and "Rad" as absorbed dose unit. Although SED has been discarded in favour of ICRU recommended Roentgen and Rad, radiotherapy establishments having orthovoltage radiotherapy facilities are still using this skin erythema as an approximate index of the skin response to the given radiation treatment and considering reddening of the skin as limiting factor to the delivery of tumorcidal doses. However, departments having megavoltage beams with skin sparing facilities must not rely on observing the development of skin reaction for the assessment of radiation response to individual treatments.

The quantity of ionizing radiation is most often expressed in terms of exposure (its ability to produce ionization in air) and absorbed dose (the amount of radiation energy imparted in a medium) [11,35,36].

The unit of exposure is roentgen which is a measure of the ionization ability of a photon beam (x or γ) in air with photon energy not higher than 3 MeV. This unit "roentgen" was originally defined as the amount of x or γ radiation required to produce 1 esu (electrostatic unit) of charge of either sign in 1 cc air at STP (standard temperature and pressure). The current definition of the unit "roentgen" is equivalent to 2.58×10^{-4} coulomb/kg dry air at STP which is equal to the original definition if the charge is expressed in coulombs (1 esu = 3.333×10^{-10} coulomb) and the volume of air is changed to mass (1 cc of air at STP weights 1.293×10^{-6} kg). ICRU–1980 defines exposure (X) as the quotient of dQ/dm where dQ is the absolute value of the total charge of the ions of one sign produced in air when all the electrons (negatrons and positrons) liberated by photons in air of mass dm are completely stopped in air. Mathematically it is expressed as

$$X = dQ \, / \, dm \qquad \ldots\ldots\ldots\ldots \qquad (5.3)$$

The system International (SI) unit for exposure is coulomb per kg (C/kg) of air. It should be emphasized here that the quantity exposure with its unit "roentgen" applies only to photon beam (x or γ) in an air medium. This exposure is a measure of the ionization in air only and cannot be used for photon having energies above 3 MeV. If the radiation is not a photon beam e.g. electron beam or if the medium is not air, e.g. tissue, then unit of exposure "roentgen" can no longer be used. In such cases, another physical term "absorbed dose" is used which describes the quantity of radiation for all types of ionizing radiation including charged and uncharged particles, all materials and all energies thereby eliminating inherent limitations in the use of exposure unit "roentgen" for quantitative measurement of ionizing radiation. The absorbed dose is a measure of radiation energy being absorbed per unit mass of the medium, which in turn measures the biologically significant effects produced as a result of the absorbed ionizing radiation. The most stringent definition of the absorbed dose or simply the dose is the quotient $d\bar{e}/dm$ where $d\bar{e}$ is the mean energy imparted by ionizing radiation to material of mass d_m[37]. The conventional (old) unit of absorbed dose is rad (an acronym for radiation absorbed dose) and represents the absorption of 100 ergs of energy per gram of the absorbing material. Thus we see that the unit of absorbed dose "rad" is much more general than the exposure unit "roentgen" since it does not specify the type and energy of the radiation nor the type of medium while exposure is confined only to photon (x or γ) having not more than 3 MeV and the medium is air only. As the unit of energy varies e.g. erg, joule. eV etc, the unit of absorbed dose also varies accordingly.

Thus   1 Rad = 100 ergs/gm = 10^{-2} J/Kg

Recently adopted SI unit for absorbed dose is the Gray (Gy) and is defined as

1 Gray = 1 J/Kg.

Thus the relationship between gray and rad is

1 Gy = 100 rads = 1 J/Kg

or 1 rad = 10^{-2} Gy

Since gray is a larger unit, a sub unit, centigray (cGy) has often been used as being equivalent to rad.
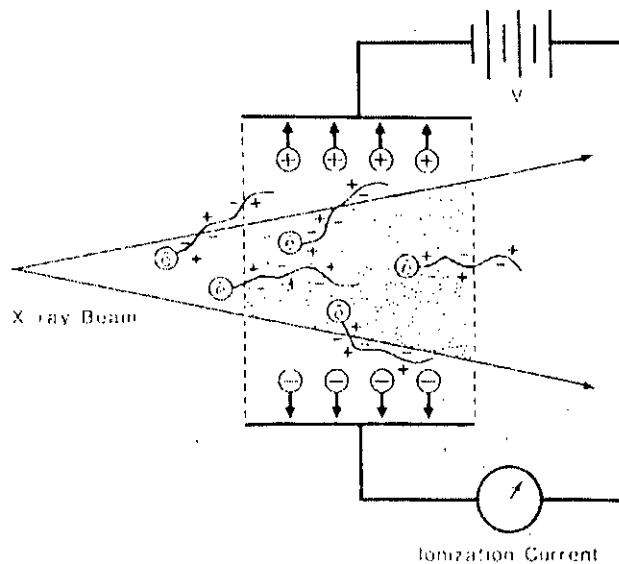
Fig.5.5 Diagram illustrating electronic equilibrium in free-air chamber

The (SI) unit for exposure is coulomb per kilogram (C/kg) but the special unit is roentgen (R).

$$1 R = 2.58 \times 10^{-4} \text{ C/kg air}$$

The definition of roentgen is illustrated in Fig.5.5. An x-ray beam in passing through air sets in motion electrons by photoelectric effect, Compton effect, or pair production. These high-speed electrons produce ionization along their tracks. Because of the electric field produced by the voltage applied

across the ion-collection plates, the positive charges move toward the positive plate and the negative charges move toward the positive plate. This constitutes a current. The collected charge of either sign can be measured by an electrometer.

According to the definition of roentgen, the electrons produced by photons in a specified volume (shaded in fig above) must spend all their energies by ionization in air enclosed by the plates (region of ion collection) and the total ionic charge of either sign should be measured. However, some electrons produced in the specified volume deposit their energy outside the region of ion collection and thus are not measured. On the other hand, electrons produced outside the specified volume may enter the ion-collecting region and produce ionization there. If the ionization loss is compensated by the ionization gained, a condition of electron equilibrium exists. Under this condition, the definition of roentgen is effectively satisfied. This is the principle of free-air ionization chamber.

5.2.1. Free-air Ionization Chamber

The free-air, or standard, ionization chamber is an instrument employed in the measurement of the roentgen according to its definition. The free-air ionization chamber is represented schematically in Fig.5.6. An x-ray beam, originating from a focal spot S, is defined by the diaphragm D and passes centrally between a pair of parallel plates. A high-voltage (field strength of the order of 100 V/cm) is applied between the plates to collect ions produced in the air between the plates. The ionization is measured for a length L defined by the limiting lines of force to the edges of the collection plate C. The lines of force are made straight and perpendicular to the collector by a guard ring G.
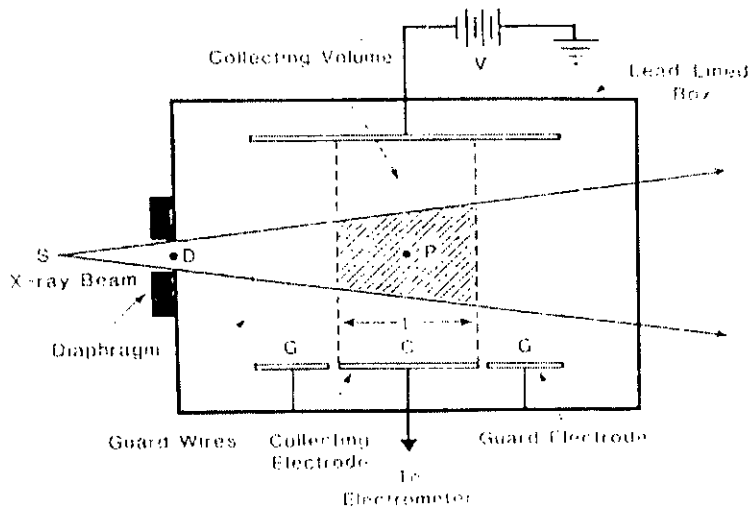
Fig.5.6 Free-air ionization chamber

In this case electrons produced by the photon beam in the specified volume (shaded in Fig.5.6) must spend all their energy by ionization of air between the plates. Such a condition can exist only if the range of the electrons liberated by the photons is less than the distance between each plate and the specified volume. For electronic equilibrium to exist, the beam intensity (photon fluence per unit time) must remain constant across the specified volume, and the separation between the diaphragm and the ion-collecting region must exceed the electron range in air.

If ΔQ is the charge collected in Coulombs and ρ is the density (kg/m^3) of air, then exposure X_p at the centre of the specified volume (point P) is

$$X_p = \frac{\Delta Q}{\rho.A_p.L} \cdot \frac{1}{2.58 \times 10^{-4}} \text{ roentgens} \qquad \text{.........5.4}$$

where A_p is the cross sectional area (in meter squared) of the beam at point P and L (in meters) is the length of the collecting volume. In practice it is more convenient to state the exposure (X) at the position of the diaphragm. Suppose f_1 and f_2 are the distances of the X-ray source to the diaphragm and point P, respectively. Since the intensity at point P and at the

diaphragm are related by an inverse square law factor $(f_1/f_2)^2$, which also relates the area of the beams at diaphragm and at point P, exposure X_D at the diaphragm is given by:

$$X_D = \frac{\Delta Q}{p.A_D.L} \cdot \frac{1}{2.58 \times 10^{-4}} \text{ roentgens} \qquad ....5.5$$

where A_D is the diaphragm aperture area.

5.2.2. Thimble Chambers

Free-air ionization chambers are too delicate and bulky for use. For laboratory a standard instrument known as a" thimble chamber" is used. The principle of this chamber is illustrated in Fig. 5.7. In this figure a spherical volume of air is shown with an air cavity at the center. Let us suppose that this sphere of air is irradiated uniformly with a photon beam and also that the distance between the outer sphere and the inner cavity is equal to the maximum range of electrons generated in air. If the number of electrons entering the cavity is the same as that leaving the cavity, electronic equilibrium exists. Additionally we may consider that we are able to measure the ionization charge produced in the cavity by the electrons liberated in the air surrounding the cavity. Then by knowing the volume or mass of air inside the cavity, we can calculate the charge per unit mass or the beam exposure at the center of the cavity. Now if the air wall in Fig.5.7a is compressed into a solid shell as in Fig.5.7b we get a thimble chamber. Although the thimble wall is solid, it is air equivalent, its effective atomic number is the same as that of air. In addition, the thickness of the thimble wall is such that the electronic equilibrium occurs inside the cavity, just as it did in Fig.5.7a. The wall thickness must be equal to or greater than the maximum range of the electrons liberated in the thimble wall [33].

Since the density of the solid air-equivalent wall is much greater than that of free air, the thickness required for electronic equilibrium in the thimble chamber are considerably reduced. For example, in the 100 to 250 kV$_p$ x-ray range, the wall thickness of the thimble (assuming unit density) is about 1mm, and in the case of ^{60}Co γ rays (average hv =1.25 Mev), it is approximately 5 mm. In practice, however, a thimble chamber is constructed with wall thickness of 1 mm or less and this is supplemented with close-fitting caps of Plexiglass or other plastic to bring the total wall thickness up to that needed for electronic equilibrium for the radiation in question.
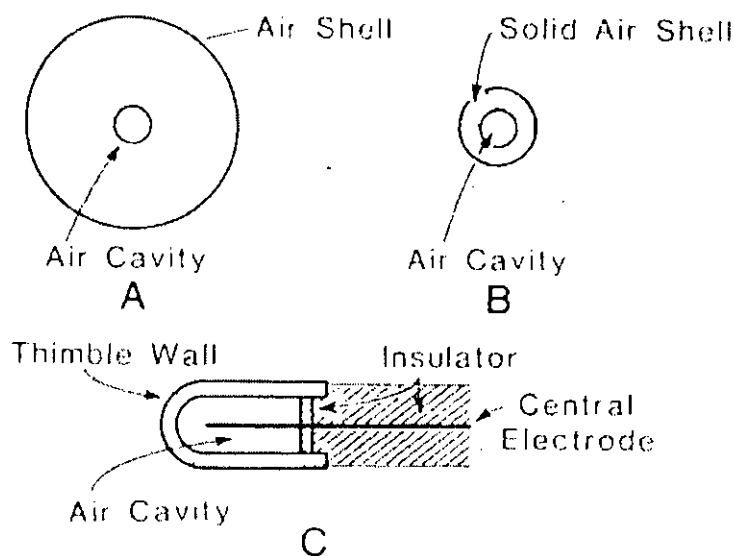
Fig.5.7. Schematic diagram illustrating the nature of the thimble ionization chamber. (A) Air shell air cavity. (B) Solid air shell with air cavity. (C) The thimble chamber.

Fig. 5.7c shows a typical thimble ionization chamber. The wall is shaped like a sewing thimble. The inner surface of the wall is coated by a special material to make it electrically conducting. This forms one electrode. The other electrode is a rod of low atomic number material such as graphite or aluminum held in the center of the thimble but electrically insulated from it. A suitable voltage is applied between the two electrodes to collect the ions produced in the air cavity. In order for the thimble chamber to be equivalent

to a free-air chamber, the thimble wall should be air equivalent. In order for the thimble chamber to be air-equivalent, the effective atomic number of the wall material and the central electrode must be such that the system as a whole behaves like a free-air chamber. Most commonly used wall materials are made either of graphite (carbon), bakelite, or a plastic coated on the inside by a conducting layer of graphite or of a conducting mixture of bakelite and graphite. The effective atomic number of the wall is generally a little less than that of air. It is closer to that of carbon (Z=6). The term "effective atomic number" is the atomic number of an element with which photons interact the same way as with the given composite material.

5.2.3. Farmer Chamber

Farmer chamber provides a stable and reliable secondary standard for x-rays and γ-rays for all energies in the therapeutic range. This chamber is shown schematically in Fig. 5.8. Actual dimensions of the thimble and the central electrode are indicated on the diagram. The thimble wall is made of pure graphite and the central is of pure aluminum. The insulator consists of polytrichlorofluorethylene. The collecting volume of the chamber is nominally 0.6 cm^3.
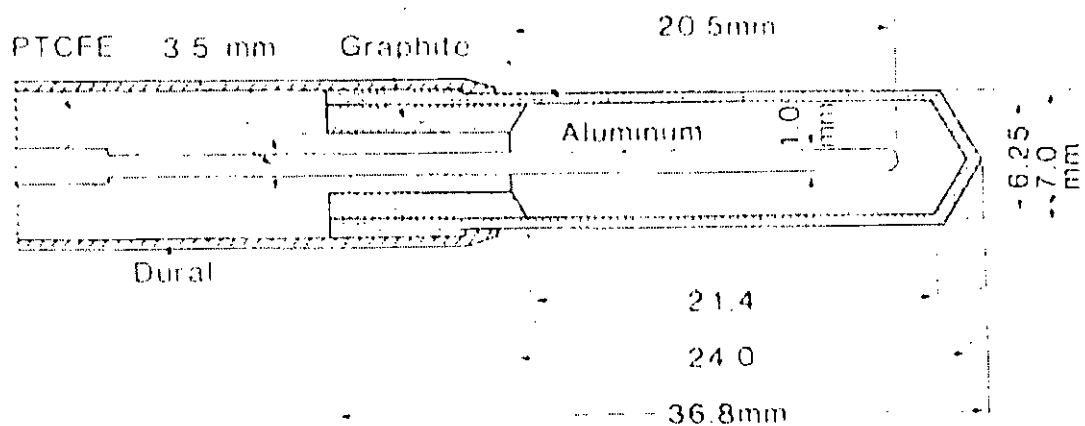
Fig. 5.8. Farmer chamber

5.2.4. Ionization Chamber Dosimetric System

An ionization dosimetric system contains an ionization chamber and a charge-measuring device called electrometer. The basic parts of an ionization chamber dosimetric system are shown in Fig. 5.9. In the present study, a 0.6 cc micro ion chamber in conjunction with a PTW UNIDOS electrometer has been used for dose measurements. The collecting electrode of the ionization chamber is connected to a charge/ current-measuring device called the electrometer. The cable should be long enough so that the electrometer can be placed outside the room at the control console of the teletherapy unit.

The PTW ionization chamber type 30001 is a standard sealed chamber for therapy dosimeter. It is watertight and equipped with a flexible stem so that it can be used in variable temperature surrounding.
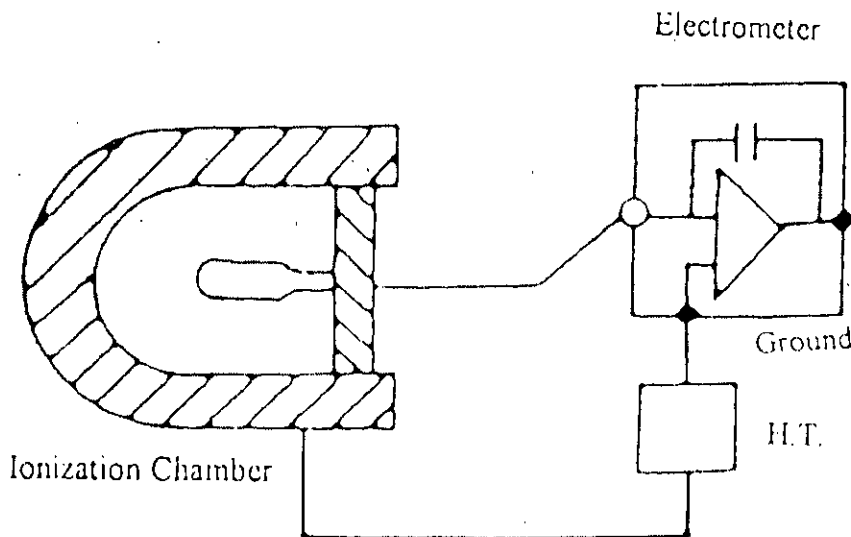
Fig. 5.9. Parts of an ionization chamber dosimetric system

Technical Specification of Ionization chamber Type PTW 30001 [38]

Volume: 0.6 cm^3

Response: 2 x 10^{-8} C/Gy

Leakage: ± 4 X 10^{-15} A

Polarizing voltage: max. 500 V

Cable Leakage: 10^{-12} C/(Gy.cm)

Wall material: PMMA ($C_5H_8O_2$)$_n$ + Graphite (C)

Wall density: 1.19 g/cm^3 (PMMA)

                          0.82 g/cm^3 (C)

Wall thickness: 0.275 mm PMMA

                          + 0.15 mm C

Area density: 45 mg/cm^2

Electrode: Aluminium;

                          1 mm ∅; 21.2 mm long

Range of temperature: + 10° C ... + 40° C

Range of rel. humidity: 20% ... 80% (<20g/m^3)

Ion collection time: 300 V : 0.18 ms

                          400 V : 0.14 ms

                          500 V : 0.11 ms

UNIDOS is a highly sensitive electrometer. It is a microprocessor controlled universal field class dosimeter. It can determine the dose by measuring the charge or by numerically integrating the dose rate, the measurement of which is based on the measurement of current. The first method is called the direct dose method, the second method integrated dose mode. The integrated dose mode enables simultaneous measurement of the dose and the dose rate.

Specifications of Universal Dosimeter UNIDOS [38]

	Digital resolution	Maximum input rating
Charge mode	10^{14} C	2.2×10^8 C
Current mode	10^{-15} A	10^{-6} A
Integrated current mode	10^{-14} C	6.5×10^{-2} C
Leakage current	$\leq 10^{-15}$ A	
Amplifier zeroing	Automatically within 75 second according to IEC	
Linearity	$\leq \pm 0.5$ according to IEC	
Long-term stability typically	$\pm 0.05\%$ per year	
Measuring quantities	Absorbed dose to water, air kerma, absorbed dose to air, photon equivalent dose, exposure	
Chamber voltage	(0 – 400)V, adjustable in 50-Volt increments, polarity selectable	
Temperature range	(10 – 40)^{0}C /(50 – 104)^{0}F	
Relative humidity	(10 – 75)% relative humidity, 20 g/m^3 max	
Signal input connector	PTW type M.INC or BNT (BNC with banana, Plug on request)	
Power supply	Line power 115/230 V[50 – 60] Hz, or iIndependent of power line, from rechargeable NiCd batteries(operating time: 7 to 9 hours)	
Case dimensions	[H x W x D] 152 x 257 x 262 mm^3 (6 x10.1 x10.3 in)	
Weight	6.4 kg	

5.3. Phantoms

Basic dose distribution data are usually measured in a water phantom, which closely approximates the radiation absorption and scattering properties of muscle and other soft tissues. Another reason for the choice of water as a phantom material is that it is universally available with reproducible radiation properties. A water phantom, however, poses some practical problems when used in conjunction with ion chambers and other detectors, which are affected by water, unless they are designed to be waterproof. In most cases, however, the detector is encased in a thin plastic (water equivalent) sleeve before immersion into the water phantom. Since it is not always possible to put radiation detector in water, solid dry phantoms have been developed as substitutes for water. Ideally, for a given material to be tissue or water equivalent, it must have the same effective atomic number, number of electron per gram and mass density. However, since the Compton effect is the most predominant mode of interaction for mega voltage photon beams in the clinical range, the necessary condition for water equivalence for such beams is the same electron density (number of electrons per cubic centimeter) as that of water.

The electron density (ρ_e) of a material may be calculated from its mass density (ρ_m) and its atomic composition according to the formula:

$$\rho_e = \rho_m . N_A . (Z/A) \qquad \qquad ....(5.6)$$

where

$$Z/A = \sum_i a_i . (Z_i / A_i) \qquad \qquad .... (5.7)$$

N_A is Avogadro's number and a_i is the fraction by weight of the ith element of atomic number Z_i and atomic weight A_i. Table-5.1 gives the properties of various phantoms, which have been frequently used for radiation dosimetry.

Table 5.1. Physical properties of various phantom materials

Material	Chemical composition	Mass density (g / cm^3)	Number of electrons/g ($\times 10^{23}$)	Z_{eff} (Photoelectric)
Water	H_2O	1	3.34	7.42
Polystyrene	$(C_8H_8)_n$	1.03 – 1.05	3.24	5.69
Plexiglas (Perspex, Lucite)	$(C_5O_2H_8)_n$	1.16 – 1.20	3.24	6.48
Polyethylene	$(CH_2)_n$	0.92	3.44	6.16
Paraffin	C_nH_{2n+2}	0.87 – 0.91	3.44	7.05
Mix D	Paraffin:60.8 Polyethylene: 30.4 MgO : 6.4 TiO$_2$: 2.4	0.99	3.41	7.05
M 3	Paraffin : 100 MgO : 29.06 CaCO$_3$: 0.94	1.06	3.34	7.35
Solid water	Exposy resin – based mixture	1.00	3.34	

5.4. Depth Dose Distribution

As the beam is incident on a patient (or a phantom), the absorbed dose in the patient varies with depth. This variation depends on many conditions: beam energy, depth, field size, and distance from source and beam collimation system. Thus the calculation of dose in the patient involves consideration in regards to these parameters and others as they affect depth dose distribution.

An essential step in the dose calculation system is to establish depth dose variation along the central axis of the beam. A number of quantities have been defined for this purpose, major ones among these being;

    a. percentage depth dose

    b. tissue-air ratios

    c. tissue-phantom ratios and

    d. tissue-maximum ratios.

These quantities are usually derived from measurements made in water phantoms using small ionization chambers.

5.5. Percentage Depth Dose

One way of characterizing the central axis dose distribution is to normalize dose at depth with respect to dose at a reference depth. The quantity percentage (or simply percent) depth dose may be defined as the quotient, expressed as a percentage, of the absorbed dose at any depth 'd' to the absorbed dose at a fixed reference depth 'd$_o$', along the central axis of the beam (Fig.3.13). Percentage depth dose (P) is thus

$$P = (D_d / D_{do}) \times 100 \quad \text{.....................} (5.8)$$

For orthovoltage (up to about 400 kV$_p$) and lower-energy x-rays, the reference depth is usually the surface (d$_o$ = 0). For higher energies, the reference depth is taken at the position of the peak absorbed dose (d$_o$ = d$_m$).

In clinical practice, the peak-absorbed dose on the central axis is sometimes called the maximum dose, the dose maximum, the given dose, or simply the D$_{max}$. Thus

$$D_{max} = D_d / P \times 100 \quad \dots\dots\dots\dots\dots\dots(5.9)$$

A number of parameters affect the central axis depth dose distribution. These include beam quality or energy, depth, field size and shape, source to surface distance and beam collimation. A discussion of these parameters will now be presented.
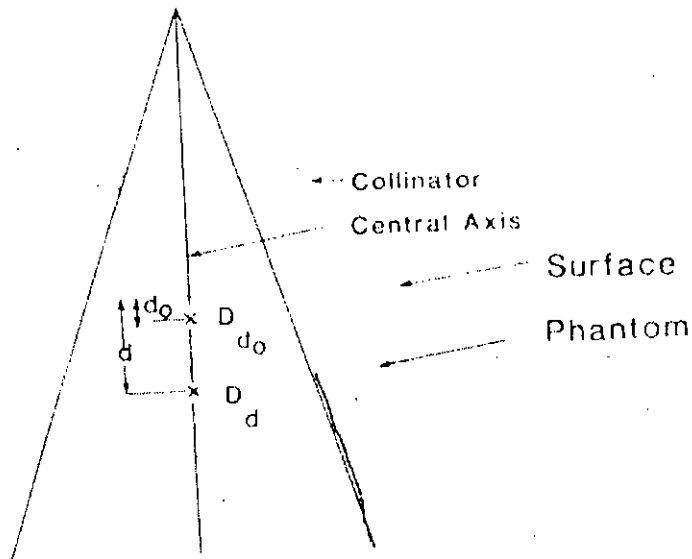
Fig.5.10. Percentage depth dose is $(D_d/D_{d0}) \times 100$, where d is any depth and d_0 is reference depth of maximum dose.

A. Dependence on Beam Quality and Depth

The percentage depth dose (beyond the depth of maximum dose) increases with beam energy. Higher energy beams have greater penetrating power and thus deliver a higher percentage depth dose (Fig.5.11). If the effects of inverse square law and scattering are not considered, the percentage depth dose variation with depth is governed approximately by exponential attenuation. Thus the beam quality affects the percentage depth dose by virtue of the average attenuation coefficient.

A1: Initial Dose Build up

As seen in Fig.5.11 the percentage depth dose decreases with depth beyond the depth of maximum dose. However, there is an initial build up of dose which become more and more pronounced as the energy is increased. In the case of the orthovoltage or lower-energy x-rays, the dose builds up to a maximum on or very close to the surface. But for higher energy beams, the points of maximum dose lie deeper in to the tissue or phantom. The region between the surface and the point of maximum dose is called the dose build up region.
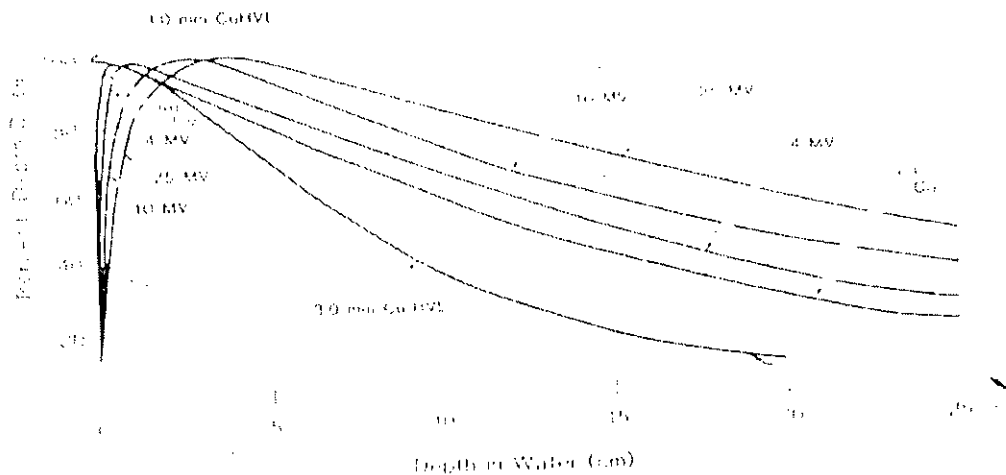
Fig.5.11. Central axis depth dose distribution for different quality photon

The dose build up effect of the higher-energy beams gives rise to what is clinically known as the skin-sparing effect. For megavoltage beams such as cobalt-60 and higher energies the surface dose is much smaller than the D_{max}. This offers a distinct advantage over the lower-energy beams for which the D_{max} occurs at the skin surface. Thus, in the case of the higher energy photon beams, higher doses can be delivered to deep-seated tumors without exceeding the tolerance of the skin. This, of course, is possible because of the higher percent depth dose at the tumor and the lower surface dose at the skin.

B. Effect of Field Size and Shape

Field size may be specified either geometrically or dosimetrically. The geometrical field size is defined as "the projection, on a plane perpendicular to the beam axis, of the distal end of the collimator as seen from the front center of the source". This definition usually corresponds to the field defined by the light localizer, arranged as if a point source of light were located at the center of the front surface of the radiation source. The dosimetric, or the physical, field size in the distance intercepted by a given isodose curve (usually 50% isodose) on a plane perpendicular to the beam axis at a stated distance from the source.

Here the field size represents as geometric field size and is defined at a predetermined distance such as the source-surface distance (SSD) or the source-axis distance (SAD). The latter term is the distance from the source to axis of gantry rotations known as the isocenter.

For a sufficiently small field, the depth dose at a point is effectively the result of the primary radiation i.e. photons which have traversed the overlying medium without interacting. The contribution of the scattered photons to the depth of dose in this case is negligibly small or zero. But as the field size is increased, the contribution of the scattered radiation to the absorbed dose increases. Since this increase in scattered dose is greater at larger depth than at the depth of D_{max}, the percent depth dose increases with increasing field size.

The increase in percent depth dose caused by increase in field size depends on beam quality. Since the scattering probability or cross-section decreases with increasing energy and since the higher-energy photon are scattered more predominantly in the forward direction, the field size dependence of percent depth dose is less pronounced for the higher-energy than for the lower-energy beams.

Percent depth dose data for the radiotherapy beams are usually tabulated for square fields. Since the majority of the treatments encountered in clinical practice required rectangular and irregularly shaped (blocked) fields, a system of equating square fields to different field shapes is required. Semi empirical methods have been developed to relate central axis depth dose data for square, rectangular, circular and irregularly shaped fields.

A simple rule of thumb method has been developed by Sterling et al. for equating rectangular and square fields. According to this rule, a rectangular field is equivalent to a square field if they have the same area/perimeter (A/P). For example, the 10x20 cm field has an A/P of 3.33. The square field which has the same A/P is 13.3x13.3 cm. The following formulas are useful for quick calculation of the equivalent field parameters: for rectangular field fields

$$A/P = (a \times b) / 2(a + b) \qquad \text{........} \qquad (5.10)$$

where 'a' is field width and b is field length. For square fields, since a = b,

$$A/P = a / 4 \qquad \text{..........} \qquad (5.11)$$

where 'a' is the side of the square. From equations (5.10) and (5.11), it is evident that the side of an equivalent square of a rectangular field is 4xA/P. For example, a 10x15-cm field has an A/P of 3.0. Its equivalent square is 12x12 cm.

C. Dependence on Source-Surface Distance

Photon fluence emitted by a point source of radiation varies inversely as the square of the distance from the source. The source-surface distance is usually chosen to be large ($\geq$80 cm) so that the source dimensions become

unimportant in relation to the variation of photon fluence with distance. In other words, the source can be considered as a point at large source-surface distances. Thus the exposure rate or "dose rate in free space" from such a source varies inversely as the square of the distance. Of course, the inverse-square law dependence of dose rate is suitable in the case of primary beam, without scatter. In a given clinical situation, however, collimation or other scattering material in the beam may cause deviation from the inverse square law.

Percent depth dose increases with SSD because of the effects of the inverse square law. Although the actual dose rate at a point decreases with increase in distance from the source, the percent depth dose, which is a relative dose with respect to a reference point, increases with SSD. This is illustrated in Fig.5.12 in which relative dose rate from a point source of radiation is plotted as a function of distance from the source, following the inverse square law. The plot shows that the drop in dose rate between two points is much greater than that at large distances. This means that the percent depth dose, which represents depth dose relative to a reference point, decreases more rapidly near the source than far away from the source.

In clinical radiotherapy, SSD is an important parameter. Since percent depth dose determines how much dose can be delivered at depth relative to the surface dose or D_{max}, the SSD needs to be as large as possible. However, since dose rate decreases with distance, the SSD, in practice, is set at a distance which provides a compromise between dose rate and percent depth dose. For the treatment of deep-seated lesions with mega voltage beams, the minimum recommended SSD is 80 cm.
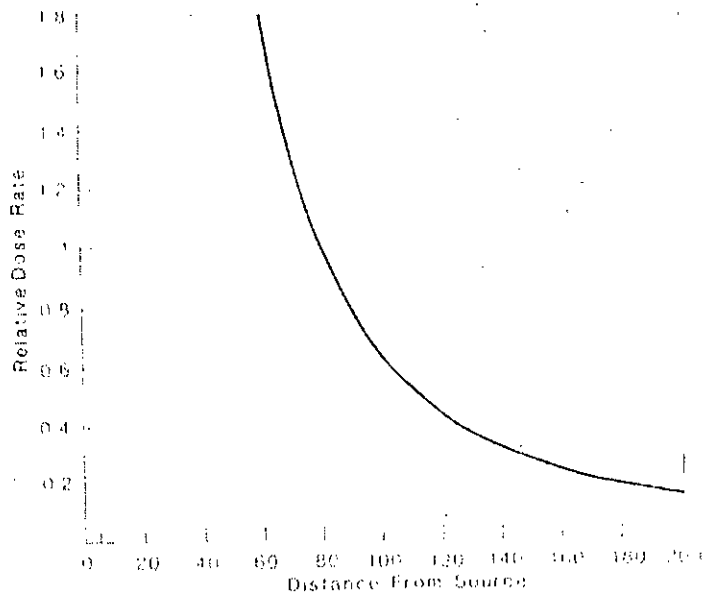
Fig.5.12. Plot of relative dose rate as inverse square law function of distance from a point source. Reference distance=80 cm.

5.6. Experimental Procedure

For investigation of photon doses in different irregular fields, solid phantoms made of acrylic sheets with dimensions 50 cm x 45 cm with average thickness of 1.5 cm were used. Routine therapy application procedures which were traceable to international norms for radiotherapy practices were followed during dose determination in solid phantoms for [60]Co- teletherapy unit. In addition an 0.6 cc ionization chamber and PTW-UNIDOS electrometer were used for this procedure. The procedure constitutes some steps. In the beginning of each step, the room temperature and the pressure were noted first according to the date. For pressure measurement, the "Fortran barometer" was used. Then the ^{60}Co teletherapy unit was adjusted to set the SSD= 80 cm on the ion chamber placed on the phantom. The trimmers of the collimator were changed to set the desired field size.

91

The "Fortran barometer" is shown in Fig.5.13 and the phantom is shown in Fig.5.14. The steps are described as follows:

1. For the determination of central axis doses in open field of ^{60}Co-teletherapy unit, ionization chamber was placed in the center of the phantom. Dose measurements were done for the field sizes 5x5 cm^2 (lateral), 10x10 cm^2 (lateral), 15x15 cm^2 (lateral), 15x15 cm^2 (vertical), 20x20 cm^2 (lateral), 25x25 cm^2 (lateral), 25x25 cm^2 (vertical), 10x10 cm^2 (both diagonal), 15x15 cm^2 (diagonal), 20x20 cm^2 (diagonal). In each field, the interested points of dose investigations were labeled with numerical 1,2,3,4...... etc. for positive and upper side and −1,-2,-3,-4 .... etc. for negative and lower side. The locations of the points of measurement to various directions for open field dose are shown in Fig. 6.1 and the corresponding data are shown in Table 1.1 to 1.11 in Chapter 6.

2. Now for dose measurement by irregular field-shaping device, the "half-beam" device was used first. For this purpose, the phantom was placed on the bed of the ^{60}Co unit. Then the collimator of the unit was adjusted to make the field size 16x17 cm^2. The half-beam was then inserted into the frame of the collimator. The SSD was adjusted to 80 cm. The machine was switched "on". The dose rates of 306 points each 1 cm apart were measured keeping the ionization chamber on the points one by one. The locations of points and the corresponding dose rates are shown in Fig. 6.2 and 6.3 respectively in Chapter 6. The corresponding data is shown in Table 2 in that Chapter.

3. Then the "half-beam device" was removed from the collimator. The field size was made 9x17 cm^2. The device was inserted again into the frame of collimator. The doses of the points numbered 127 to 306 of the same phantom were then measured following the same process. The half-

beam device is shown in Fig 5.15. The corresponding data are shown in Table 3 and Tables 4.1 to 4.18 in Chapter 6.

4. Now inserting various rectangular shaped small blocks (made of led alloy) (Fig 5.17) into the shielding tray (Fig. 6.18), three other irregular field shaping devices named (a) inverted 'Y' block, (b) two-cornered block, (c) four-cornered block etc. were prepared. The dose rates using these devices were measured for field size 15x15 cm^2 for points shown in Figures 6.4, 6.5, 6.6 in Chapter 6. The corresponding data are shown in Tables 5 – 7, in that chapter.

5. Data for comparison between measured and calculated dose rates of blocked field i.e. for calculation of percentage of deviation are given in Tables 8.1 – 8.6 for field size 15x15 cm.

6. Then the dose rates for different fields 15x15 cm, 20x20 cm and 25x25 cm for points (Fig 6.7) were measured using a special irregular field shaping device (block) with tissue compensator (wax). The corresponding data are shown in Tables 9.1 – 9.3.
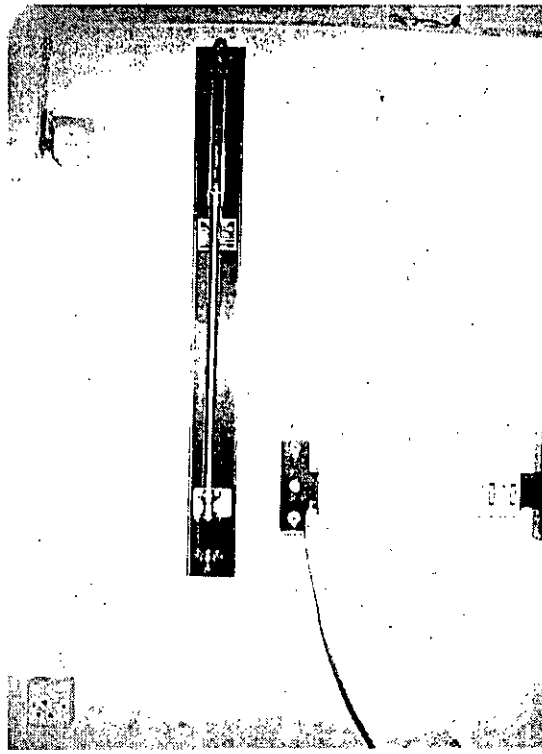
Fig. 5.13. Fortran Barometer
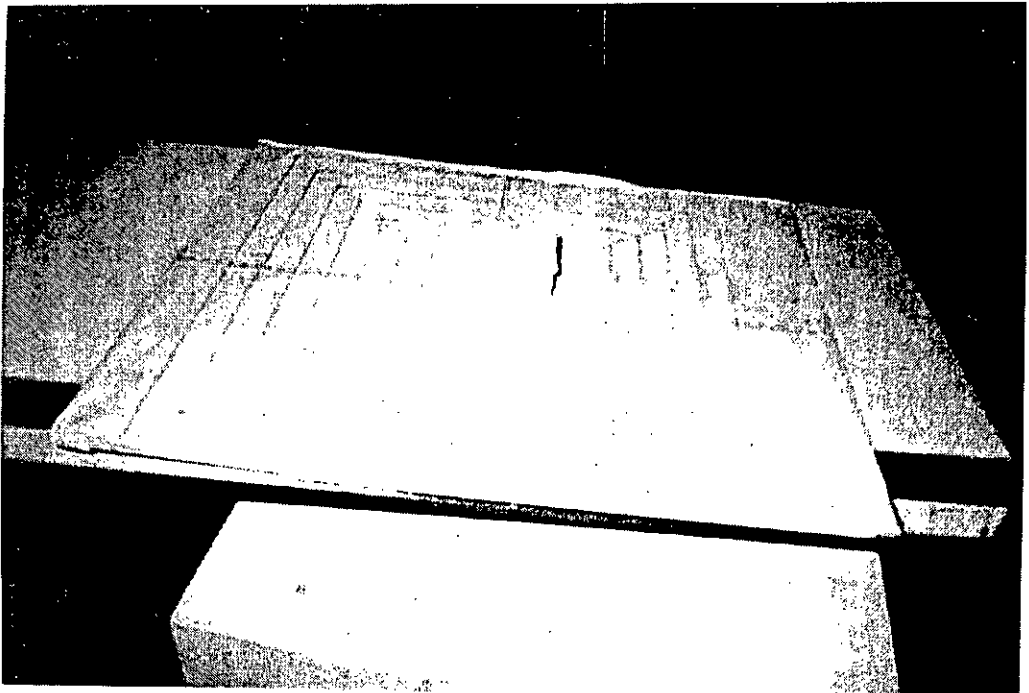
Fig. 514. Phantom
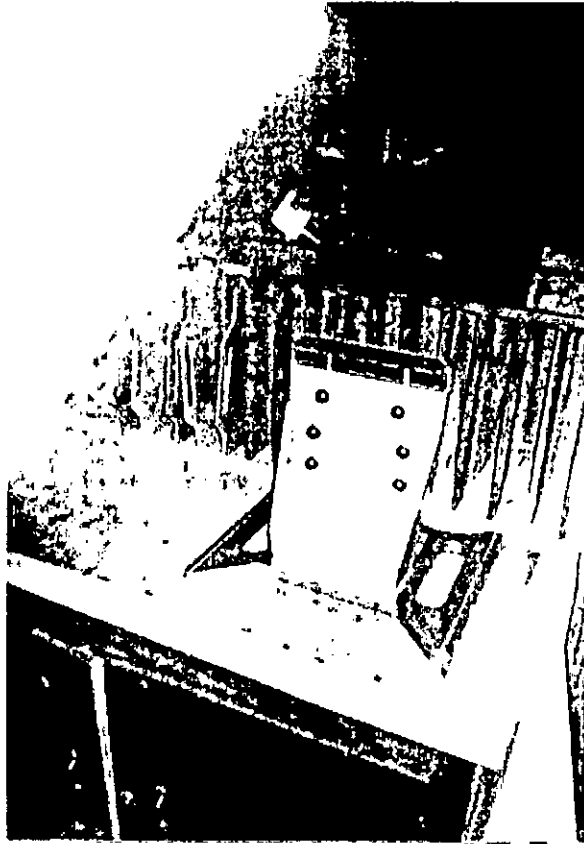
Fig. 5.15. Half-beam device

Fig. 5.16. Control room for ^{60}Co teletherapy unit
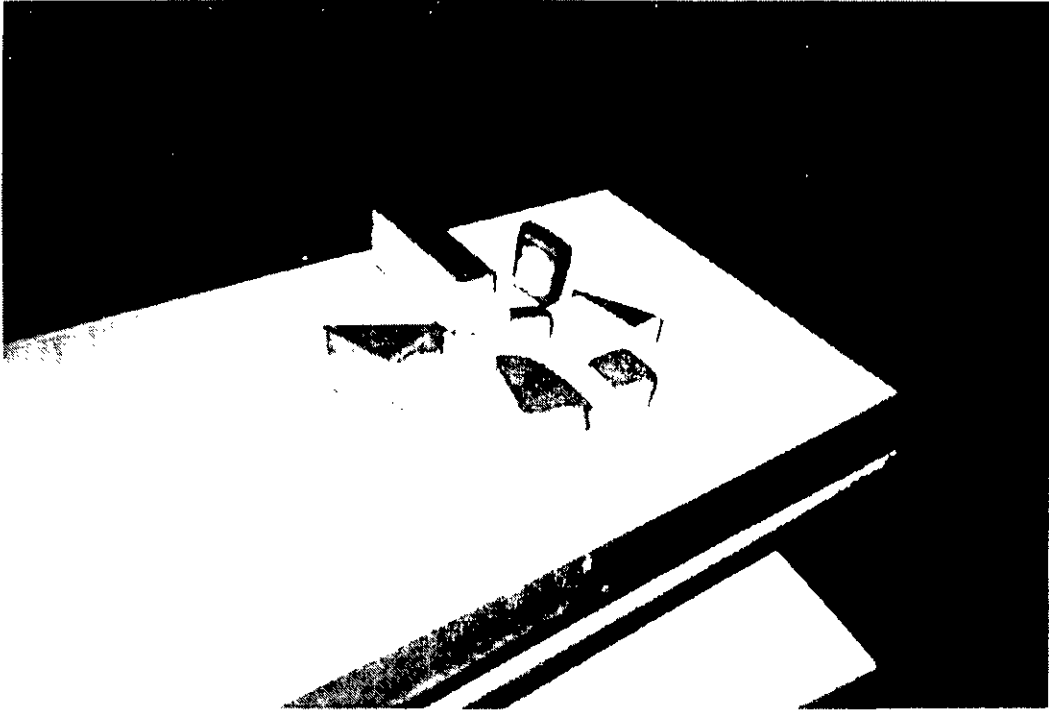
Fig. 5.17. Blocks

Fig. 5.18. Shielding tray
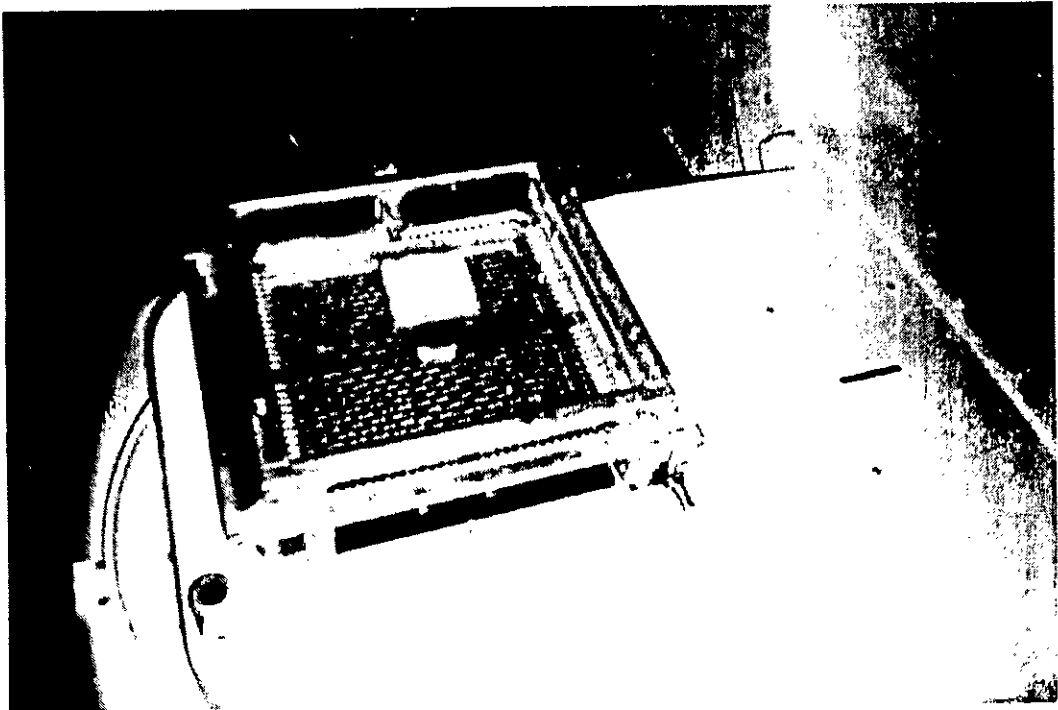
CHAPTER 6   Results and Discussion

6.1. Results and Discussion

The aim of this thesis work was to investigate the dose distribution by irregular field-shaping device for photon beam radiation. In order to serve the purpose, a device known as " half-beam device" as an irregular field-shaping device was used, which is used for breast cancer treatment. Three blocked fields namely "inverted Y" field, "two-cornered blocked" field, "four-cornered blocked" field were then used as other irregular field-shaping devices. These were made by inserting small rectangular blocks into the shielding tray. For the measurement of doses for ^{60}Co teletherapy unit, a solid phantom made of acrylic sheets with dimensions 40cmx40cm with average thickness of 1.5 cm were used. Another irregular field-shaping device was used for calculation of doses for different field sizes for the treatment of pelvis cancer, which was made of a special shaped block (led) and tissue-compensator (in this case wax) inserting into the shielding tray.

Data of dose rates for some open fields were taken first. Tables 1.1 to 1.11 represent the open field data of the dose rate of different field size for lateral, diagonal, vertical distance of point's 1 cm apart. Fig. 6.1 represents the location of the points of measurement to various directions. First, the dose rates were found in mR as the electrometer was set on that unit. Dose in mGy were obtained by multiplying by the conversion factor 0.876.

Table 2 represents the data of dose rate in mGy on field size 16x17 cm of 306 points which are 1 cm apart using the half – beam device. Fig. 6.2 and Fig. 6.3 represent the points and dose rates in mGy respectively.

Table 3 represents the data of dose rate on field size 9x17cm of 127 to 306 alternative points using the half beam device. Tables 4.1 to 4.18 represent the data of dose rates in mGy of vertical points of the 16x17 cm field and

the corresponding data, which represent the effect of the use of half-beam device. As the half-beam device is used for the treatment of breast cancer, the above graphs show that the side of the treatment field is blocked by the device so that the dose rate is low. As a result the breast wall and lung get lower dose. Portion of the treatment field is partially shielded because the area is normal tissues.

Table 5.1 represents the data of uncorrected dose rate in mGy of both sided points of lateral distance for "inverted Y" field. The field is shown in Fig. 6.4. The dose rate is corrected for temperature and pressure by multiplying the correction factor C_{TP} = 1.01. The corresponding graph is shown in the same page. Table 5.2 to 5.5 represent the data of calculated dose rate, TAR, off – axis factors respectively and corresponding graphs. Though in Fig. 6.4, the dose rates of 10 points on both sides of central axis were measured, the points up to 7 were used for calculation of SAR. Because as the field size is 15x15 cm, the SAR (scatter–air-ratio) for the points outside the field cannot be calculated. The inverted "Y" is placed in the middle of the treatment field, so that the spinal cord is saved from the radiation, as the dose to spinal cord is limited. Here it should be mentioned that the dose limit to spinal cord of the patient depends on its diameter.

Similarly, Tables 6.1 to 6.5 represent the same data for "two-cornered blocked field" and Tables 7.1 to 7.5 represent the data for "four-cornered blocked field". Figs. 6.5 and 5.6 represent the arrangement for the "two-cornered blocked field" and "four-cornered blocked field" respectively. The off-axis factors of each blocked field were calculated as shown in the appendix. An example of calculation of TAR is shown in Fig. 1 and Table of the appendix by Clarkson's method. The calculated value of each measured dose was found by using the Eq.1 in appendix. Then for getting the value of percentage of deviation of dose rates, the open field data for 15x15 cm (termed as standard field size in radiotherapy) and the data of each blocked fields were used separately. For getting the data, the value of corresponding

TAR were used to get the calculated dose rate from the open field data by using Eq.2 in the appendix. Then the percentage of deviation of dose rates were calculated by comparing the measured dose rate of each blocked field and the calculated dose rate. Table 8.1 represents the open field data. Tables 8.2 to 8.6 represent the data of comparison and percentage of deviation of dose rates for blocked fields. From the above tables it is seen that though the percentage of deviation of doses should not be more than 5%, in some cases the value is more than that value. The reasons for the variation may be due to the variation of distance between central axis point and off-axis point. Another reason may be due to decay of Co-60 source, as the open field dose rate was measured about four months before the blocked field dose rate. The Co-60 source decays as described in Eq-3 (Appendix A). Table 8.6 shows that the value of percentage of deviation of dose rates are inconsistent for points −1,0,1,2, because for these points there are no value of SAR. Another important point for each blocked field is that, there are different dose rates between the two sided value of central axis. This may be due to asymmetry of placing the blocks on the phantom.

Tables 9.1, 9.2, 9.3 represent the irregular field data for dose rates of blocked field with wax for field size 20x20 cm, 25x25 cm, 15x15 cm respectively. The corresponding figures are shown in the same pages. This type of blocks are used for the cancer treatment. Fig. 6.7 represents the points of dose measurement for 15x15 cm field size for this block.
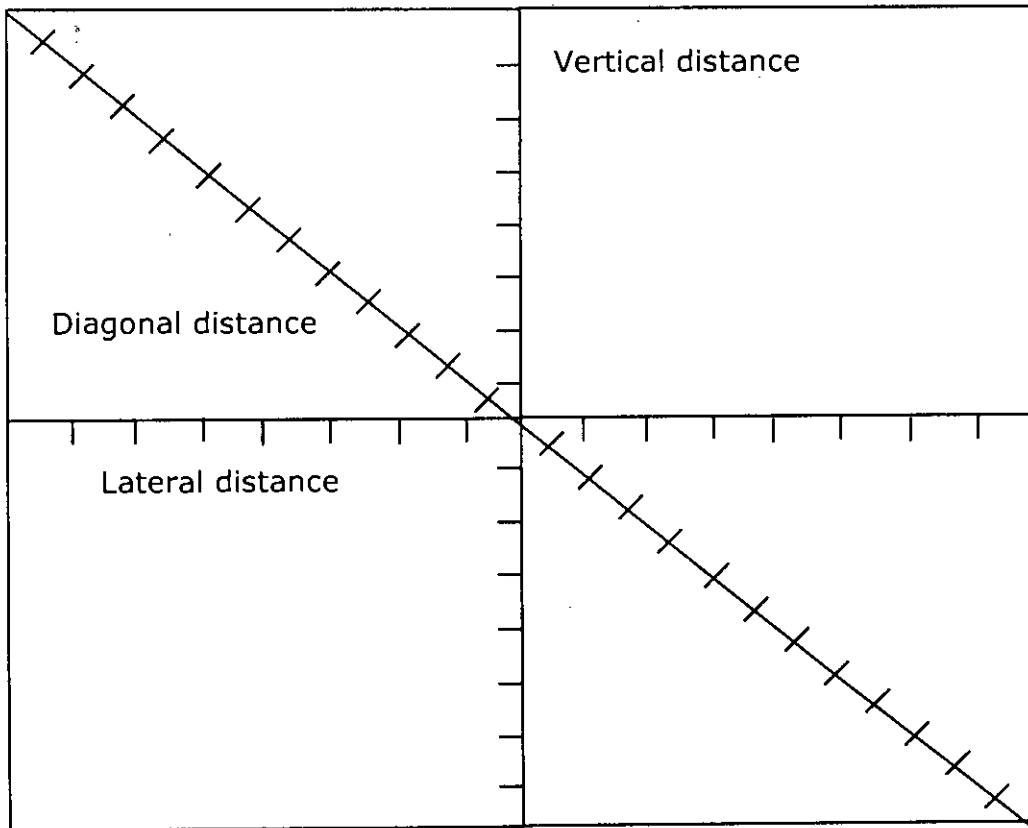
Fig. 6.1. Location of the points of measurement to various directions for open field dose

Fig:- No. of points of measurement
of absorbed dose rate using half
beam device

1	2	3	4	5	6	7	8	9	10	11	12	13	14	15	16	17	18
19	20	21	22	23	24	25	26	27	28	29	30	31	32	33	35	35	36
37	38	39	40	41	42	43	44	45	46	47	48	49	50	51	52	53	54
55	56	57	58	59	60	61	62	63	64	65	66	67	68	69	70	71	72
73	74	75	76	77	78	79	80	81	82	83	84	85	86	87	88	89	90
91	92	93	94	95	96	97	98	99	100	101	102	103	104	105	106	107	108
109	110	111	112	113	114	115	116	117	118	119	120	121	122	123	124	125	126
127	128	129	130	131	132	133	134	135	136	137	138	139	140	141	142	143	144
145	146	147	148	149	150	151	152	153	154	155	156	157	158	159	160	161	162
163	164	165	166	167	168	169	170	171	172	173	174	175	176	177	178	179	180
181	182	183	184	185	186	187	188	189	190	191	192	193	194	195	196	197	198
199	200	201	202	203	204	205	206	207	208	209	210	211	212	213	214	215	216
217	218	219	220	221	222	223	224	225	226	227	228	229	230	231	232	233	234
235	236	237	238	239	240	241	242	243	244	245	246	247	248	249	250	251	252
253	254	255	256	257	258	259	260	261	262	263	264	265	266	267	268	269	270
271	272	273	274	275	276	277	278	279	280	281	282	283	284	285	286	287	288
289	290	291	292	293	294	295	296	297	298	299	300	301	302	303	304	305	306

9 x 17 cm →

16 cm ↕

17 cm →

16 X 17 cm Field size

Fig. 6.2. Number of points for 16x17 cm field size of dose measurement using half beam device

Step 1 — Dose rate (mGy) using half-beam device opening 16×17 cm field size.
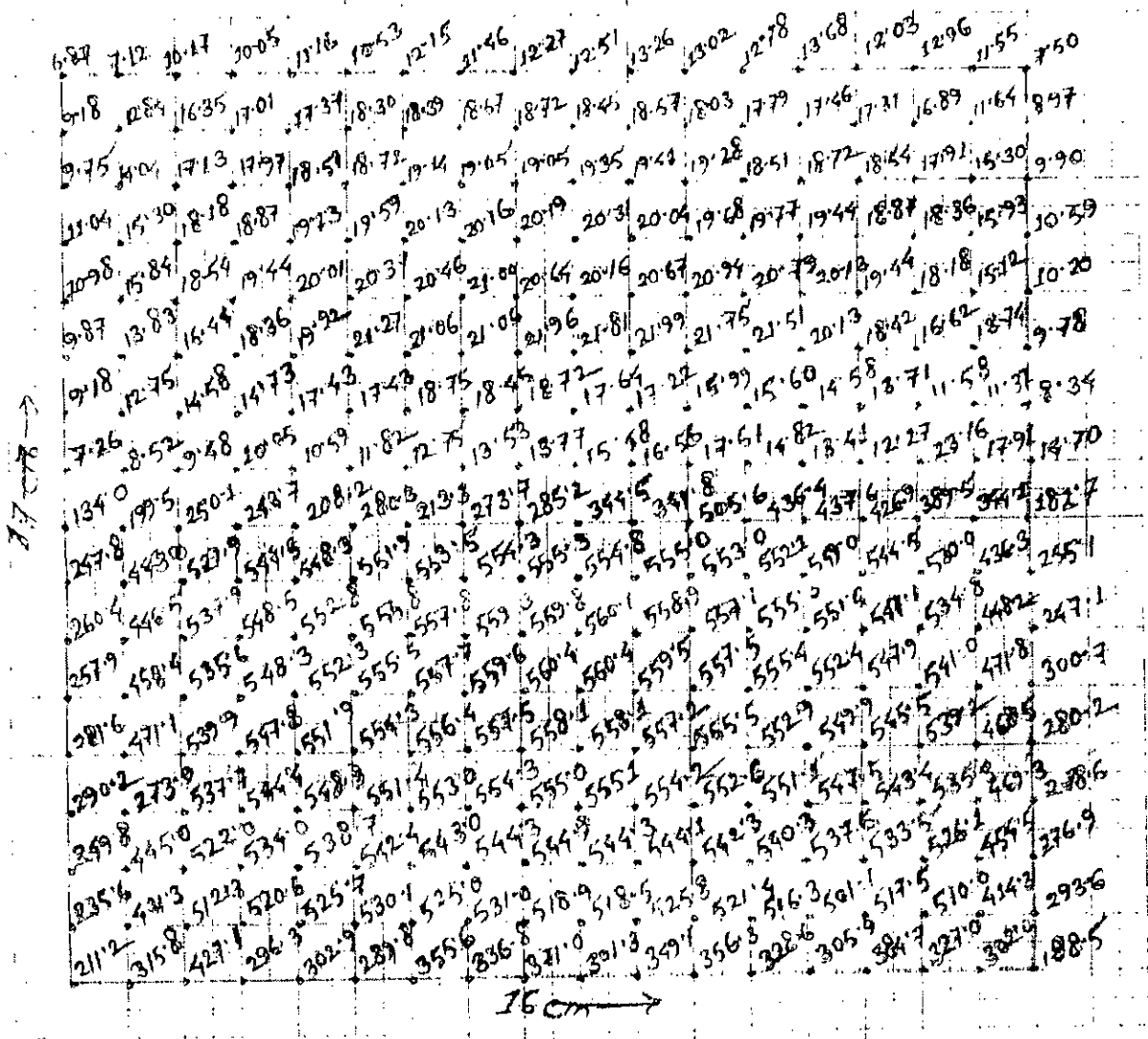
Fig. 6.3. Dose rate in mGy for 16x17 cm field size using half-beam device
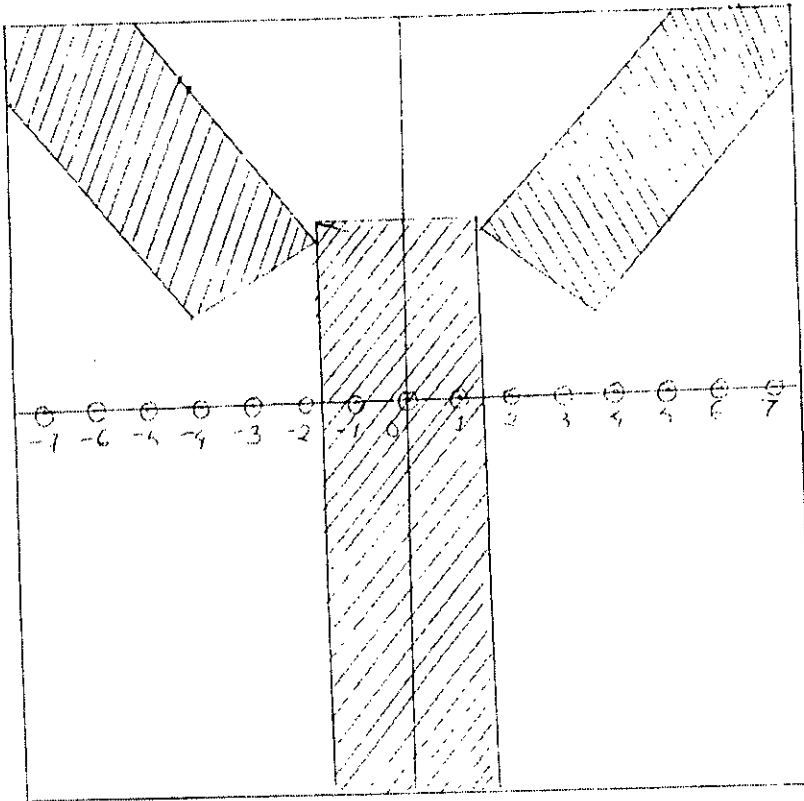
Fig. 6.4. Number of points of dose measurement for inverted 'Y' field

103
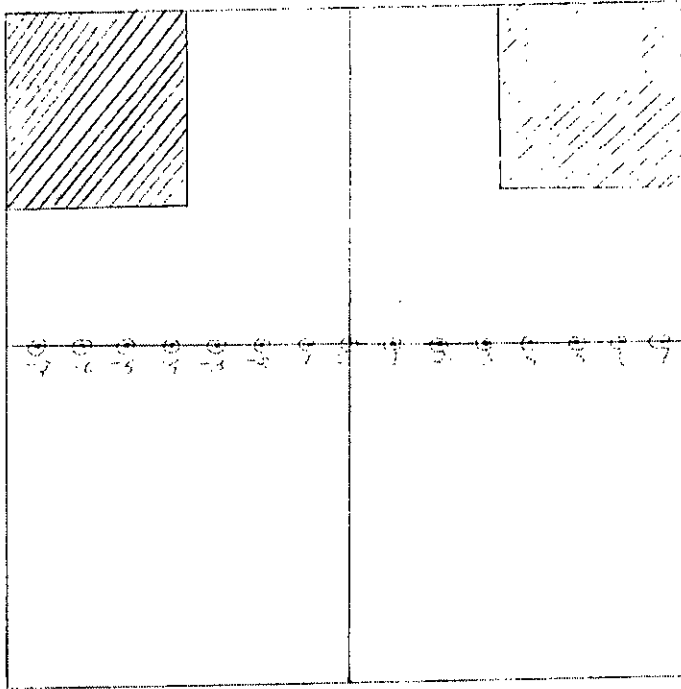
Fig. 6.5. Number of points of dose measurement for two-cornered blocked field
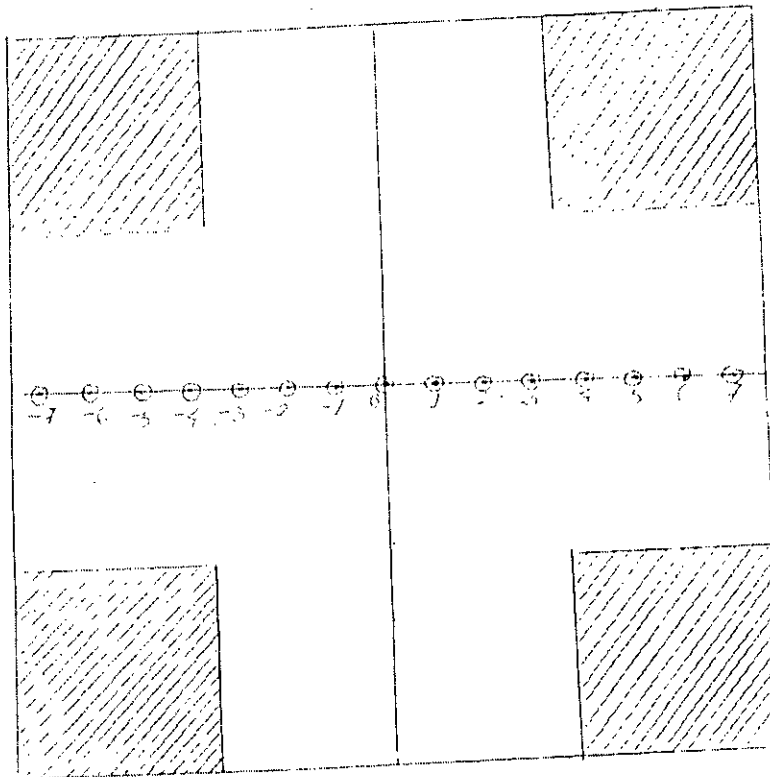
Fig. 6.6. Number of points of dose measurement for four-cornered blocked field
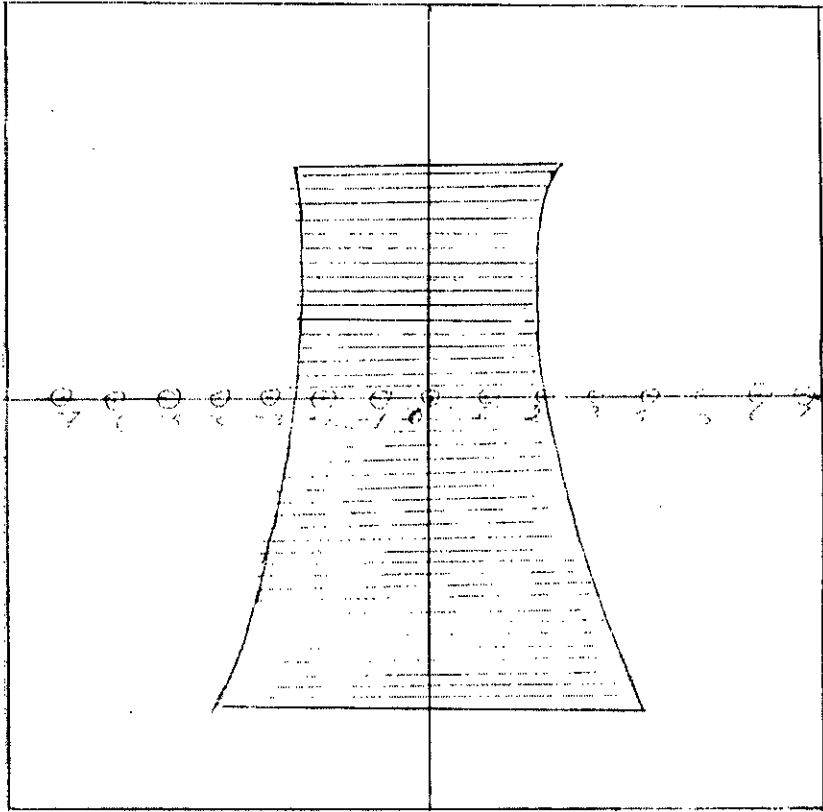
Fig. 6.7. Number of points of dose measurement for 15x15 cm field size for block with tissue compensator

6.2. Tables of Different Data

1. Table for open field data

Table-1.1
· SSD = 80 cm
· Field Size = 5x5 cm
· Electrometer PTW – UNIDOS
· Ionization chamber = 0.6 c.c

* Lateral distance in cm	Dose rate in mR	Dose rate in mGy
7	3.42	3.00
6	4.9	4.29
5	8.55	7.49
4	21.2	18.57
3	205.73	180.22
2	443.8	388.77
1	542.4	475.14
0	549	480.92
-1	541.14	474.04
-2	443.48	388.49
-3	204.61	179.24
-4	21.95	19.23
-5	8.35	7.31
-6	4.59	4.02
-7	3.32	2.91
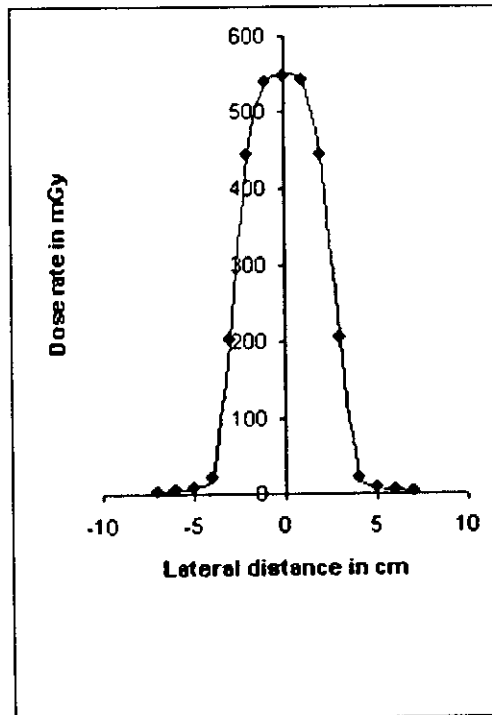
* Reference Fig. 6.1

1. Table for open field data

Table-1.2
- SSD = 80 cm
- Field size = 10 x 10
- Electrometer PTW - UNIDOS
- Ionization chamber = 0.6 c.c

Lateral distance in cm	Dose rate in mR	Dose rate in mGy
-20	2.46	2.15
-19	2.7	2.37
-18	2.88	2.52
-17	3.24	2.84
-16	3.54	3.10
-15	3.6	3.15
-14	3.93	3.44
-13	4.5	3.94
-12	5.22	4.57
-11	6.27	5.49
-10	7.74	6.78
-9	9.66	8.46
-8	13.68	11.98
-7	22.17	19.42
-6	58.89	51.59
-5	294.1	257.63
-4	532.9	466.82
-3	566.9	496.60
-2	569.3	498.71
-1	570.6	499.85
0	571.2	500.37
1	570.4	499.67
2	568.8	498.27
3	565.8	495.64
4	511.7	448.25
5	237.5	208.05
6	44.43	38.92
7	19.44	17.03
8	12.96	11.35
9	9.36	8.20
10	7.35	6.44
11	6.12	5.36
12	5.22	4.57
13	4.56	3.99
14	3.96	3.47
15	3.6	3.15
16	3.36	2.94
17	3.06	2.68
18	2.7	2.37
19	2.46	2.15
20	2.31	2.02
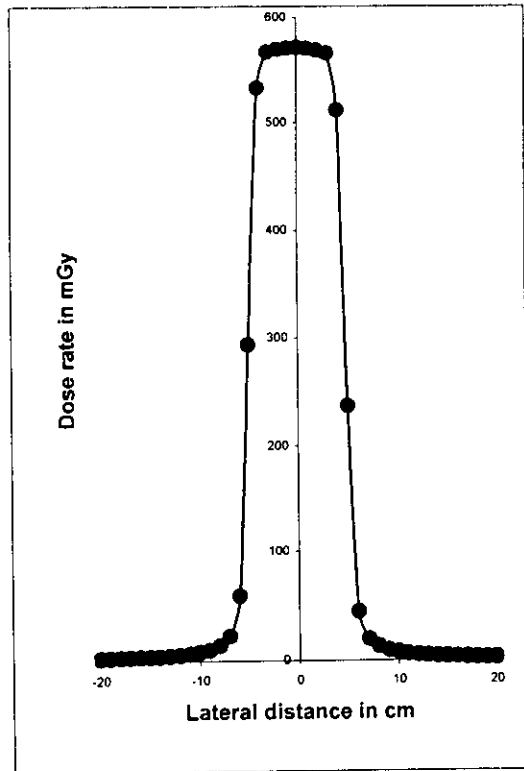
1. Table for open field data

Table-1.3
· SSD = 80 cm
· Electrometer PTW – UNIDOS
· Ionization chamber = 0.6 c.c
· Field size = 15 x 15 cm

Lateral positive distance in cm	Dose rate in mR	Dose rate in mGy	Central axis dose rate in mGy	Lateral negative distance in cm	Dose rate in mR	Dose rate in mGy
23	3.03	2.65		-1	587.1	514.30
22	3.42	3.00		-2	586	513.34
21	3.96	3.47		-3	584.4	511.93
20	4.41	3.86		-4	580.8	508.78
19	5.04	4.42		-5	576.6	505.10
18	5.4	4.73		-6	565.8	495.64
17	5.94	5.20		-7	397.4	348.12
16	6.84	5.99		-8	138.7	121.50
15	8.1	7.10		-9	34.62	30.33
14	9.51	8.33	523.32	-10	22.92	20.08
13	11.61	10.17		-11	16.92	14.82
12	14.58	12.77		-12	13.29	11.64
11	19.11	16.74		-13	10.62	9.30
10	23.48	20.57		-14	8.82	7.73
9	43.8	38.37		-15	7.56	6.62
8	212.2	185.89		-16	6.33	5.55
7	492.9	431.78		-17	5.58	4.89
6	581.7	509.57		-18	5.07	4.44
5	586.7	513.95		-19	4.65	4.07
4	591.6	518.24		-20	4.2	3.68
3	594.7	520.96		-21	3.6	3.15
2	596.3	522.36		-22	3.15	2.76
1	597.4	523.32		-23	2.76	2.42
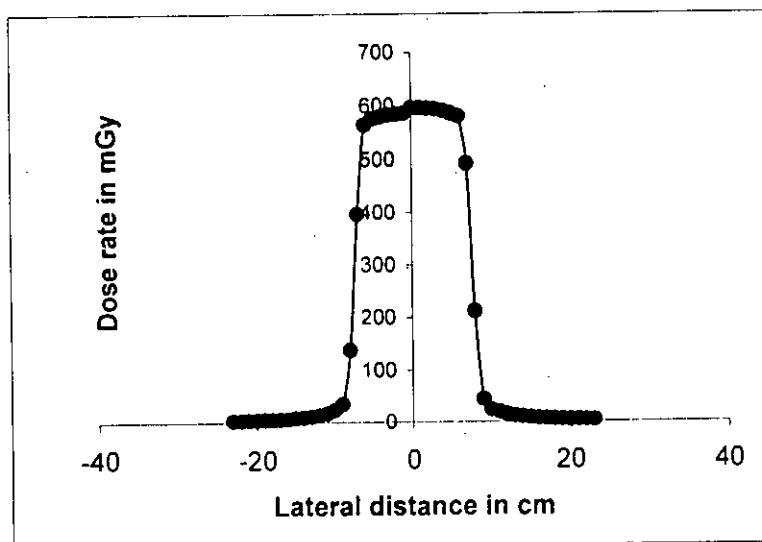
1. Table for open field data

Table-1.4
· S.S.D = 80 cm
· Field Size = 15 x 15 cm (Vertical)
· Electrometer PTW – UNIDOS
· Ionization Chamber = 0.6 CC

* Vertical distance in cm	Dose rate in mR	Dose rate in mGy	Central axis dose rate in mGy	Vertical distance in cm	Dose rate in mR	Dose rate in mGy
15	6.12	5.36		-1	588.3	515.3508
14	7.14	6.25		-2	586.3	513.5988
13	8.46	7.41		-3	583.8	511.4088
12	10.44	9.15		-4	581.1	509.0436
11	13.41	11.75		-5	576	504.576
10	18	15.77		-6	567.5	497.13
9	29.91	26.20		-7	424.1	371.5116
8	99.33	87.01		-8	89.85	78.7086
7	435.4	381.41		-9	30.69	26.88444
6	572.9	501.86	516.23	-10	19.77	17.31852
5	579.1	507.29		-11	14.49	12.69324
4	583.5	511.15		-12	11.13	9.74988
3	586.2	513.51		-13	9	7.884
2	588.2	515.26		-14	7.38	6.46488
1	589.2	516.14		-15	6.3	5.5188
0	589.3	516.23				

* Reference Fig.6.1

1. Table for open field data

Table-1.5
· S.S.D = 80 cm
· Field Size = 20 x 20 cm (Lateral)
· Electrometer PTW – UNIDOS
· Ionization Chamber = 0.6 CC

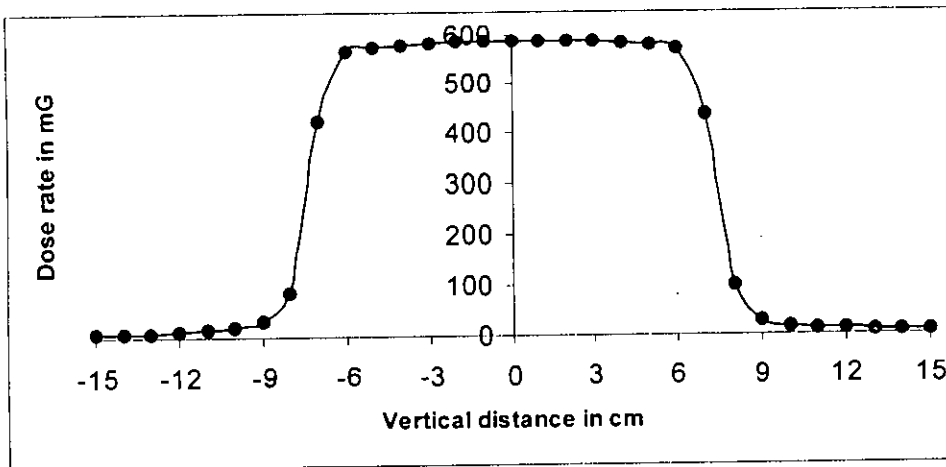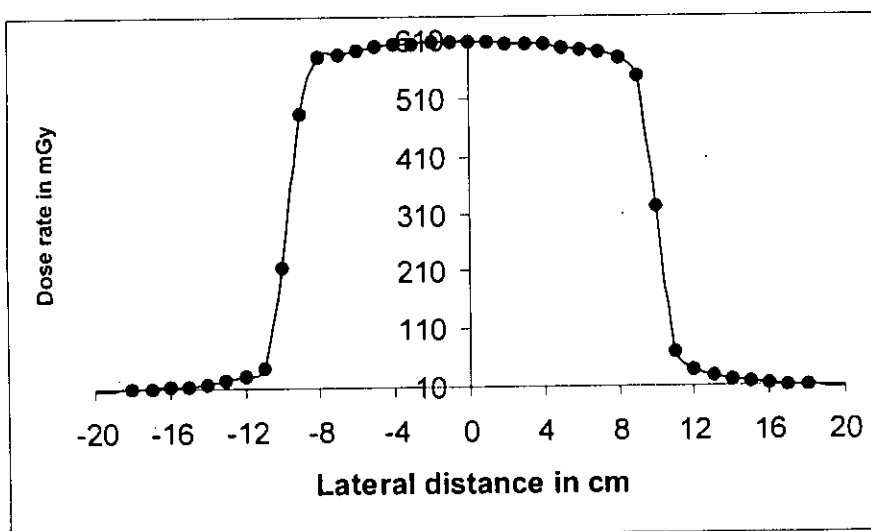| Lateral distance in cm	Dose rate in mR	Dose rate in mGy	Central axis dose rate in mGy	Lateral distance in cm	Dose rate in mR	Dose rate in mGy
20	7.05	6.18		-1	606.6	531.38
19	7.92	6.94		-2	605.7	530.59
18	9.18	8.04		-3	604.1	529.19
17	10.74	9.41		-4	601.8	527.18
16	13.08	11.46		-5	597.9	523.76
15	15.93	13.95		-6	593.3	519.73
14	19.5	17.08		-7	587.4	514.56
13	25.83	22.63		-8	580.9	508.87
12	37.11	32.51		-9	484.8	424.68
11	69.3	60.71		-10	217.5	190.53
10	322.7	282.69		-11	46.14	40.42
9	548.2	480.22	531.47	-12	31.95	27.99
8	578.7	506.94		-13	23.19	20.31
7	588.5	515.53		-14	17.73	15.53
6	593.9	520.26		-15	14.7	12.88
5	597.8	523.67		-16	12.21	10.70
4	601.5	526.91		-17	10.26	8.99
3	603.1	528.32		-18	8.49	7.44
2	604.6	529.63		-19	7.38	6.46
1	605.2	530.16		-20	6.3	5.52
0	606.7	531.47				

1. Table for open field data

Table-1.6
- S.S.D = 80 cm
- Field Size = 25 x 25 cm (Lateral)
- Electrometer PTW – UNIDOS
- Ionization Chamber = 0.6 CC

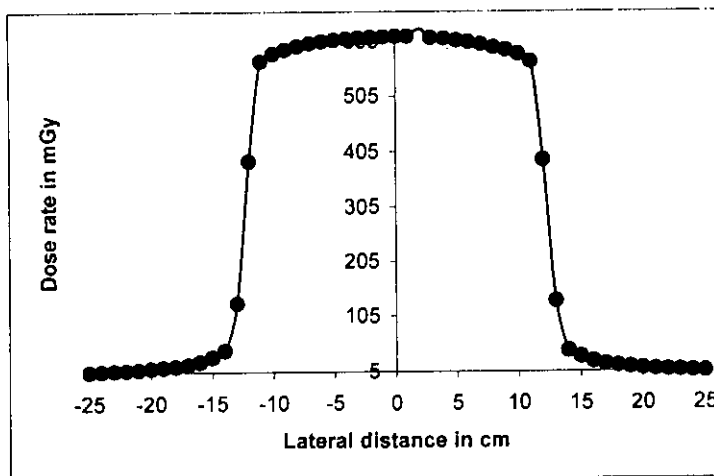| Lateral distance in cm	Dose rate in mR	Dose rate in mGy	Central axis dose rate in mGy	Lateral distance in cm	Dose rate in mR	Dose rate in mGy
25	5.67	4.97		-1	613.9	537.78
24	6.15	5.39		-2	613.5	537.43
23	7.05	6.18		-3	612.1	536.20
22	8.04	7.04		-4	610.7	534.97
21	9.3	8.15		-5	608.3	532.87
20	11.1	9.72		-6	605.7	530.59
19	12.96	11.35		-7	602.2	527.53
18	15.36	13.46		-8	597.1	523.06
17	18.39	16.11		-9	590.4	517.19
16	23.1	20.24		-10	583.2	510.88
15	31.2	27.33		-11	568.8	498.27
14	42.57	37.29		-12	388.4	340.24
13	131.9	115.54	538.65	-13	128.4	112.48
12	390.2	341.82		-14	43.05	37.71
11	568.6	498.09		-15	31.02	27.17
10	582.5	510.27		-16	22.89	20.05
9	590.1	516.93		-17	18	15.77
8	594.7	520.96		-18	15.09	13.22
7	600.6	526.13		-19	12.99	11.38
6	604.6	529.63		-20	11.13	9.75
5	607.5	532.17		-21	9.33	8.17
4	611	535.24		-22	8.04	7.04
3	611.9	536.02		-23	7.05	6.18
2	629	551.00		-24	6.15	5.39
1	614.9	538.65		-25	5.28	4.63
0	614.9	538.65				

1. Table for open field data

Table-1.7
· S.S.D = 80 cm
· Field Size = 25 x 25 cm (Vertical)
· Electrometer PTW – UNIDOS
· Ionization Chamber = 0.6 CC

Lateral distance in cm	Dose rate in mR	Dose rate in mGy	Central axis dose rate in mGy	Lateral distance in cm	Dose rate in mR	Dose rate in mGy
25	4.89	4.28		-1	613.8	537.69
24	5.61	4.91		-2	613.7	537.60
23	6.6	5.78		-3	612.7	536.73
22	7.38	6.46		-4	610.8	535.06
21	8.1	7.10		-5	607.1	531.82
20	9.42	8.25		-6	604.8	529.80
19	11.43	10.01		-7	595.6	521.75
18	13.29	11.64		-8	591.6	518.24
17	16.14	14.14		-9	586.5	513.77
16	20.19	17.69	538.3	-10	568.8	498.27
15	27.33	23.94		-11	562.5	492.75
14	42.15	36.92		-12	341.8	299.42
13	156.8	137.36		-13	69.69	61.05
12	468.7	410.58		-14	36.69	32.14
11	574.3	503.09		-15	26.1	22.86
10	582.6	510.36		-16	19.44	17.03
9	589.6	516.49		-17	15.24	13.35
8	595.6	521.75		-18	12.78	11.20
7	601.5	526.91		-19	10.47	9.17
6	604.8	529.80		-20	9	7.88
5	608.2	532.78		-21	7.65	6.70
4	611	535.24		-22	6.78	5.94
3	612.6	536.64		-23	5.94	5.20
2	614.3	538.13		-24	5.22	4.57
1	614.7	538.48		-25	4.65	4.07
0	614.5	538.30				
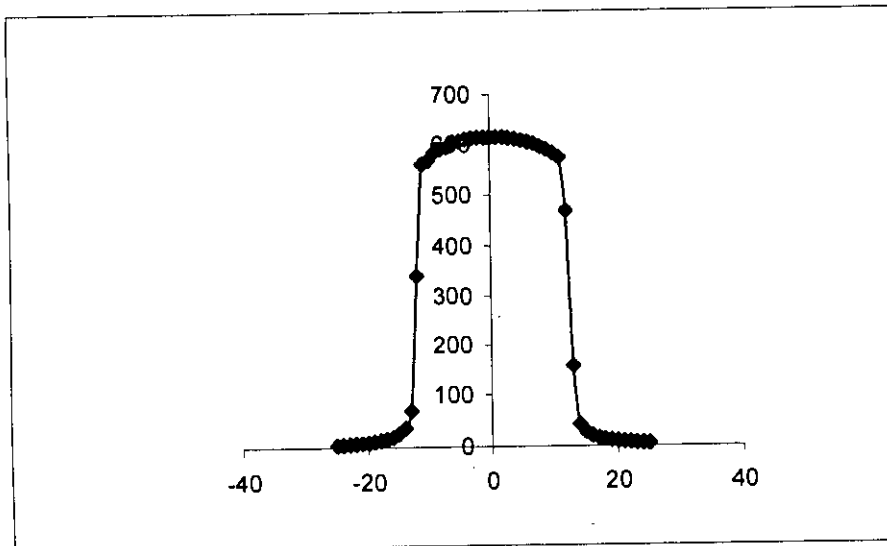
1. Table for open field data

Table-1.8
· S.S.D = 80 cm
· Field Size = 10 x10cm (diagonal distance)
· Electrometer PTW – UNIDOS
· Ionization Chamber = 0.6 CC

* Diagonal distance in cm	Dose rate in mR	Dose rate in mGy	Central axis dose rate in mGy	Diagonal distance in cm	Dose rate in mR	Dose rate in mGy
10	3.24	2.84		-1	558.9	489.60
9	4.14	3.63		-2	555.4	486.53
8	5.58	4.89		-3	544.9	477.33
7	8.13	7.12		-4	429	375.80
6	16.2	14.19		-5	156.2	136.83
5	157	137.53	490.38	-6	18.69	16.37
4	426.4	373.53		-7	8.16	7.15
3	537.4	470.76		-8	5.55	4.86
2	554.9	486.09		-9	3.96	3.47
1	558.5	489.25		-10	3.06	2.68
0	559.8	490.38				

* Reference Fig.6.1

1. Table for open field data

Table-1.9
· S.S.D = 80 cm
· Field Size = 10 x 10 cm (Diagonal distance)
· Electrometer PTW – UNIDOS
· Ionization Chamber = 0.6 CC

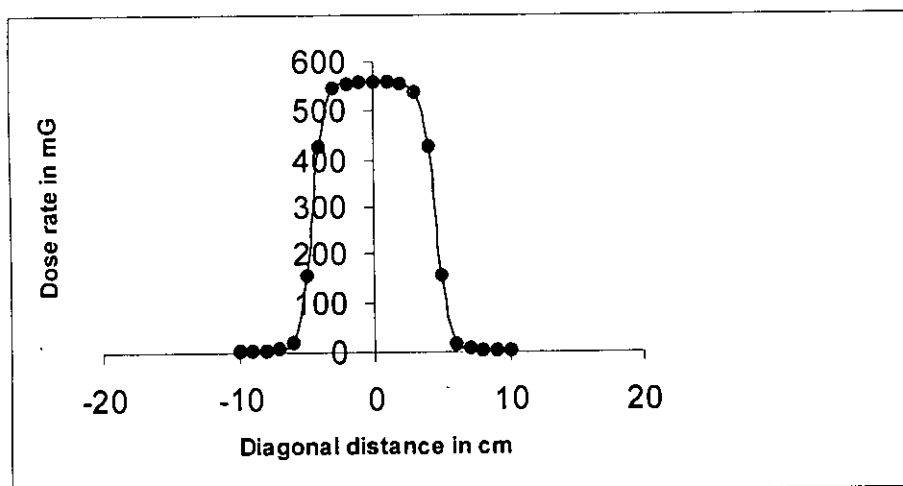| Diagonal distance in cm	Dose rate in mR	Dose rate in mGy	Central axis dose rate in mGy	Diagonal distance in cm	Dose rate in mR	Dose rate in mGy
10	3.15	2.76		-1	558.6	489.33
9	3.96	3.47		-2	555	486.18
8	5.37	4.70		-3	545.1	477.51
7	7.86	6.89		-4	442.4	387.54
6	15.48	13.56		-5	148.9	130.44
5	123.3	108.01		-6	15.54	13.61
4	445.1	389.91	489.95	-7	7.83	6.86
3	544.2	476.72		-8	5.25	4.60
2	554.2	485.48		-9	3.96	3.47
1	557.9	488.72		-10	3.06	2.68
0	559.3	489.95				

1. Table for open field data

Table-1.10
· S.S.D = 80 cm
· Field Size = 15 x 15 cm (Diagonal distance)
· Electrometer PTW – UNIDOS
· Ionization Chamber = 0.6 CC

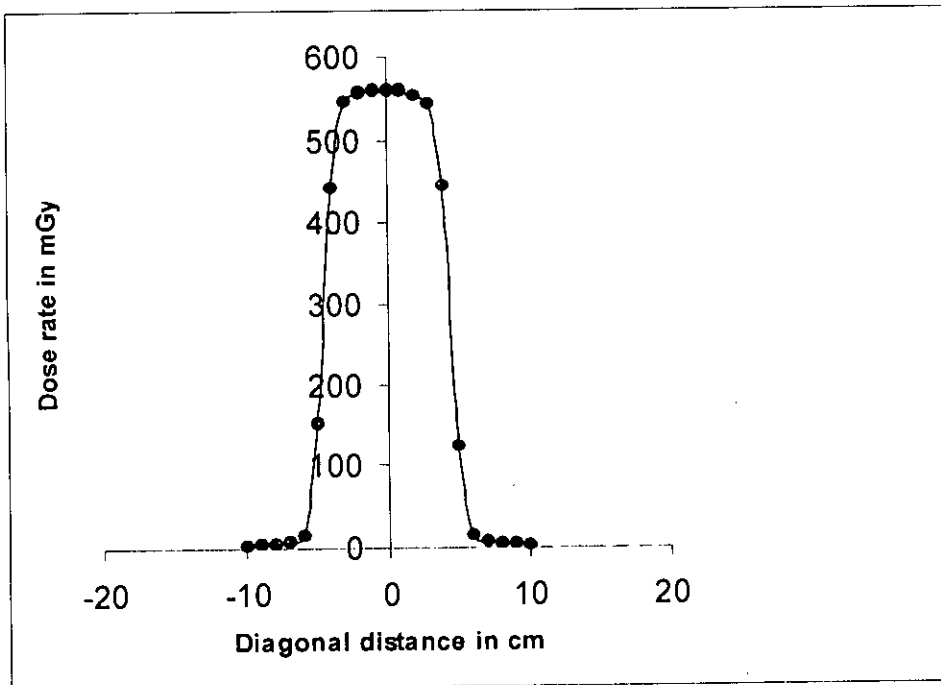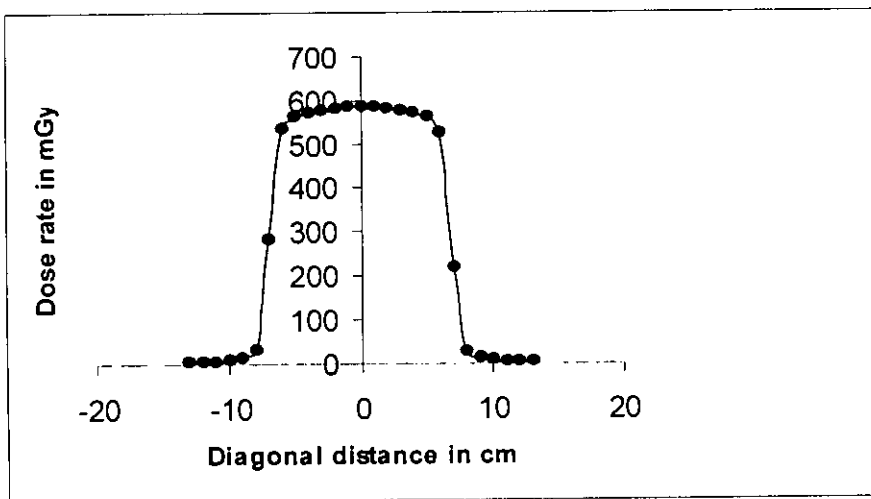| Diagonal distance in cm	Dose rate in mR	Dose rate in mGy	Central axis dose rate in mGy	Diagonal distance in cm	Dose rate in mR	Dose rate in mGy
13	3.96	3.47		-1	585.6	512.99
12	4.89	4.28		-2	583.1	510.80
11	6.48	5.68		-3	578.7	506.94
10	8.88	7.78		-4	572.1	501.16
9	13.8	12.09		-5	563.8	493.89
8	27.12	23.76		-6	534.3	468.05
7	219	191.84		-7	283.1	248.00
6	527.8	462.35	513.34	-8	34.08	29.85
5	562.8	493.01		-9	14.04	12.30
4	570.7	499.93		-10	9	7.88
3	577.2	505.63		-11	6.51	5.70
2	581.9	509.74		-12	5.01	4.39
1	585.4	512.81		-13	3.96	3.47
0	586	513.34				

1. Table for open field data

Table-1.11
· S.S.D = 80 cm
· Field Size = 20 x 20 cm (Diagonal distance)
· Electrometer PTW – UNIDOS
· Ionization Chamber = 0.6 CC

Diagonal distance in cm	Dose rate in mR	Dose rate in mGy	Central axis dose rate in mGy	Diagonal distance in cm	Dose rate in mR	Dose rate in mGy
16	4.2	3.68		-1	600.6	526.13
15	5.22	4.57		-2	599.6	525.25
14	6.78	5.94		-3	596.1	522.18
13	9.06	7.94		-4	591.6	518.24
12	12.81	11.22		-5	586	513.34
11	20.31	17.79		-6	577.7	506.07
10	86.82	76.05		-7	568.2	497.74
9	396.1	346.98		-8	553.4	484.78
8	544.7	477.16	527.09	-9	443.3	388.33
7	563.9	493.98		-10	142.1	124.48
6	572	501.07		-11	22.14	19.39
5	584.4	511.93		-12	13.11	11.48
4	590.3	517.10		-13	9.18	8.04
3	595.7	521.83		-14	6.87	6.02
2	599.2	524.90		-15	5.34	4.68
1	601.3	526.74		-16	4.32	3.78
0	601.7	527.09				
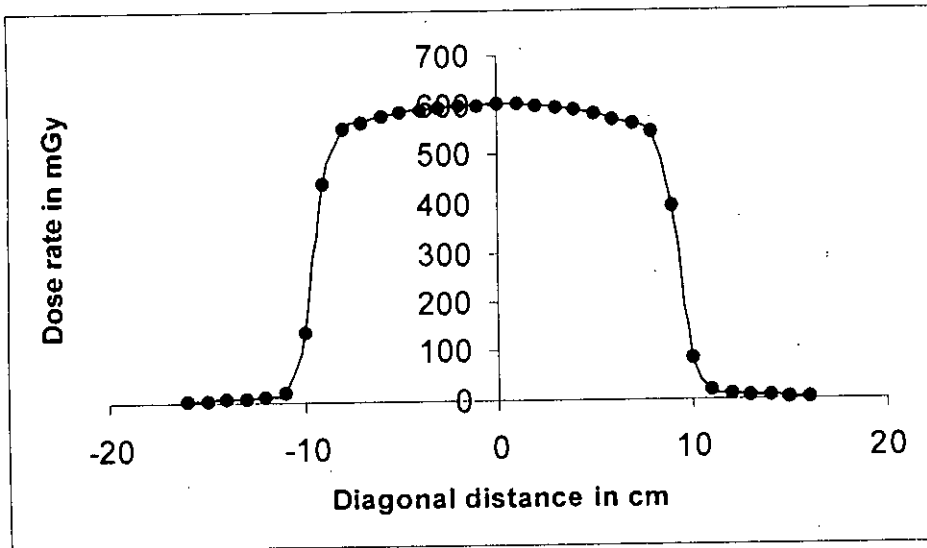
2. Table for first setup using half beam device

- S.S.D = 80 cm
- Field Size = 16 x 17 cm
- Electrometer PTW – UNIDOS
- Ionization Chamber = 0.6 CC
- Temperature = 23 deg. Celcius

Pressure:

Date	No. of points	Pressure
01.04.2004	From 1 to 48	Has not been known
22.04.2004	From 49 to 104	1000.03 hpa
06.05.2004	From 105 to 154	1012.8 hpa
12.05.2004	From 155 to 202	1001.01 hpa
13.05.2004	From 203 to 250	1000.2 hpa
19.05.2004	From 251 to 306	1002.6 hpa

* No. of Points	Dose/min in mGy (Uncorrected)	No. of Points	Dose/min in mGy (Uncorrected)	No. of Points	Dose/min in mGy (Uncorrected)	No of Points	Dose/min in mGy (Uncorrected)	No. of Points	Dose/min in mGy (Uncorrected)
1	6.89	63	20.19	125	11.31	187	557.8	249	543.4
2	9.12	64	20.31	126	8.34	188	559.3	250	535.3
3	10.17	65	20.04	127	7.26	189	559.8	251	469.3
4	10.05	66	19.68	128	8.52	190	560.1	252	278.6
5	11.16	67	19.77	129	9.48	191	558.9	253	249.8
6	10.53	68	19.44	130	10.05	192	557.1	254	445
7	12.15	69	18.87	131	10.59	193	555.3	255	522
8	11.46	70	18.36	132	11.82	194	551.6	256	534.9
9	12.27	71	15.93	133	12.75	195	547.1	257	538.7
10	12.51	72	10.59	134	13.53	196	534.8	258	542.4
11	13.26	73	10.98	135	13.77	197	444.2	259	543
12	13.02	74	15.84	136	15.48	198	247.1	260	544.3
13	12.78	75	18.54	137	16.56	199	257.9	261	544.9
14	13.68	76	19.44	138	17.61	200	458.4	262	544.3
15	12.03	77	20.01	139	14.82	201	535.6	263	544.1
16	12.96	78	20.37	140	13.41	202	548.3	264	542.3
17	11.55	79	20.46	141	12.27	203	552.3	265	540.3
18	7.5	80	21	142	23.16	204	555.5	266	537.6
19	9.18	81	20.64	143	17.91	205	557.7	267	533.5
20	12.84	82	20.16	144	14.7	206	559.6	268	526.1
21	16.35	83	20.67	145	134	207	560.4	269	454.5
22	17.01	84	20.94	146	199.5	208	560.4	270	276.9
23	17.37	85	20.79	147	250.1	209	559.5	271	235.6
24	18.3	86	20.13	148	243.7	210	557.5	272	431.3
25	18.39	87	19.44	149	208.2	211	555.4	273	512.3
26	18.57	88	18.18	150	280.3	212	552.4	274	520.6
27	18.72	89	15.12	151	213.3	213	547.9	275	525.7
28	18.45	90	10.2	152	273.7	214	541	276	530.1
29	18.57	91	9.87	153	285.2	215	471.8	277	525
30	18.03	92	13.83	154	344.5	216	300.7	278	531
31	17.79	93	16.44	155	341.8	217	282.6	279	518.9
32	17.46	94	18.36	156	505.6	218	471.1	280	518.5
33	17.31	95	19.92	157	436.4	219	539.9	281	525.8
34	16.89	96	21.27	158	437.6	220	547.8	282	521.4
35	11.64	97	21.6	159	426.9	221	551.9	283	516.3
36	8.97	98	21.6	160	389.5	222	554.3	284	501.1
37	9.75	99	21.96	161	344.1	223	556.4	285	517.5
38	14.04	100	21.81	162	182.7	224	557.5	286	510
39	17.13	101	21.99	163	247.8	225	558.1	287	414.3
40	17.97	102	21.75	164	443	226	558.1	288	293.6
41	18.51	103	21.51	165	527.9	227	557.2	289	211.2
42	18.72	104	20.13	166	544.5	228	555.5	290	315.8
43	19.14	105	18.42	167	548.3	229	552.9	291	427.1
44	19.05	106	16.62	168	551.9	230	549.9	292	296.3
45	19.05	107	13.74	169	553.5	231	545.5	293	302.9
46	19.35	108	9.87	170	554.3	232	539.2	294	289.8
47	19.41	109	9.18	171	555.3	233	468.5	295	355.6
48	19.23	110	12.75	172	554.8	234	280.2	296	336.8
49	18.51	111	14.58	173	555	235	290.2	297	371
50	18.72	112	14.73	174	553	236	473.9	298	310.3
51	18.54	113	17.43	175	552.1	237	537.7	299	349.1
52	17.91	114	17.43	176	549	238	544.4	300	356.3
53	15.3	115	18.75	177	544.5	239	548.3	301	328.6
54	9.9	116	18.45	178	530	240	551.4	302	305.9
55	11.04	117	18.72	179	436.3	241	553	303	384.7
56	15.3	118	17.64	180	255.1	242	554.3	304	327
57	18.18	119	17.22	181	260.4	243	555	305	302
58	18.87	120	15.99	182	446.5	244	555.1	306	188.5
59	19.23	121	15.6	183	537.9	245	554.2		
60	19.59	122	14.58	184	548.5	246	552.6		
61	20.13	123	13.71	185	552.8	247	551.1		
62	20.16	124	11.58	186	555.8	248	547.5		

* 1 point = 1 cm

117

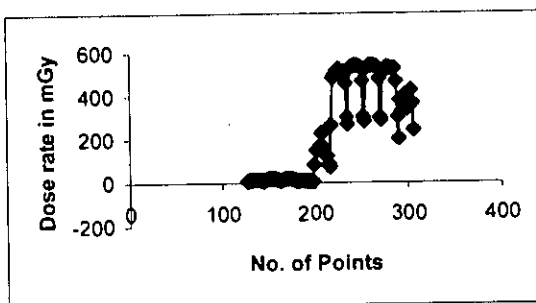## 3. Table for second setup using half beam device

- S.S.D = 80 cm
- Field Size = 9 x 17 cm
- Electrometer PTW – UNIDOS
- Ionization Chamber = 0.6 CC
- Temperature = 25 deg.Celcius

Pressure:

Date	No. of points	Pressure
20.05.2004	From 127 to 189	74.5 cm
02.06.2004	From 191 to 252	1004.9 hpa
03.06.2004	From 253 to 306	1002.7 hpa

* No. of Points	Dose/min in mGy (Uncorrected)	No. of Points	Dose/min in mGy (Uncorrected)	No. of Points	Dose/min in mGy (Uncorrected)	No. of Points	Dose/min in mGy (Uncorrected)
127	6.09	183	7.56	239	534	295	350.7
129	10.89	185	8.94	241	537.9	297	404.9
131	11.85	187	9.27	243	538.9	299	337.5
133	12.57	189	9.57	245	538.8	301	379.1
135	12.42	191	8.7	247	536	303	424.3
137	11.85	193	8.47	249	530.6	305	364.5
139	12.27	195	7.56	251	468.7	306	241.8
141	11.43	197	6.6	252	301.2		
143	9.54	198	5.31	253	283.2		
144	6.84	199	82.35	255	526.4		
145	7.2	201	145.6	257	535.6		
147	13.74	203	155	259	538.9		
149	16.95	205	167.1	261	540.8		
151	17.85	* 207	226.3	263	540.2		
153	17.82	209	161.1	265	537.2		
155	17.97	211	126.3	267	530.9		
157	17.67	213	122.4	269	477.4		
159	15.9	215	83.61	270	298.5		
161	11.85	216	73.68	271	288.4		
162	7.92	217	263.4	273	504.4		
163	7.47	219	483.8	275	522.7		
165	13.32	221	497.7	277	532.6		
167	16.8	223	515.4	279	530.2		
169	18.72	225	524.2	281	526.9		
171	18.09	227	508.2	283	524.6		
173	18.45	229	500.4	285	526.1		
175	18.33	231	511.4	287	465.5		
177	15.39	233	456.9	289	302.5		
179	11.7	234	300	290	201.9		
180	7.74	235	267.6	291	378		
181	5.22	237	522.7	293	323.4		

* 1 Point = 1 cm

118

4. Table for irregular shaped field data using half-beam device (3rd Setup)

Table-4.1
· Co- 60 Photon beam
· SSD=80cm
· Open field size=16 x17cm

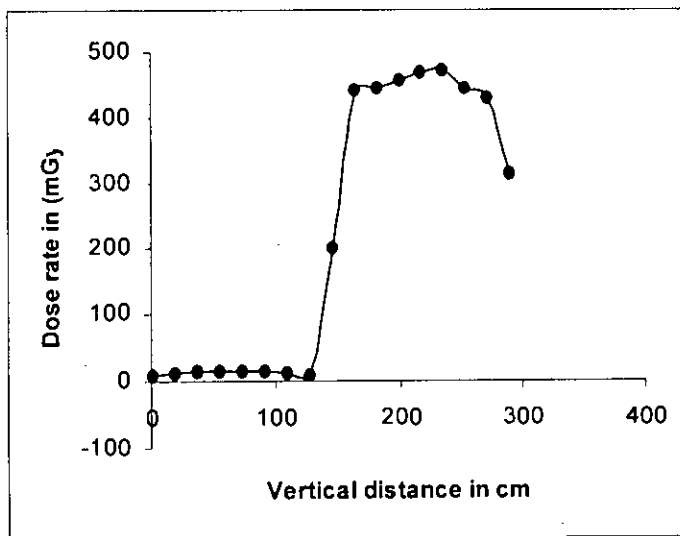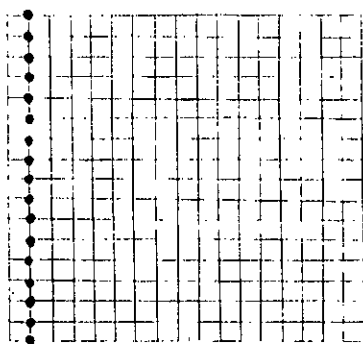| Vertical distance in cm	(Dose rate mGy)
1	6.87
19	9.18
37	9.75
55	11.04
73	10.98
91	9.87
109	9.18
127	7.26
145	134
163	247.8
181	260.4
199	257.9
217	281.6
235	290.2
253	249.8
271	235.6
289	211.2
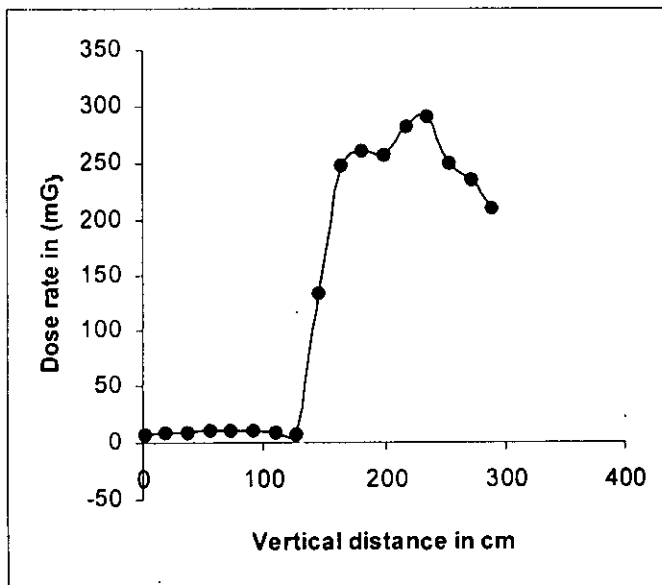
Fig:Dose rates on same line of the field
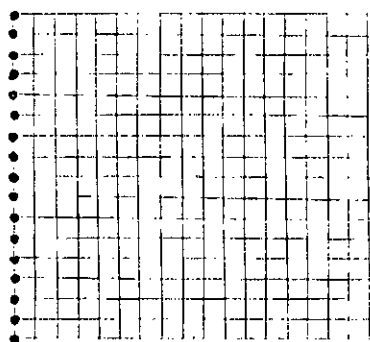
4. Table for irregular shaped field data using half-beam device (3rd Setup)

Table-4.2

· Co- 60 Photon beam
· SSD=80cm
· Open field size=16 x17cm

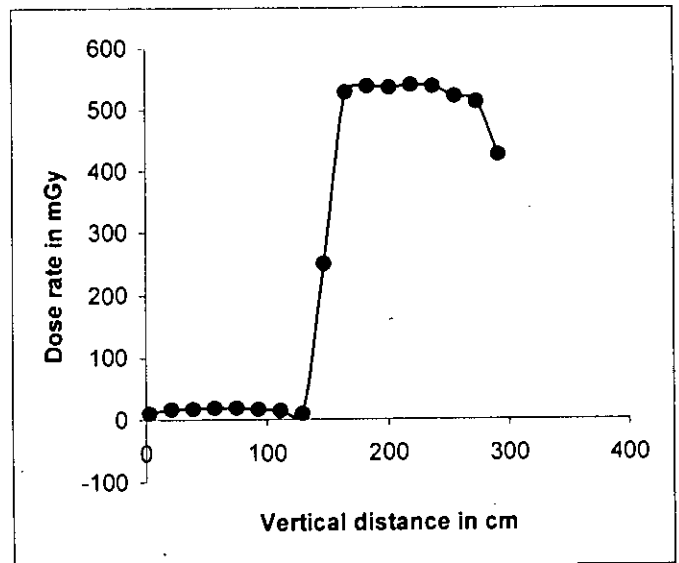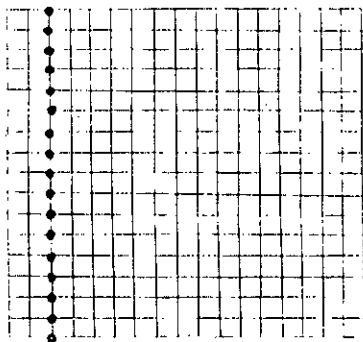| Vertical distance in cm	Dose rate(mGy)
2	9.12
20	12.84
38	14.04
56	15.3
74	15.84
92	13.83
110	12.75
128	8.52
146	199.5
164	443
182	446.5
200	458.4
218	471.1
236	473.9
254	445
272	431.3
290	315.8

Fig:Dose rates on same line of the field

4. Table for irregular shaped field data using half-beam device (3rd Setup)

Table-4.3

· Co- 60 Photon beam
· SSD=80cm
· Open field size=16 x17cm

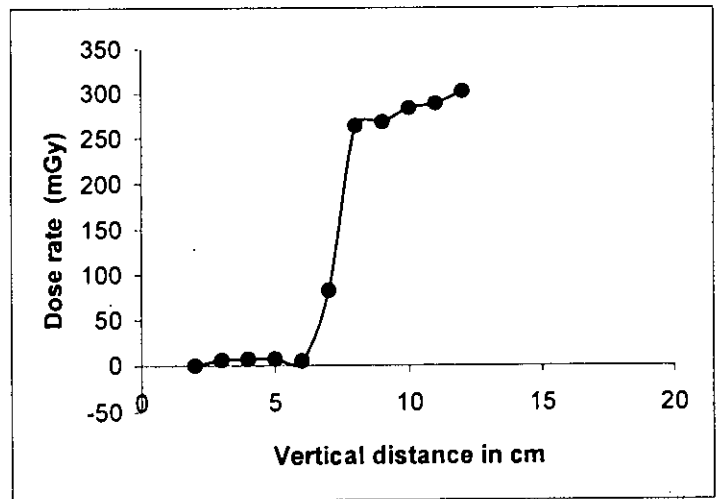| Vertical distance in cm	Dose rate(mGy)
3	10.17
21	16.35
39	17.13
57	18.88
75	18.54
93	16.44
111	14.58
129	9.48
147	250.1
165	527.9
183	537.9
201	535.6
219	539.9
237	537.7
255	522
273	512.3
291	427.1

Fig:Dose rates on same line of the field

4. Table for irregular shaped field data using half-beam device (3rd Setup)

Table-4.4
· Co- 60 Photon beam
· SSD=80cm
· Open field size=16 x17cm

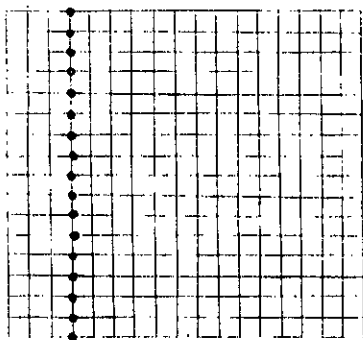| Vertical distance in cm	Dose rate(mGy)
4	10.05
22	17.01
40	17.97
58	18.87
76	19.44
94	18.36
112	14.73
130	10.05
148	243.7
166	544.5
184	548.5
202	548.3
220	547.8
238	544.4
256	534
274	520.6
292	296.3

Fig:Dose rates on same line of the field

4. Table for irregular shaped field data using half-beam device (3rd Setup)

Table-4.5
- Co- 60 Photon beam
- SSD=60cm
- Open field size=16 x17cm

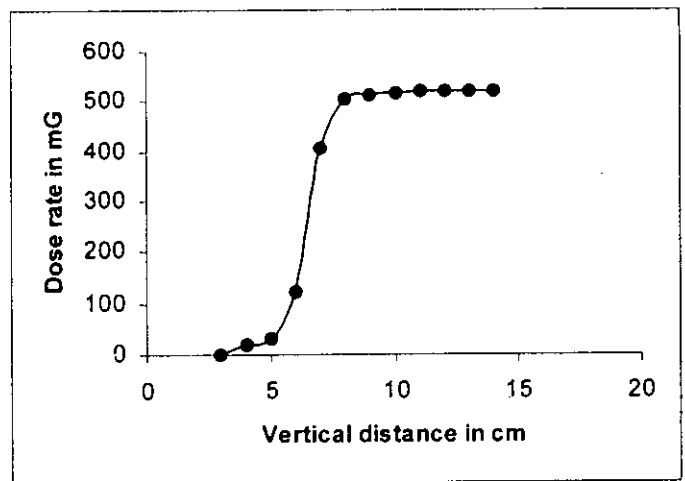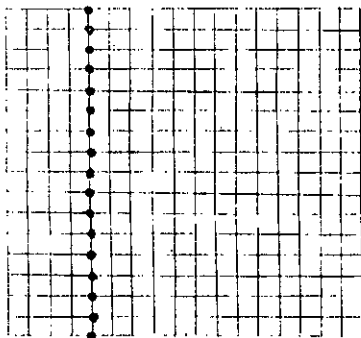| Vertical distance in cm	Dose rate(mGy)
5	11.16
23	17.37
41	18.51
59	19.23
77	20.01
95	19.92
113	17.43
131	10.59
149	208.2
167	548.3
185	552.8
203	552.3
221	551.9
239	548.3
257	538.7
275	525.7
293	302.9

Fig:Dose rates on same line of the field

4. Table for irregular shaped field data using half-beam device (3rd Setup)

Table-4.6
· Co- 60 Photon beam
· SSD=80cm
· Open field size=16 x17cm

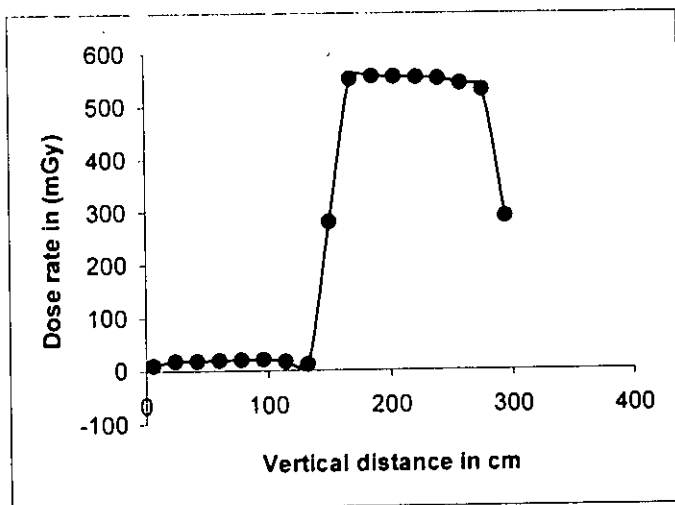| Vertical distance in cm	Dose rate(mGy)
6	10.53
24	18.3
42	18.72
60	19.59
78	20.37
96	21.27
114	17.43
132	11.82
150	280.3
168	551.9
186	555.8
204	555.5
222	554.3
240	551.4
258	542.4
276	530.1
294	289.8

Fig:Dose rates on same line of the field

4. Table for irregular shaped field data using half-beam device (3rd Setup)

Table-4.7
· Co- 60 Photon beam
· SSD=80cm
· Open field size=16 x17cm

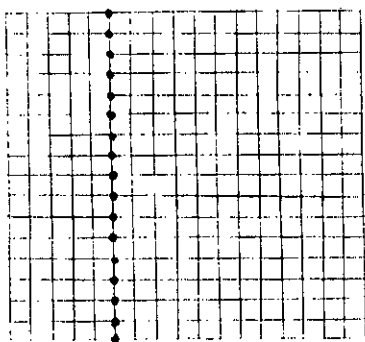| Vertical distance in cm	Dose rate(mGy)
7	12.15
25	18.39
43	19.14
61	20.13
79	20.46
97	21.6
115	18.75
133	12.75
157	436.4
169	553.5
187	557.8
205	557.7
223	556.4
241	553
259	543
277	525
295	355.6

Fig:Dose rates on same line of the field

4. Table for irregular shaped field data using half-beam device (3rd Setup)

Table-4.8
· Co- 60 Photon beam
· SSD=80cm
· Open field size=16 x17cm

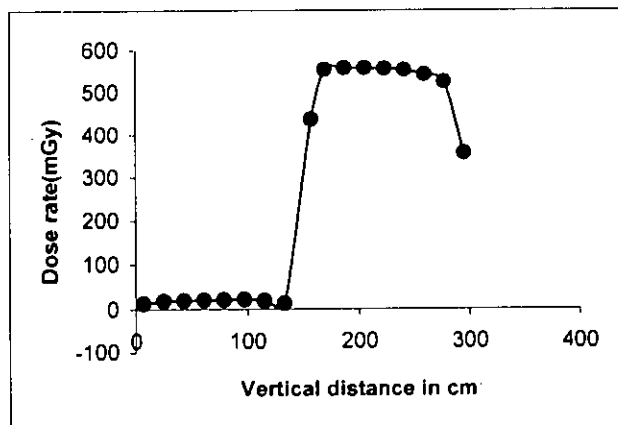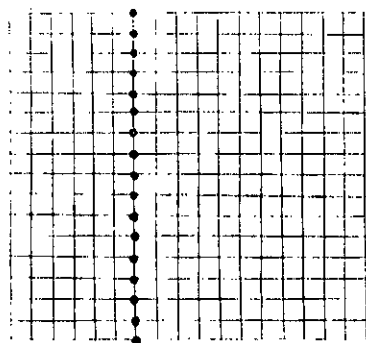| Vertical distance in cm	Dose rate(mGy)
8	11.46
26	18.57
44	19.05
62	20.16
80	21
98	21.6
116	18.45
134	13.53
152	273.7
170	554.3
188	559.3
206	559.6
224	557.5
242	554.3
260	544.3
278	531
296	336.8

Fig:Dose rates on same line of the field

4. Table for irregular shaped field data using half-beam device (3rd Setup)

Table-4.9
Co- 60 Photon beam
SSD=80cm
Open field size=16 x17cm

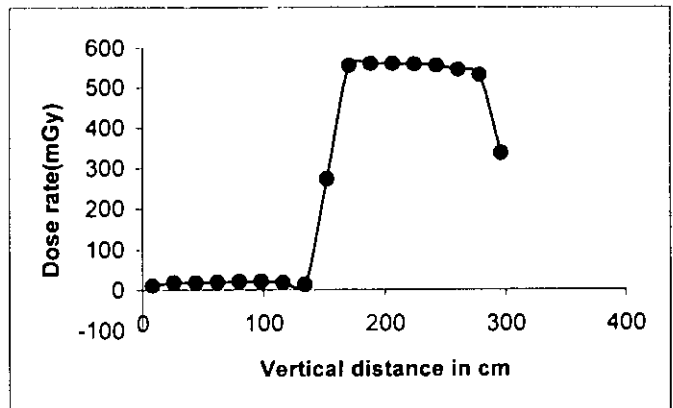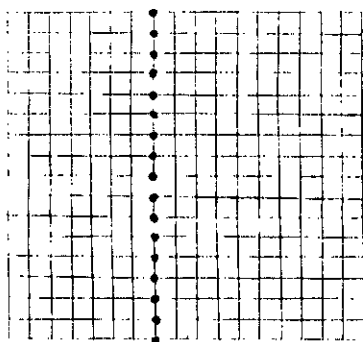| Vertical distance in cm	Dose rate(mGy)
9	12.27
27	18.72
45	19.05
63	20.19
81	20.64
99	21.96
117	18.72
135	13.77
153	285.2
171	555.3
189	559.8
207	560.4
225	558.1
243	555
261	544.9
279	518.9
297	371

Fig:Dose rates on same line of the field

4. Table for irregular shaped field data using half-beam device (3rd Setup)

Table-4.10
· Co- 60 Photon beam
· SSD=80cm
· Open field size=16 x17cm

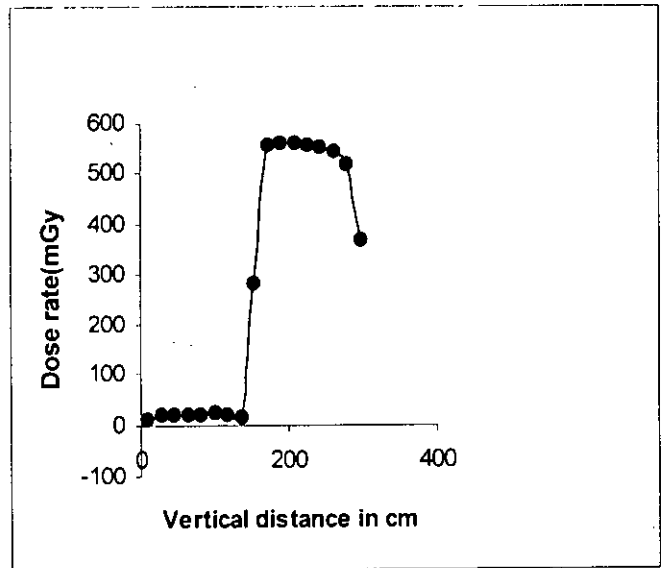| Vertical distance in cm	Dose rate(mGy)
10	12.51
28	18.45
46	19.35
64	20.31
82	20.16
100	21.81
118	17.64
136	15.48
154	344.5
172	554.8
190	560.1
208	560.4
226	558.1
244	555.1
262	544.3
280	518.5
298	310.3

Fig:Dose rates on same line of the field

4. Table for irregular shaped field data using half-beam device (3rd Setup)

Table-4.11
· Co- 60 Photon beam
· SSD=80cm
· Open field size=16 x17cm

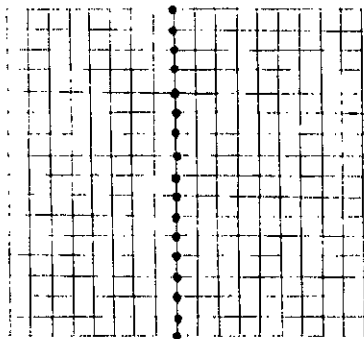| Vertical distance in cm	Dose rate(mGy)
11	13.26
29	18.57
47	19.41
65	20.04
83	20.67
101	21.99
119	17.22
137	16.56
155	341.8
173	555
191	558.9
209	559.5
227	557.2
245	554.2
263	544.1
281	525.8
299	349.1

Fig:Dose rates on same line of the field

129

4. Table for irregular shaped field data using half-beam device (3rd Setup)

Table- 4.12
· Co- 60 Photon beam
· SSD=80cm
· Open field size=16 x17cm

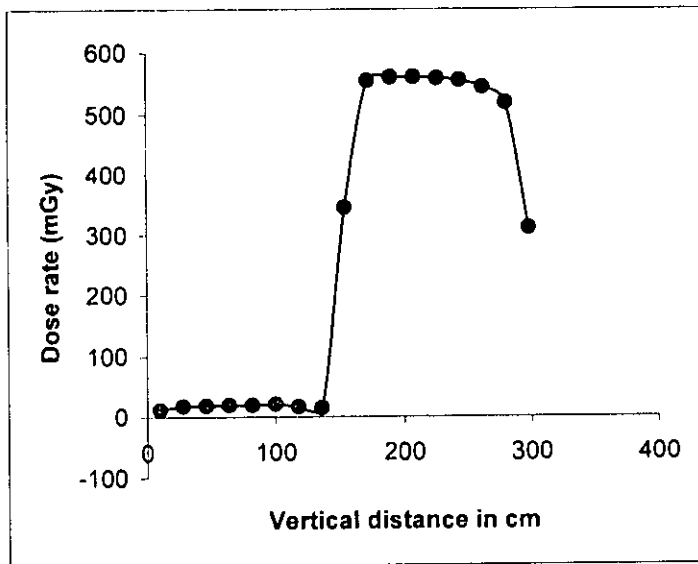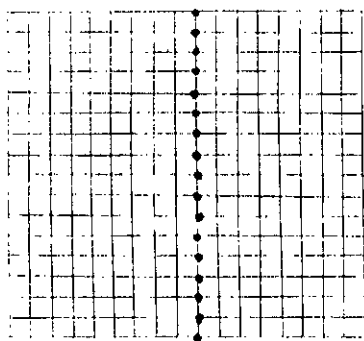| Vertical distance in cm	Dose rate(mGy)
12	13.02
30	18.03
48	19.23
66	19.68
84	20.94
102	21.75
120	15.99
138	17.61
156	505.6
174	553
192	557.1
210	557.5
228	555.5
246	552.6
264	542.3
282	521.4
300	356.3

Fig:Dose rates on same line of the field

4. Table for irregular shaped field data using half-beam device (3rd Setup)

Table-4.13
· Co- 60 Photon beam
· SSD=80cm
· Open field size=16 x17cm

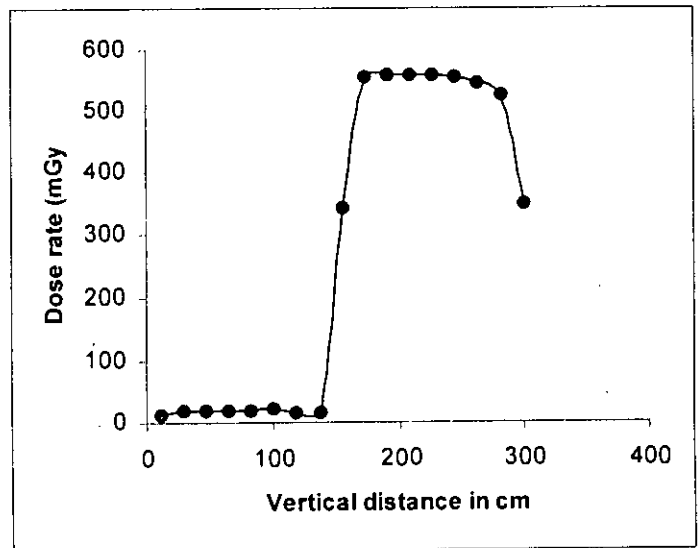| Vertical distance in cm	Dose rate(mGy)
13	12.78
31	17.79
49	18.51
67	19.77
85	20.79
103	21.51
121	15.6
139	14.82
157	436.4
175	552.1
193	555.3
211	555.4
229	552.9
247	551.1
265	540.3
283	516.3
301	328.6

Fig:Dose rates on same line of the field

4. Table for irregular shaped field data using half-beam device (3rd Setup)

Table-4.14
· Co- 60 Photon beam
· SSD=80crn
· Open field size=16 x17cm

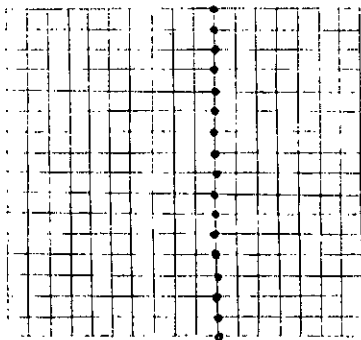| Vertical distance in cm	Dose rate(mGy)
14	13.68
32	17.46
50	18.72
68	19.44
86	20.13
104	20.13
122	14.58
140	13.41
158	437.6
176	549
194	551.6
212	552.4
230	549.9
248	547.5
266	537.6
284	501.1
302	305.9

Fig:Dose rates on same line of the field

4. Table for irregular shaped field data using half-beam device (3rd Setup)

Table-4.15
· Co- 60 Photon beam
· SSD=80cm
· Open field size=16 x17cm

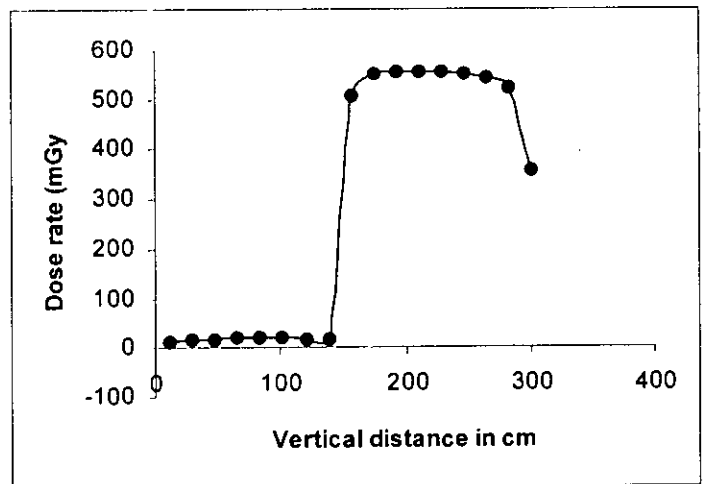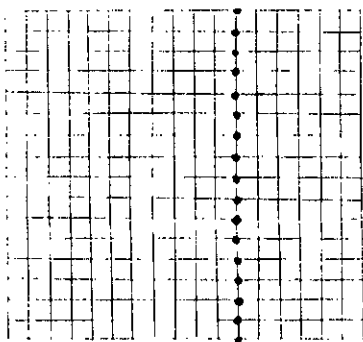| Vertical distance in cm	Dose rate(mGy)
15	12.03
33	17.31
51	18.54
79	20.46
87	19.44
105	18.42
123	13.71
141	12.27
159	426.9
177	544.5
195	547.1
213	547.9
231	545.5
249	543.4
267	533.5
285	517.5
303	384.7
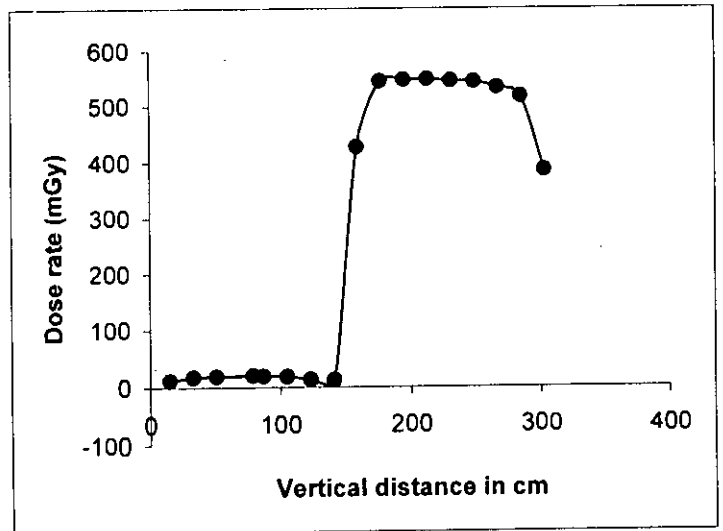
Fig:Dose rates on same line of the field
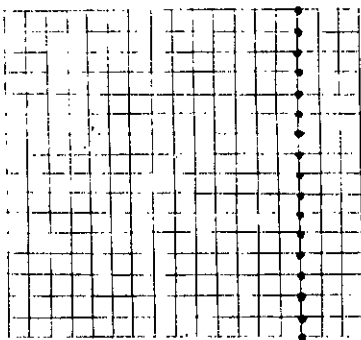
4. Table for irregular shaped field data using half-beam device (3rd Setup)

Table-4.16
· Co- 60 Photon beam
· SSD=80cm
· Open field size=16 x17cm

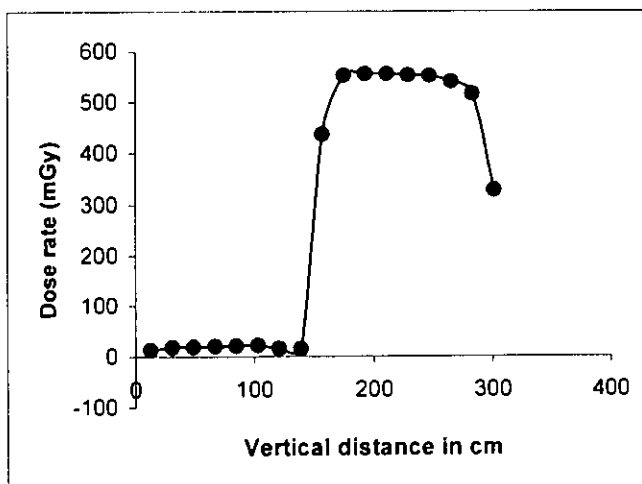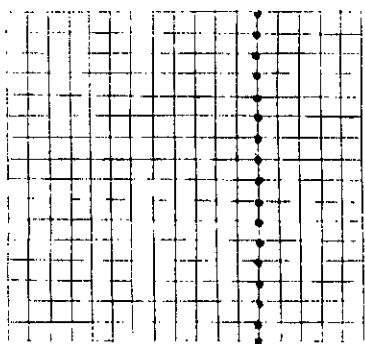| Vertical distance in cm	Dose rate(mGy)
16	12.96
34	16.89
52	17.91
70	18.36
88	18.18
106	16.62
124	11.58
142	23.16
160	389.5
178	530
196	534.8
214	541
232	539.2
250	535.3
268	526.1
286	510
304	327
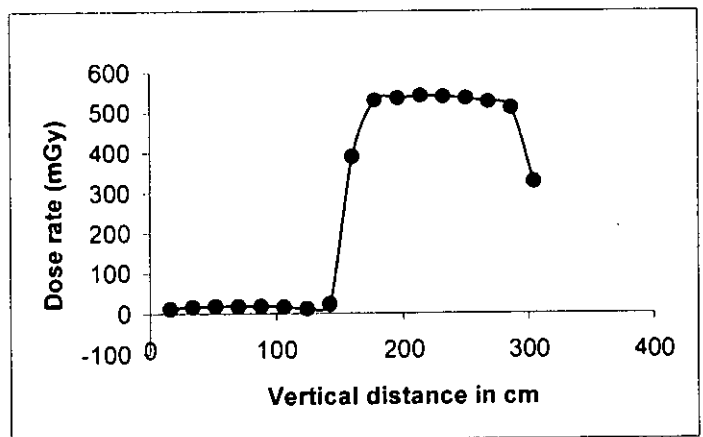
Fig:Dose rates on same line of the field
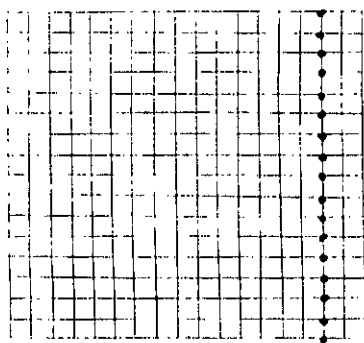
4. Table for irregular shaped field data using half-beam device (3rd Setup)

Table-4.17
· Co- 60 Photon beam
· SSD=80cm
· Open field size=16 x17cm

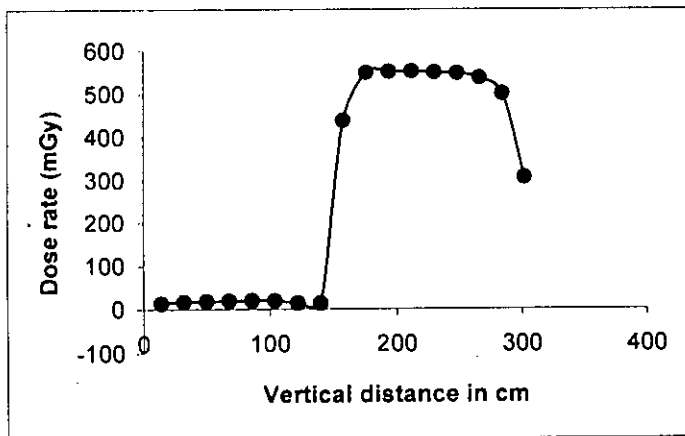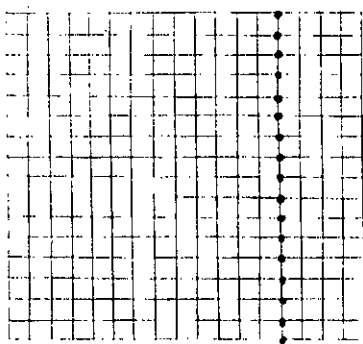| Vertical distance in cm	Dose rate(mGy)
17	11.55
35	11.64
53	15.3
71	15.93
89	15.12
107	13.74
125	11.31
143	17.91
161	344.1
179	436.3
197	444.2
215	471.8
233	468.5
251	469.3
269	454.5
287	414.3
305	302
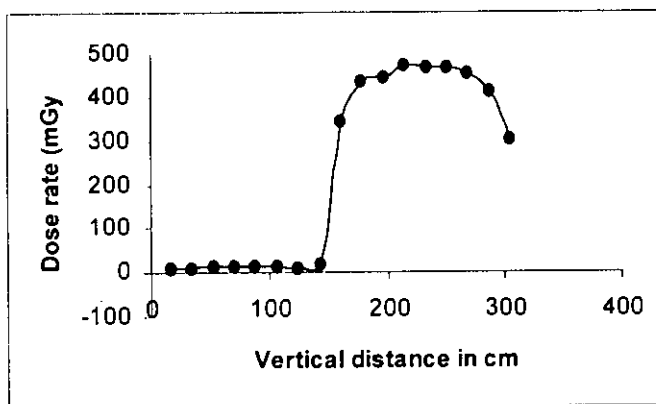
Fig:Dose rates on same line of the field
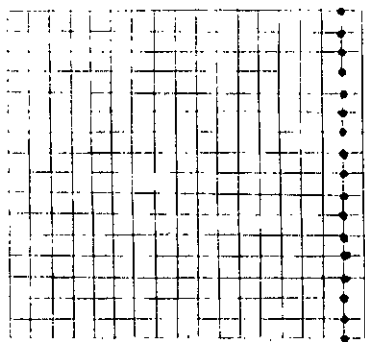
4. Table for irregular shaped field data using half-beam device (3rd Setup)

Table-4.18
· Co- 60 Photon beam
· SSD=80cm
· Open field size=16 x17cm

Vertical distance in cm	Dose rate(mGy)
18	7.5
36	8.97
54	9.9
72	10.59
90	10.2
108	9.78
126	8.34
144	14.7
162	182.7
180	255.1
198	247.1
216	300.7
234	280.2
252	278.6
270	276.9
288	293.6
306	188.5
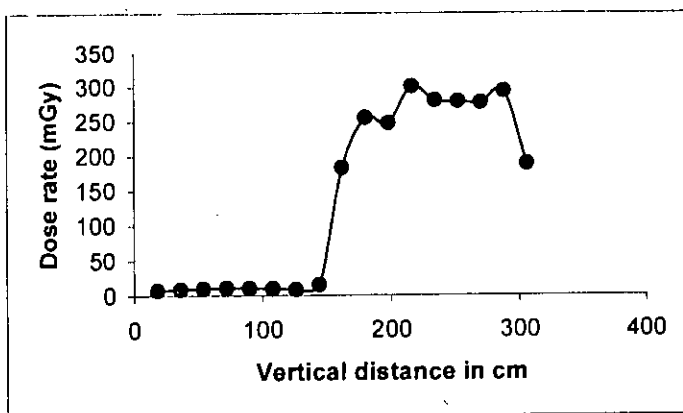
Fig:Dose rates on same line of the field
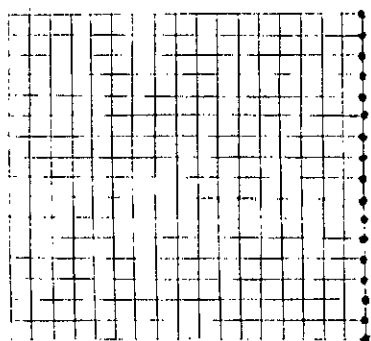
5. Table for irregular blocked field data (Inverted"Y" Field)

Table-5.1

· S.S.D = 80 cm
· Field Size = 15 x 15 cm (Lateral distance)
· Electrometer PTW – UNIDOS
· Ionization Chamber = 0.6 CC
· Temperature = 24 deg. Celcius
· Pressure = 1000.6 hpa

Lateral distance in cm	Uncorrected measured dose rate(mGy)	Correction factor	Corrected measured dose rate(mGy)
10	18.51		18.70
9	29.91		30.21
8	167		168.67
7	450.7		455.21
6	505.1		510.15
5	509		514.09
4	509.3		514.39
3	505		510.05
2	442.1		446.52
1	150.3	1.01	151.80
0	36.66		37.03
-1	139.2		140.59
-2	486.7		491.57
-3	508.4		513.48
-4	501.6		506.62
-5	498.2		503.18
-6	485		489.85
-7	356.9		360.47
-8	59.28		59.87
-9	27.27		27.54
-10	17.46		17.63

Fig. Inverted 'Y"
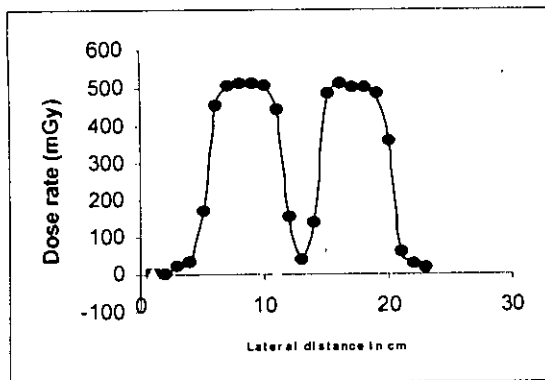
5. Table for irregular blocked field data (Inverted"Y" Field)

Table-5.2
· S.S.D = 80 cm
· Field Size = 15 x 15 cm (Lateral distance)
· Electrometer PTW – UNIDOS
· Ionization Chamber = 0.6 CC
· Temperature = 24 deg. Celcius
· Pressure = 1000.6 hpa

Lateral distance in cm	Measured dose(mGy)
7	450.7
6	505.1
5	509
4	509.3
3	505
2	442.1
1	150.3
0	36.66
-1	139.2
-2	486.7
-3	508.4
-4	501.6
-5	498.2
-6	485
-7	356.9
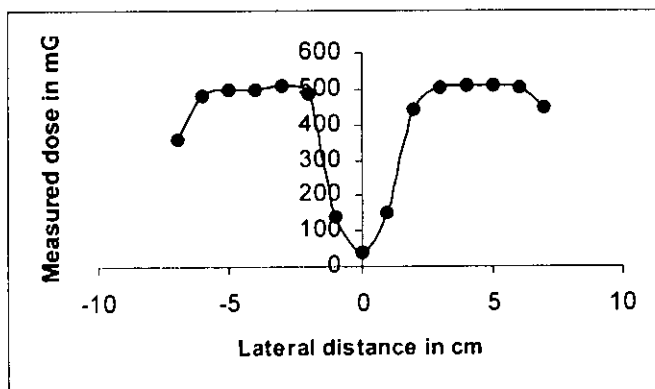
Table-5.3

Lateral distance in cm	Calculated dose(mGy)
7	418.38
6	530.71
5	540
4	540.32
3	535.7
2	469.03
1	157.92
0	38.52
-1	146.26
-2	516.34
-3	539.36
-4	532.15
-5	528.54
-6	509.59
-7	331.31
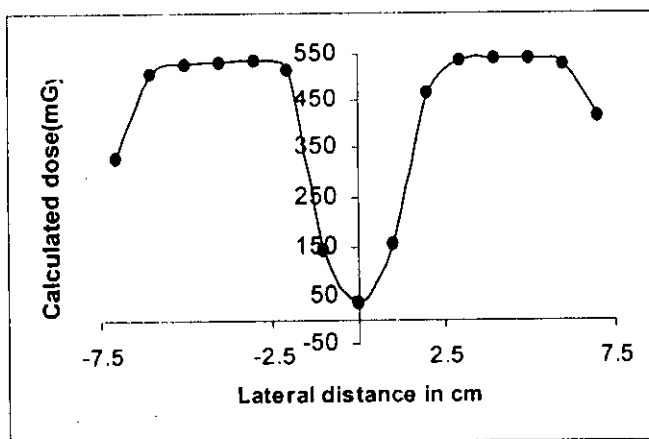
5. Table for irregular blocked field data (Inverted"Y" Field)

Table-5.4
- S.S.D = 80 cm
- Field Size = 15 x 15 cm (Lateral distance)
- Electrometer PTW – UNIDOS
- Ionization Chamber = 0.6 CC
- Temperature = 24 deg. Celcius
- Pressure = 1000.6 hpa

Lateral distance in cm	TAR(Tissue-air ratio)
7	0.91
6	1.03
5	1.04
4	1.04
3	1.04
2	1.04
1	1.03
0	1.03
-1	1.03
-2	1.04
-3	1.04
-4	1.04
-5	1.04
-6	1.03
-7	0.91
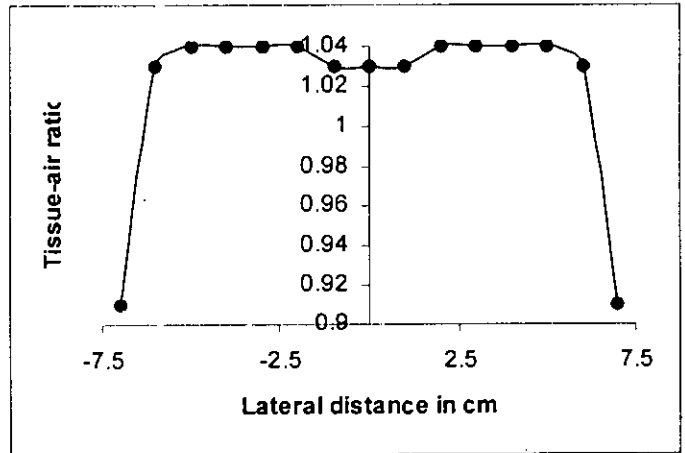
Table-5.5

| Lateral distance in cm	OAF(off-axis factor)
7	0.86
6	1
5	1
4	1
3	1
2	1
1	1
0	1
-1	1
-2	1
-3	1
-4	1
-5	1
-6	1
-7	0.86

6. Table for irregular blocked field (Two cornered blocked field)

Table- 6.1
· S.S.D = 80 cm
· Field Size = 15 x 15 cm (Lateral distance)
· Electrometer PTW – UNIDOS
· Ionization Chamber = 0.6 CC
· Temperature = 24 deg. Celcius
· Pressure = 1000.4 hpa

Lateral distance (cm)	Uncorrected measured dose rate(mGy)	Correction factor	Corrected measured dose rate(mGy)
10	20.31		20.51
9	29.94		30.24
8	121.8		123.02
7	408		412.08
6	506.2		511.26
5	511.5		516.62
4	516.4		521.56
3	519.4		524.59
2	521.3		526.51
1	522.3	1.01	527.52
0	522.8		528.03
-1	520.6		525.81
-2	519.4		524.59
-3	518.2		523.38
-4	516		521.16
-5	510.2		515.30
-6	503.4		508.43
-7	402.7		406.73
-8	120.1		121.30
-9	28.57		28.86
-10	19.99		20.19

6. Table for irregular blocked field (Two cornered blocked field)

Table-6.2
· S.S.D = 80 cm
· Field Size = 15 x 15 cm (Lateral distance)
· Electrometer PTW – UNIDOS
· Ionization Chamber = 0.6 CC
· Temperature = 24 deg. Celcius
· Pressure = 1000.4 hpa

Lateral distance in cm	Measured dose rate (mGy)
7	408
6	506.2
5	511.5
4	516.4
3	519.4
2	521.3
1	522.3
0	522.8
-1	520.6
-2	519.4
-3	518.2
-4	516
-5	510.2
-6	503.4
-7	402.7
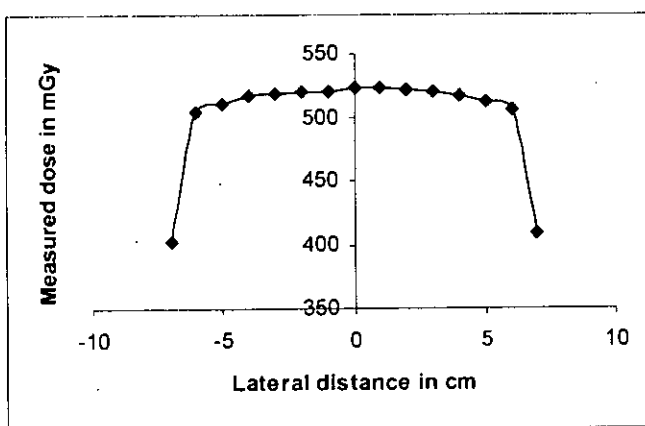
Table-6.3

Lateral distance in cm	Calculated dose rate (mGy)
7	382.9
6	537.03
5	542.65
4	547.85
3	556.33
2	558.37
1	559.44
0	559.97
-1	557.62
-2	556.33
-3	555.05
-4	547.43
-5	541.27
-6	534.06
-7	377.93
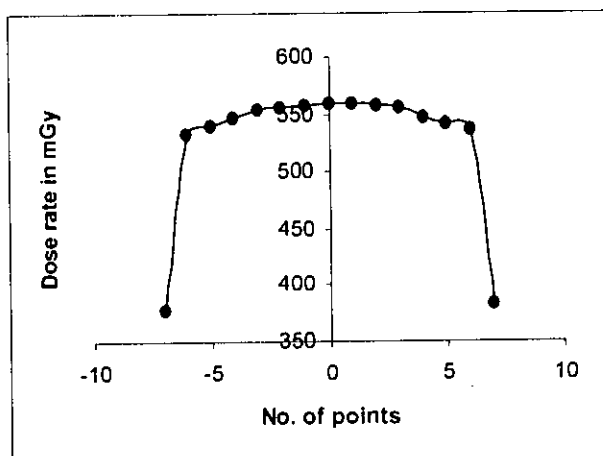
6. Table for irregular blocked field (Two cornered blocked field)

Table-6.4
- S.S.D = 80 cm
- Field Size = 15 x 15 cm (Lateral distance)
- Electrometer PTW – UNIDOS
- Ionization Chamber = 0.6 CC
- Temperature = 24 deg. Celcius
- Pressure = 1000.4 hpa

Lateral distance in cm	TAR(Tissue-air ratio)
7	0.92
6	1.04
5	1.04
4	1.04
3	1.05
2	1.05
1	1.05
0	1.05
-1	1.05
-2	1.05
-3	1.05
-4	1.04
-5	1.04
-6	1.04
-7	0.92
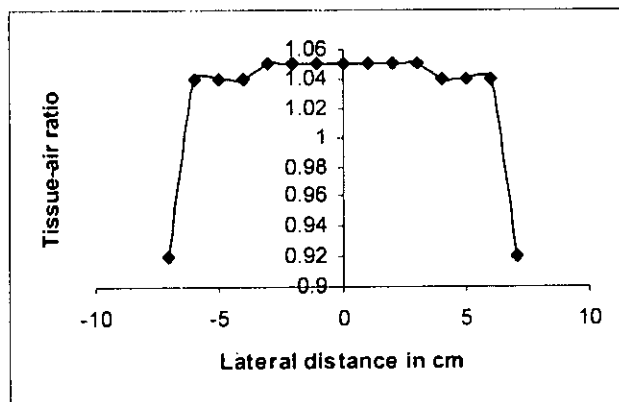
Table-6.5

Lateral distance in cm	OAF(off-axis factor)
7	0.86
6	1
5	1
4	1
3	1
2	1
1	1
0	1
-1	1
-2	1
-3	1
-4	1
-5	1
-6	1
-7	0.86

7. Table for irregular blocked field (Four corner- blocked field)

Table - 7.1
- S.S.D = 80 cm
- Field Size = 15 x 15 cm (Lateral distance)
- Electrometer PTW – UNIDOS
- Ionization Chamber = 0.6 CC
- Temperature = 24 deg. Celcius
- Pressure = 1000.4 hpa

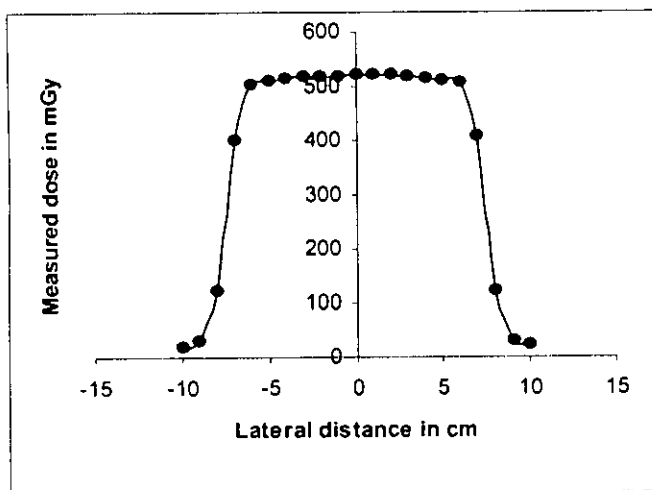| Lateral distance in cm	Uncorrected measured dose(mGy)	Correction factor	Corrected measured dose(mGy)
10	16.32		16.48
9	25.5		25.76
8	76.44		77.20
7	353.6		357.14
6	505.7		510.76
5	511.7		516.82
4	515.6		520.76
3	518.8		523.99
2	521.2	1.01	526.41
1	521.5		526.72
0	522.4		527.62
-1	521.3		526.51
-2	521.7		526.92
-3	519		524.19
-4	514.4		519.54
-5	511.3		516.41
-6	506.1		511.16
-7	352.2		355.72
-8	77		77.77
-9	25.1		25.35
-10	15.99		16.15
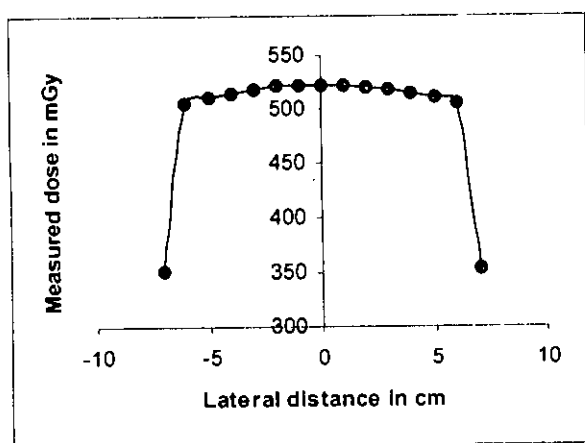
7. Table for irregular blocked field (Four corner- blocked field)

Table 7.2
- S.S.D = 80 cm
- Field Size = 15 x 15 cm (Lateral distance)
- Electrometer PTW – UNIDOS
- Ionization Chamber = 0.6 CC
- Temperature = 24 deg. Celcius
- Pressure = 1000.4 hpa

Lateral distance in cm	Measured dose(mGy)
7	353.6
6	505.7
5	511.7
4	515.6
3	518.8
2	521.2
1	521.5
0	522.4
-1	521.3
-2	521.7
-3	519
-4	514.4
-5	511.3
-6	506.1
-7	352.2
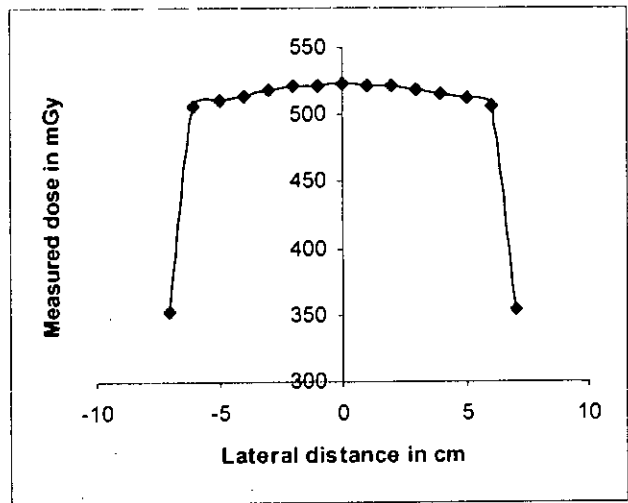
Table- 7.3

Lateral distance in cm	Calculated dose (mGy)
7	321.03
6	536.5
5	542.86
4	547
3	550.4
2	552.94
1	553.26
0	554.22
-1	553.05
-2	553.47
-3	550.61
-4	545.73
-5	542.44
-6	536.92
-7	319.76
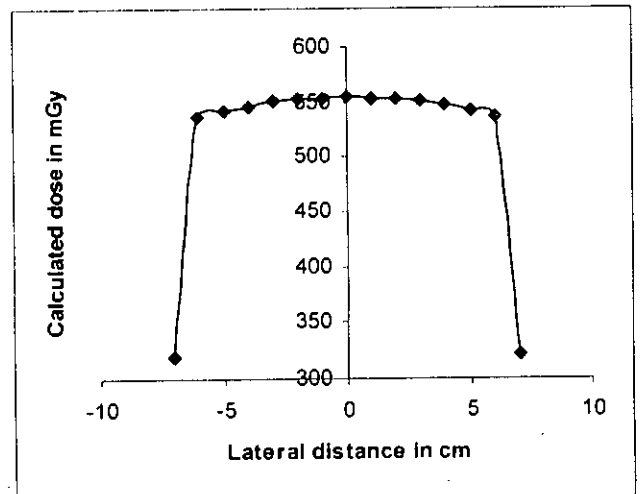
7. Table for irregular blocked field (Four corner- blocked field)

Table 7.4
- S.S.D = 80 cm
- Field Size = 15 x 15 cm (Lateral distance)
- Electrometer PTW – UNIDOS
- Ionization Chamber = 0.6 CC
- Temperature = 24 deg. Celcius
- Pressure = 1000.4 hpa

Lateral distance in cm	TAR (tissue-air ratio)
7	0.89
6	1.04
5	1.04
4	1.04
3	1.04
2	1.04
1	1.04
0	1.04
-1	1.04
-2	1.04
-3	1.04
-4	1.04
-5	1.04
-6	1.04
-7	0.89
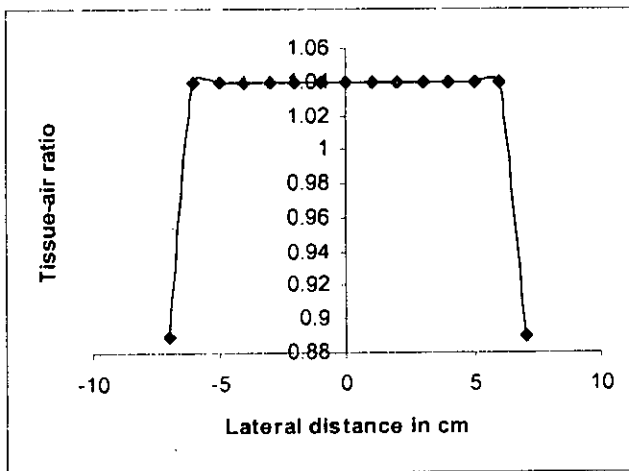
Table- 7.5

Lateral distance in cm	OAF (off-axis factor)
7	0.86
6	1
5	1
4	1
3	1
2	1
1	1
0	1
-1	1
-2	1
-3	1
-4	1
-5	1
-6	1
-7	0.86

145

8. Table for comparison between measured data & calculated data of blocked field

Table for Open -field
· Co- 60 Photon beam
· SSD=80cm
· Field size =15x15 cm
· Depth=0.5cm

Lateral distance in cm	Uncorrected dose rate(mR)	Conversion factor	Corrected dose rate(mGy)	Correction factor	Corrected dose (mGy)
7	435.4		381.41		385.22
6	572.9		501.86		506.88
5	579.1		507.29		512.36
4	583.5		511.15		516.26
3	586.2		513.51		518.65
2	588.2		515.26		520.42
1	589.2		516.14		521.30
0	589.3	0.876	516.23	1.01	521.39
-1	588.3		515.35		520.50
-2	586.3		513.60		518.73
-3	583.8		511.41		516.52
-4	581.1		509.04		514.13
-5	576		504.58		509.62
-6	567.5		497.13		502.10
-7	424.1		371.51		375.23

8. Table for comparison between measured data & calculated data of blocked field

8.1 - Table for blocked field
(Two cornered block)

· Co- 60 Photon beam
· SSD=80cm
· Field size =15x15 cm
· Depth=0.5cm

Lateral distance in cm	Uncorrected dose rate(mGy)	TAR (Tissue- air-ratio)	Correction factor	Corrected dose (mGy)
7	408	0.92		412.08
6	506.2	1.04		511.26
5	511.5	1.04		516.62
4	516.4	1.04		521.56
3	519.4	1.05		524.59
2	521.3	1.05		526.51
1	522.3	1.05		527.52
0	522.8	1.05	1.01	528.03
-1	520.6	1.05		525.81
-2	519.4	1.05		524.59
-3	518.2	1.05		523.38
-4	516	1.04		521.16
-5	510.2	1.04		515.30
-6	503.4	1.04		508.43
-7	402.7	0.92		406.73

8.2 - Table for percentage of deviation

Lateral distance in cm	Measured dose at block (mGy)	Calculated dose(mGy)	% of deviation
7	412.08	357.95	-13.14
6	511.26	532.43	4.14
5	516.62	538.18	4.17
4	521.56	542.28	3.97
3	524.59	550.03	4.85
2	526.51	551.91	4.82
1	527.52	552.84	3.76
0	528.03	552.93	4.72
-1	525.81	551.92	4.98
-2	524.59	550.11	4.87
-3	523.38	547.77	4.66
-4	521.16	540.04	3.62
-5	515.3	535.30	3.88
-6	508.43	527.41	3.73
-7	406.73	348.66	-14.28

8. Table for comparison between measured data & calculated data of blocked field

8.3 - Table for blocked field
(Four-block)

· Co- 60 Photon beam
· SSD=80cm
· Field size =15x15 cm
· Depth=0.5cm

Lateral distance in cm	Uncorrected dose rate(mGy)	TAR (Tissue- air-ratio)	Correction factor	Corrected dose (mGy)
7	353.6	0.89		357.14
6	505.7	1.04		510.76
5	511.7	1.04		516.82
4	515.6	1.04		520.76
3	518.8	1.04		523.99
2	521.2	1.04		526.41
1	521.5	1.04		526.72
0	522.4	1.04	1.01	527.62
-1	521.3	1.04		526.51
-2	521.7	1.04		526.92
-3	519	1.04		524.19
-4	514.4	1.04		519.54
-5	511.3	1.04		516.41
-6	506.1	1.04		511.16
-7	352.2	0.89		355.72

8.4 - Table for percentage of deviation

(Four-block)

Lateral distance in cm	Measured dose at block (mGy)	Calculated dose(mGy)	% of deviation
7	357.14	346.27	-3.04
6	510.76	532.43	4.24
5	516.82	538.18	4.13
4	520.76	542.28	4.13
3	523.99	544.79	3.97
2	526.41	546.65	3.84
1	526.72	547.57	3.96
0	527.62	547.67	3.8
-1	526.51	546.73	3.84
-2	526.92	544.87	3.41
-3	524.19	542.55	3.5
-4	519.54	540.04	3.95
-5	516.41	535.30	3.66
-6	511.16	527.41	3.18
-7	355.72	337.29	-5.18

8. Table for comparison between measured data & calculated data of blocked field

8.5 - Table for blocked field
(Inverted Y)

· Co- 60 Photon beam
· SSD=80cm
· Field size =15x15 cm
· Depth=0.5cm

Lateral distance in cm	Uncorrected dose rate(mGy)	TAR (Tissue- air-ratio)	Correction (TP) factor	Corrected dose (mGy)
7	450.7	0.91		455.21
6	505.1	1.03		510.15
5	509	1.04		514.09
4	509.3	1.04		514.39
3	505	1.04		510.05
2	442.1	1.04		446.52
1	150.3	1.03		151.80
0	36.66	1.03	1.01	37.03
-1	139.22	1.03		140.61
-2	486.7	1.04		491.57
-3	508.4	1.04		513.48
-4	501.6	1.04		506.62
-5	498.2	1.04		503.18
-6	485	1.03		489.85
-7	356.9	0.91		360.47

8.6 - Table for percentage of deviation
(Inverted Y)

Lateral distance in cm	Measured dose at block (mGy)	Calculated dose(mGy)	% of deviation
7	455.21	354.06	-22.22
6	510.15	527.31	3.36
5	514.09	538.18	4.69
4	514.39	542.28	5.42
3	510.05	544.79	6.81
2	446.52	-	-
1	151.8	-	-
0	37.03	-	-
-1	140.59	-	-
-2	91.57	-	-
-3	513.48	542.55	5.66
-4	506.62	540.04	6.60
-5	503.18	535.30	6.38
-6	489.85	522.33	6.63
-7	360.47	344.87	-4.33

9. Table for data for blocked field with wax

Table - 9.1
· Co- 60 Photon beam
· SSD=80cm
· Field size =20x20 cm
· Depth=0.5cm

Distance in cm	Dose rate in mR	Dose rate in mGy	Central axis dose rate in mGy	Distance in cm	Dose rate in mR	Dose rate in mGy
-12.5	55.71	48.80		0.5	62.28	54.56
-12	75.12	65.81		1	64.89	56.84
-11.5	125.9	110.29		1.5	65.91	57.74
-11	204.6	179.23		2	73.53	64.41
-10.5	290.1	254.13		2.5	98.34	86.15
-10	375.3	328.76		3	129.6	113.53
-9.5	437.5	383.25		3.5	207.6	181.86
-9	459.2	402.26		4	220.2	192.90
-8.5	463	405.59		4.5	273.5	239.59
-8	467.4	409.44		5	289.3	253.43
-7.5	469	410.84		5.5	406	355.66
-7	469.4	411.19		6	427.6	374.58
-6.5	466.4	408.57		6.5	466.4	408.57
-6	455.2	398.76	54.56	7	466.5	408.65
-5.5	406	355.66		7.5	469	410.84
-5	328.2	287.50		8	467.1	409.18
-4.5	273.5	239.59		8.5	463	405.59
-4	242.2	212.17		9	460.7	403.57
-3.5	207.6	181.86		9.5	437.5	383.25
-3	161.1	141.12		10	416.7	365.03
-2.5	105.9	92.77		10.5	290.1	254.13
-2	73.8	64.65		11	237.3	207.87
-1.5	65.91	57.74		11.5	125.9	110.29
-1	63.48	55.61		12	93.57	81.97
-0.5	62.28	54.56		12.5	55.71	48.80
0	62.28	54.56				
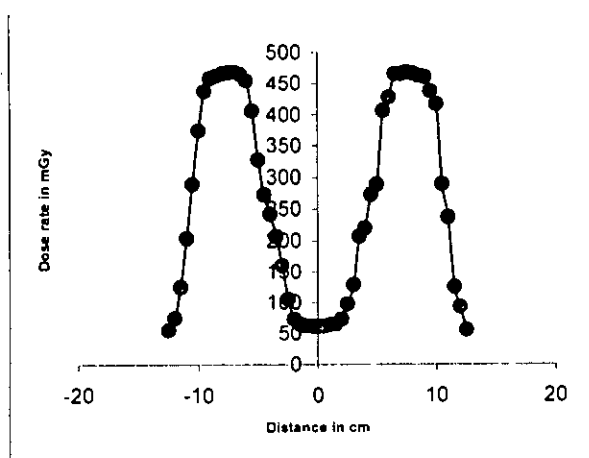
9. Table for data for blocked field with wax

Table - 9.2
· Co- 60 Photon beam
· SSD=80cm
· Field size =25x25 cm
· Depth=0.5cm

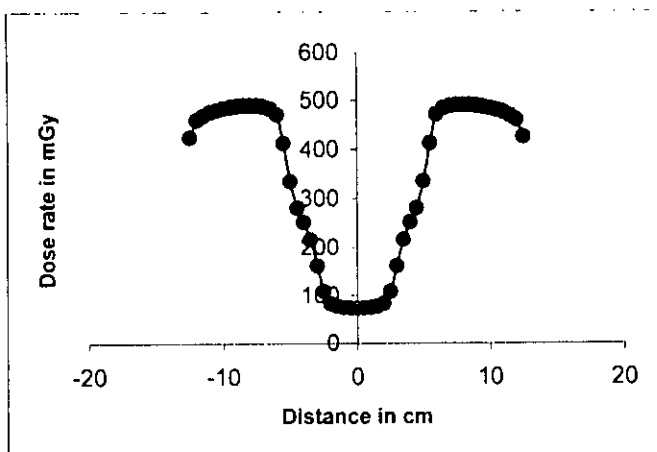| Distance in cm	Dose rate in mR	Dose rate in mGy	Central axis dose rate in mGy	Distance in cm	Dose rate in mR	Dose rate in mGy
-12.5	425.4	372.65		0.5	73.38	64.28
-12	460.8	403.66		1	74.49	65.25
-11.5	469.5	411.28		1.5	77.01	67.46
-11	476.5	417.41		2	83.04	72.74
-10.5	480.4	420.83		2.5	108.5	95.05
-10	484.4	424.33		3	161.5	141.47
-9.5	486.9	426.52		3.5	216.5	189.65
-9	489	428.36		4	252.2	220.93
-8.5	490.4	429.59		4.5	281.1	246.24
-8	490.7	429.85		5	335.8	294.16
-7.5	490.4	429.59		5.5	413.1	361.88
-7	488.4	427.84		6	471.9	413.38
-6.5	484.1	424.07		6.5	484.1	424.07
-6	471.9	413.38	64.23	7	488.4	427.84
-5.5	413.1	361.88		7.5	490.4	429.59
-5	335.8	294.16		8	490.7	429.85
-4.5	281.1	246.24		8.5	490.4	429.59
-4	252.2	220.93		9	489	428.36
-3.5	216.5	189.65		9.5	486.9	426.52
-3	161.5	141.47		10	484.4	424.33
-2.5	108.5	95.05		10.5	480.4	420.83
-2	83.04	72.74		11	476.5	417.41
-1.5	77.01	67.46		11.5	469.5	411.28
-1	74.49	65.25		12	460.8	403.66
-0.5	73.38	64.28		12.5	425.4	372.65
0	73.32	64.23				

9. Table for data for blocked field with wax

Table - 9.3
· Co- 60 Photon beam
· SSD=80cm
· Field size =15x15 cm
· Depth=0.5cm

Distance in cm	Dose rate in mR	Dose rate in mGy	Central axis dose rate in mGy	Distance in cm	Dose rate in mR	Dose rate in mGy
-10	38.32	33.57		0.5	50.01	43.81
-9.5	46.65	40.87		1	50.49	44.23
-9	71.85	62.94		1.5	51.84	45.41
-8.5	131.3	115.02		2	59.61	52.22
-8	209.3	183.35		2.5	90.33	79.13
-7.5	304.7	266.92		3	138.6	121.41
-7	382	334.63		3.5	184.7	161.80
-6.5	425.9	373.09		4	219.3	192.11
-6	429.8	376.50		4.5	246.8	216.20
-5.5	378.7	331.74	49.29	5	290.6	254.57
-5	317.1	277.78		5.5	365.2	319.92
-4.5	252.3	221.01		6	425.9	373.09
-4	228.3	199.99		6.5	433.9	380.10
-3.5	198.2	173.62		7	417.6	365.82
-3	154.4	135.25		7.5	351	307.48
-2.5	98.43	86.22		8	277.6	243.18
-2	61.17	53.58		8.5	190	166.44
-1.5	51.72	45.31		9	107.1	93.82
-1	49.65	43.49		9.5	58.32	51.09
-0.5	49.2	43.10		10	43.71	38.29
0	49.29	43.18				
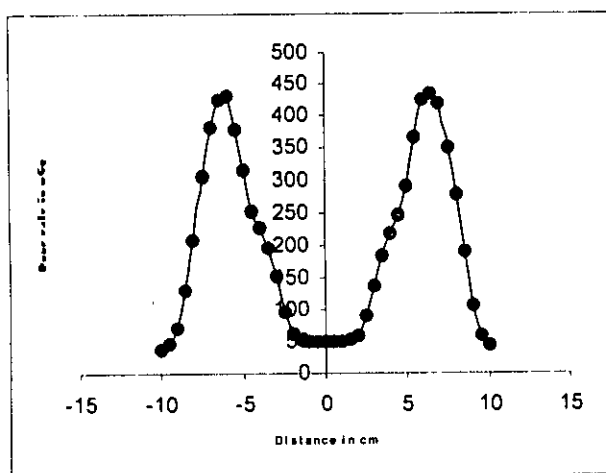
CHAPTER-7 Summary, Recommendation and Conclusion

7.1. Summary

The number of cancer patients in our country is increasing day by day. Among them the number of breast cancer patients is not so small. Cancer treatment is very much expensive all over the world. In our country, its treatment is improving also. In the present work, as the main objective was to investigate the doses using irregular field-shaping device, so the work was carried out giving emphasis mainly on finding the effect of the devices so that the treatment can be given to the cancer cells without affecting the normal tissues.

The motive of this study was to analyze the data of dose distribution for Co-60 photon beam for irregular field shaping device. For this purpose phantom of size 50 x 45 cm, thickness 1.5 cm and the irradiation facilities Co-60 teletherapy unit were used. For dose measurement 0.6 cc ionization chamber and PTW-UNIDOS electrometer were used. Open field doses for various field sizes such as 5x5 cm, 10x10cm, 15x15cm, 20x20 cm and 25x25 cm for lateral, vertical and diagonal distances were investigated first. The 'Half-beam device', which is used, for the breast cancer treatment was used as one of the irregular field-shaping devices. Three other irregular field-shaping devices were used. These were prepared with several rectangular blocks made of shielding material inserting the blocks into the shielding tray. The doses on points of both side of the central axis were measured by using the irregular field shaping devices.

The data were analyzed by making graphs using the points of dose measurement vs. the dose rate of these points and thus showing the effect of the irregular field-shaping device, which are used for the treatment of cancer.

Another special block made of lead alloy, which is routinely used for the pelvis cancer treatment was used with tissue-compensator for the dose measurement of various points, thus to find the effect of tissue-compensator. For finding the percentage of deviation for doses, the open field data was compared the blocked field data for the same field size 15x15 cm. The estimated deviations were 5%, which is very much within the limit of acceptability.

7.2. Recommendations

In our country, for the improvement of cancer treatment more works have to be done, so that people do not go abroad for treatment. For this, more and more seminars and workshops must be carried out throughout the country about the cancer disease. Scientists should be given opportunity to work on cancer treatment.

a) We have to increase the public awareness, specially for the illiterate peoples/ women residing in villages. For this purpose relevant data are necessary. The govt. should have a well-thought execution plan for solving the problem.

b) This awareness programme should have the target to fight against the problem when it is in the primary stage and thus will allow us to go for the solution adopting relatively an easier method.

c) Treatment facilities for cancer patients specially for breast cancer patients are very limited in the country. This has happened not only because of our financial crisis, rather the lack of a suitable national plan, which is more important. Such a plan may be implemented effectively when strong and capable hands of both government and non-government organizations are brought together.

d) A major problem for solving this type of a vital issue in our country is definitely shortage of resource personnel, who need to be trained from abroad. They must, at the same time be meritorious enough side by side having interest to work in this field. Making them interested for the work is the task of the govt. This should be ensured first.

e) For field level work, training activities should initially be arranged for the workers who will work in this level. This training should be started from the center of the country and subsequently be extended outwards to ultimately enclose the remote areas of the country.

7.3. Conclusion

In the case of half-beam device we tried to analyze the data making a graph using the points against the measured dose rate. So that it can be easy to give treatment to breast cancer patients without affecting much the normal tissues. From the name as 'half-beam' of the device it is clear that it makes the beam to the phantom or patient just half, so when the device is used, the field size of the treatment area becomes half. Hence carefully using this device, the affected area can be treated well without affecting the normal tissue. The objective of the present work was to find out the effect of this device, so that it can be useful for breast cancer treatment.

The data analysis in the case of irregular shaped fields; two-cornered blocked field, four-cornered blocked field and 'Inverted Y field' show that the dose rate varies with the distance of the central axis point i.e. with off-axis distance. Again for blocked field, the calculated dose is related to TAR (Tissue-air-ratio), so it depends also on the area of the blocks. Here another point is to be mentioned that the area of the block that we observe on the phantom is not the actual area of the blocks. Because as the blocks are

inserted into the shielding tray placed into the collimators, we see the shadow of the blocks on the phantom. So when we use the Clarkson's method to calculate the TAR value, we need the shadow area of the blocks. The other point is that as the calculated dose rate is related to the value of TAR, C_{TP} – temperature pressure factor, decay constant, then changing the above factors can change the value of calculated dose rate. As a result, though the percentage of deviation between measured and calculated value of dose should be below 5%, we found it different for different blocked field.

Considering the above discussion, it may be concluded that the treatment of cancer can be improved by making a careful use of these factors.

References

1. Sources of National Cancer Institute Information, Cancer Information Service, NCI Online Internet

2. A web module produced by Committee of the International Commission on Radiological Protection(ICRP)

3. Special Evaluation Review. The Agency's Technical Co operation Activities related to Quality Assurance and safety in Radiotherapy: Bangladesh. Evaluation Section, TCPC. Department of technical Co-operation. International Atomic Energy Agency IAEA-FER-98/03, Vienna, Austria, December 1998; pl-3.

4. Safety report series No.17 Lessons learned from accidental exposures in radiotherapy. IAEA, Vienna, Austria, 2000;p6

5. Design and Development of a Radiotherapy Programme: Medical Physics, Radiation Protection and safety Aspects, IAEA- TECDOC 1040, Vienna, Austia, 1998;pl-5

6. A E Nahnum. Extention of the Spencer Attix cavity thory to the 3 media situation for electron beam. Dosimetry in Radiotherapy proceedings of a Sympsium, Vienna, Austria, 31 August-4 September 1987, organized by IAEA in co operation with WHO. Vol. 1, IAEA, Vienna, Austria 1988;p87

7. PMK Leung, Physical Basis of Radiotherapy. Revised Ed. 1978; pl-2,84-85 , 144 , 212.

8. H E Johns. The physics of radiology Pub. Charles C Thomas Illinois, 3rd Ed. 1978; p272-303

9. William R. Hendee and Geofrey. Radiation Therapy physics. Pub. Mosby, Year Book . Inc. 11830 Westline Industrias Park. St. Louis, Missori. 2nd Ed. 1996; p428-429.

10. Technical Report Series No. 374. Calibration of Dosimeters used in Radiotherapy. IAEA, Vienna, Austria, 1994;p96-99.

11. James E Turner, Atom, Radiation and Radiation protection. Pub. Pergamon Press Inc 1st Ed. New York, 1986, P225-238

12. Mevatrons performance specifications, Medical linear accelerator for X-ray and electron ration therapy. Siemen's medical laborataries Inc. 5617-741 500 3U10 Revk May 15 ,1988 ; Pl- 1-3-3;

13. Jones DEA. A note on back –scatter and depth dose for elongated rectangular X-ray fields. Br. J Radiol 1949 ; 22; 342.

14. Belli JA. And Andrews Jr. Relationship between humor growth and radio sensitivity. J Nat Cancer Inst. 1963; 3 I : 689

15. Du Sault LA. The influence of the time factor on the dose response curve. Amer J Roentgen. 1962; 87; 567;.

16. Fowler JF. and Stern B.E. Dose – time relationships in radio therapy and the validity of survival curve models. Brit. J Radiold. 1963; 36: 163

17. Whitsome GF. , Gulyas S. and Botond J. Radiation senditivity throughout the cell cycle and its relationships to recovery. In cellular radiation biology '18th. Ann. Sym. Md Anderson Hospital Baltimore, williams & Wilkins. 1965; p423

18. Withers HR. Dose survival relationship for irradiaton of epithelial cells of mouse skin. Brt J Radio. 1967 ; 40 ; 335.

19. Alison P Casarett. Radiation Biology . Pub. Prentice- Hall Inc. Englewood cliffs, New Jersy, 1968; 32-72

20. Johns HE , Cunninhum Jr. The physics of Radiology 3rd Ed. Spring field. Illiois, Pub. Charles C Thomas 1969; p 210-238

21. Ulrich Quast, Dosimetry of non regular beams including TBI. Proceeding of the workshop on medical physics in radiotherapy and nuclear medicine, Dhaka, Banladesh, 5-10 December 1999; p15.

22. BJR, British Journal of Radiology, Supplement 25, 1997.

23. AAPM Task Group-21, A protocol for the Determination of Absorbed Dose from High Energy Photon and electron Beams, Med., Phy.1983.

24. TRS 398, Absorbed Dose Determination in External Beam Radiotherapy, IAEA, Vienna, 2000.

25. Cember H, Introduction to health physics, 2nd edition, McGraw-Hill, Inc. 1992.

26. P.H. van der Giessen, Dose outside the irradiated volume in radiradiotherapy, Dr. Bernard Verbeeten Institute, Tilburg, Netherlands, 1997.

27. Martin A and Harbison SA, An introduction to radiation protection, 2nd edition, Chapman and Hall Ltd.,1982.

28. ICRU, publication 60, Vol. 21, No. 1-3, 1990, Recommendations of the international commission on radiological protection, Pergamon press, Oxford UK, 1991.

29. Hendee WR, Medical Radiation Physics, 2nd edition, year book medical publishers inc., Chicago, London, 1979.

30. Ter-Pogossian M, The physical aspects of diagnostic radiology, Harper & Raw, New York, 1967.

31. Meredith W, Massey J, Fundamental physics of radiology, Williams and Wilkins Co., Baltimore, 1968.

32. Spiers F, Doses in bone, in clinical dosimetry, ICRU, report 10d, national bureau of standards handbook 87, 1963 (Appendix-II).

33. FM Khan, The Physics of radiotherapy, 2nd edition, Williams & Wilkins publishers, USA,1987.

34. Design and implementation of a radiotherapy programme. Clinical medical physics, radiation protection and safety aspects. IAEA, Vienna, Austria, September 1998 .

35. Khan F.M. Replacement correction (P$_{repl}$) for ion chamber dosimetry. Med Phys 1991;18: 1244.

36. Technical Report Series No. 277. Absorbed Dose determination in photon and electron beams. An international code of practice, 2nd ed. IAEA, Vienna, Austria, 1997.

37. Gray LH. An ionization method for the absolute measurement of gamma-ray energy. Proc. R Soc 1936, A 156-576.

38. Instruction Manual PTW-UNIDOS[D 196.131.0/5]

39. Technical Report Series No. 381.IAEA,Vienna, Austria, 1997;p24,49-51.

40. Technical Report Series No.374.Calibration of Dosimeters used in Radiotherapy.IAEA,Vienna,Austria,1994;p96-99

41. Greene. D., Massey J B. and Meredith W.J. Exposure dose measurements in megavoltage therapy. Phy. Med. Biol. 1962;6:551

42. F m Khan. The physics of Radiation Therapy. Pub. Lippincott Williams & Wilkins, 351 West Camden St, Baltimore,2nd Ed.1994; p94,98,101,117,138,181,300-325,328.

43. International Commission on Radiological Units and Measurements. Physical aspects of irradiation ICRU Report 10b, US National Bureau of Standards. 1964.

44. International Commission on Radiological Units and Measurements. Radiation quantities and units ICRU Report 33. 1980.

45. ICRU Report 10b, Handbook 85, US Nat.Bur of Standards Washington DC, 1962.

46. American Association of Physicists in Medicine. RTC Task groups 21. Protocols for the determination of absorb dose from high-energy photons and electron beams. Med. Phys 1983; 10:741

47. Walters and Miller's Text Book of Radiotherapy, Radiation Physics, Therapy and Oncology. Pub.Churchill Livingstone, Longman Group UK Ltd. 1993;p71, 84 – 85.

48. Radhe Mohan and Chen-Shou Chui, "Use of fast Fourier transformations in calculating dose distributions for irregularly shaped field for three-dimensional treatment planning",Med.Phys.,1987 Jan/Feb 14(1):70-77

49. Jun Lian, Cristian Cotrutz, and Lei Xing, "Therapeutic treatment plan optimization with probability density-based dose prescription", Med. Phys. 2003 April 30(4):655-665.

50. Dietmar Georg,Jorgen Olofss,Thomas Kunzler and Mikael Karlsson, " On empirical methods to determine scatter factors for irregular MLC shaped beams",Med.Phys. 2004 August 31(8):2222-2229

51. P.Vadash and B.E. Bjarngard, Med. Phys. 20,733-734(1993)

52. M.G. Devis, J.L. Horton, and J.A.Bencomo, "Use of simple quality assurance procedures in the analysis of beam asymmetries on Cobalt-60 treatment units", Med. Phys. 1996, April 23 (4): 523 – 524.

53. Michael K. fix, Harald Keller, and Peter Ruegsegger, Ernst J. Born, "Simple beam models for Montec Carlo photon beam dose calculation in radiotherapy", Med. Phys. 2000 December 27 (12); 2739 – 2746.

54. T.B. Tiourina ,W.J.F. Dries, and P.M. van der Linden, "Measurements and calculations of the absorbed dose distribution around a ^{60} Co source", Med. Phys. 1995 May 22(5):549-554

55. Chen-Show Chuy, Linda Hong, Margie Hund and Beryl McCormick, "A simplified intensity modulated radiation therapy technique for the breast", Med. Phys. 2002 April 29(4); 522 – 528.

56. H. Rashid, "Investigation of doses in irregular photon fields", Ph.D. thesis, April 2003.

Appendix

1. Equation for dose calculation:

$$\text{Time} = \frac{\text{Dose}}{\text{TAR X Output X SSD Factor X } C_{TP}}$$

Or, Dose =Time X TAR X Output X SSD factor X C_{TP} ... ...(1)

Where, Time= 1 min

TAR=Tissue-air ratio

Output =Measured dose rate in mGy

SSD factor =$(80.5/80)^2$
=1.01

C_{TP} =Temp.pressure correction factor

$$\text{Where,} C_{TP} = \frac{P_0}{P} \times \frac{273+t}{T_0}$$

$$= (\frac{1013}{P}) \text{ hpa X } (\frac{273+t}{22})^0k$$

Where, t = room temperature

p =room pressure in hpa

2. Conversion of pressure unit to SI unit (pascal)

To convert 1 mmHg pressure to 1 Pa(pascal) the conversion factor is 133.322. Hence, 1 atmospheric pressure is equal to 1.01325×10^5.

Now, hpa = hecto(10^2) Pa

Hence 1 atm pressure (760 cm)

$$= 1.013 \times 10^5 \text{ Pa}$$
$$= 1013 \text{ hpa}$$

3. Off-axis factor

The ratio of the primary component on the central axis to the primary component at some point off-axis is called the off-axis factor (OAF). The value of off-axis factors are given in chart 1.

4. TAR (Tissue-air-ratio)

$$\text{TAR} = \text{TA}\theta. \text{OAF} + \overline{\text{SAR}} \qquad \text{... ... ...(2)}$$

Where, TAθ is designed for 'zero' field size TAR. This 'zero area' TAR (TAθ) represents the primary component of the beam. The value of TAθ is 1 in this case.

$\overline{\text{SAR}}$ is termed as the average-scatter-air ratio and is calculated by Clarkson's method. The value of SAR is given in Chart 2

The example of calculation of $\overline{\text{SAR}}$ (i.e. TAR) is shown in Fig. 1 (two-cornered blocked field) and Table 1.

5. Calculation of percentage of deviation of dose rates

To get percentage of deviation of dose rates the following formula is used.

Calculated dose= open field dose X TAR X SSD factor ... ...(3)
(hypothetical)   (same point)   (at that point)

6. Decay factor

Decay factor =Dose/decay constant = Dose/1.011 ... ...(4)

Chart 1 for the value of off-axis factor

Field Length at 80 cm (cm)	0.75	0.775	0.80	0.825	0.85	0.875	0.90	0.925	0.95	0.975	1.00	1.025	1.05	1.075	1.1
						Reduced Off-Axis Distance in Either Direction†									
10	1.00	0.98	0.98	0.97	0.9.	0.88	0.84	0.78	0.70	0.63	0.53	0.43	0.34	0.29	0.16
15	1.00	1.00	1.00	0.97	0.97	0.94	0.92	0.86	0.79	0.71	0.53	0.38	0.25	0.19	0.09
20	1.00	1.00	1.00	1.00	1.00	0.98	0.96	0.91	0.85	0.75	0.53	0.33	0.18	0.11	0.06
30	1.00	1.00	1.00	1.00	1.00	1.00	0.99	0.95	0.89	0.80	0.53	0.28	0.12	0.04	

† The overall OAF is the product of OAF for each direction. For reduced off-axis distances less than 0.75 the OAF is 1.00

Chart 2 for the value of SAR (scatter-air-ratio)

| Depth (cm)	1	2	3	4	Field radius in cm at depth d 5	6	7	8	9	10	11	12
				0.025	0.033	0.037	0.051	0.043	0.054	0.058	0.063	0.067
1				0.048	0.020	0.065			0.091	0.023		0.028
		0.025	0.037	0.048	0.083	0.102	0.102	0.112	0.121	0.127		
	0.023	0.045	0.064	0.080	0.093	0.130	0.130	0.147	0.154	0.161	0.166	0.172
3	0.032	0.061	0.084	0.103	0.118	0.130	0.162	0.170	0.170	0.186	0.191	0.197
4	0.038	0.071	0.099	0.121	0.117	0.151	0.179	0.189	0.198	0.206	0.212	0.218
5	0.041	0.076	0.107	0.134	0.152	0.166	0.190	0.201	0.211	0.219	0.226	0.234
6	0.042	0.080	0.114	0.141	0.140	0.176	0.190	0.209	0.220	0.229	0.239	0.246
7	0.042	0.081	0.115	0.143	0.164	0.181	0.196	0.209	0.220	0.236	0.246	0.254
8	0.041	0.080	0.114	0.142	0.165	0.185	0.199	0.214	0.225	0.240	0.251	0.260
9	0.040	0.073	0.112	0.140	0.164	0.183	0.200	0.216	0.228	0.240	0.252	0.262
10	0.038	0.075	0.109	0.136	0.161	0.181	0.199	0.215	0.229	0.242	0.252	0.262
11	0.036	0.071	0.104	0.132	0.157	0.179	0.197	0.213	0.227	0.241	0.252	0.262
12	0.035	0.069	0.099	0.128	0.153	0.174	0.194	0.210	0.225	0.239	0.251	0.261
13	0.034	0.066	0.095	0.124	0.149	0.170	0.190	0.207	0.223	0.237	0.249	0.260
14	0.032	0.063	0.063	0.092	0.120	0.168	0.186	0.204	0.220	0.235	0.247	0.258
15	0.031	0.060	0.089	0.116	0.140	0.162	0.182	0.200	0.216	0.231	0.211	0.255
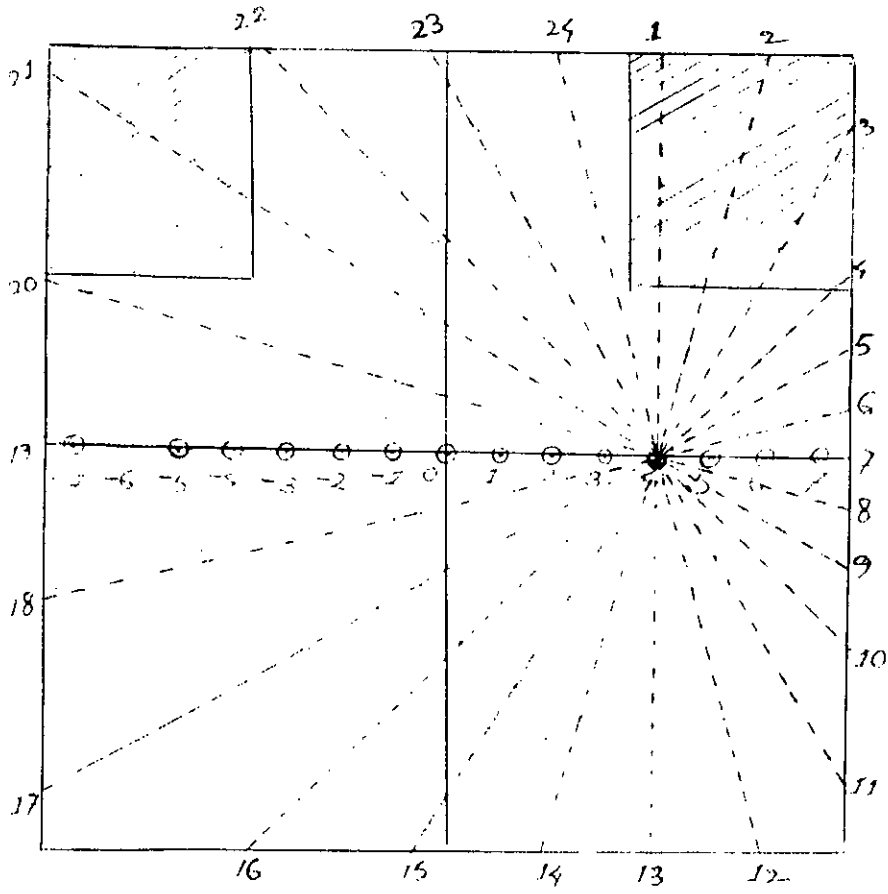
Fig.1 Example of the process of calculation of SAR using Clarkson's method for two-cornered blocked field for 15x15 cm field size

Table for example of calculation of TAR for point.4 of two-cornered blocked field

Radius no.	Nearest length (cm)	SAR (Chart 2)
1	4	0.026
2	4	0.026
3	4	0.026
4	5	0.032
5	4	0.026
6	5	0.032
7	4	0.026
8	4	0.026
9	4	0.026
10	5	0.032
11	7	0.043
12	8	0.048
13	8	0.048
14	8	0.048
15	9	0.054
16	11	0.063
17	14	0.073
18	12	0.067
19	12	0.067
20	11	0.063
21	9	0.054
22	11	0.063
23	9	0.054
24	8	0.048

$$\Sigma \ SAR = 1.07$$

$$\text{Therefore, } \overline{SAR} = \frac{1.07}{24}$$

$$= 0.04$$

Reduced off-axis distance for point is $\dfrac{4}{7.5} = 0.53$

which is less than 0.75 then from Table 2 we get OAF = 1.

Hence. $\overline{TAR}$ = TAθ . OAF + SAR = 1.1 + 0.04 = 1.04

Where TAθ = TAR for 0x0 field size = 1